International Journal of Polymer Science

Advanced Smart Materials from Natural Fibre Reinforced Polymer Composites

Lead Guest Editor: Khalina Abdan
Guest Editors: Ching Hao Lee, Hyun-Joong Kim, and Abu Bakar Sulong

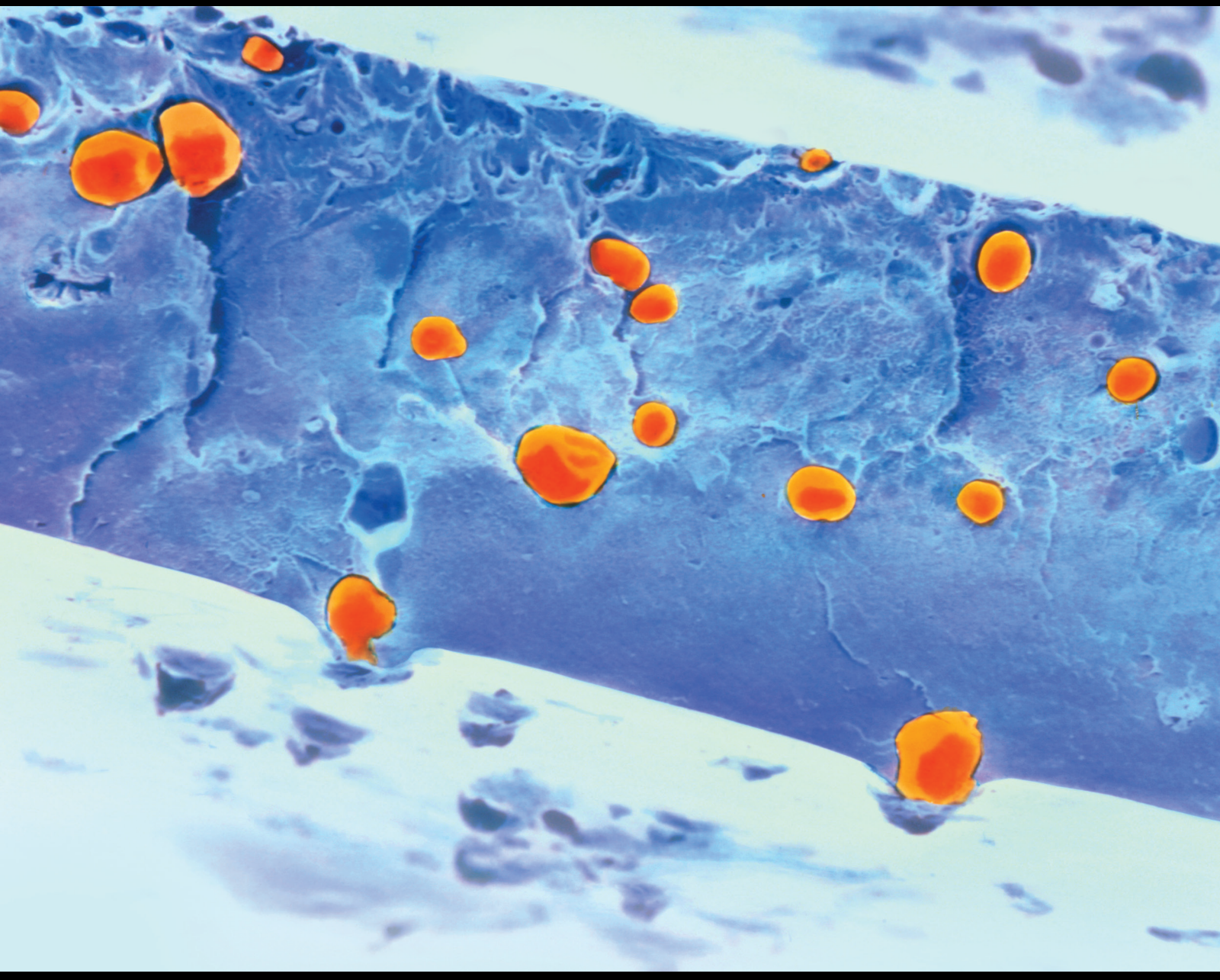

Advanced Smart Materials from Natural Fibre Reinforced Polymer Composites

International Journal of Polymer Science

Advanced Smart Materials from Natural Fibre Reinforced Polymer Composites

Lead Guest Editor: Khalina Abdan
Guest Editors: Ching Hao Lee, Hyun-Joong Kim, and Abu Bakar Sulong

Contents

Hindawi
International Journal of Polymer Science
Volume 2022, Article ID 7253136, 20 pages
https://doi.org/10.1155/2022/7253136

Research Article

Physical, Mechanical, and Thermal Properties and Characterization of Natural Fiber Composites Reinforced Poly(Lactic Acid): Miswak (*Salvadora Persica* L.) Fibers

A. F. Nur Diyana,[1] A. Khalina,[1,2] M. S. Sapuan,[3] C. H. Lee,[4] H. A. Aisyah,[1] M. N. Nurazzi,[1] and R. S. Ayu[1]

[1]*Laboratory of Bio Composite Technology, Institute of Tropical Forestry and Forest Products (INTROP), Universiti Putra Malaysia, Serdang, Malaysia*
[2]*Department of Agriculture and Biotechnological Engineering, Universiti Putra Malaysia, Serdang, 43400 Selangor, Malaysia*
[3]*Department of Mechanical Engineering, Universiti Putra Malaysia, Serdang, 43400 Selangor, Malaysia*
[4]*Mechanical Department, School of Computer Science and Engineering, Taylor's University, 47500 Subang Jaya, Selangor, Malaysia*

Correspondence should be addressed to A. Khalina; khalina@upm.edu.my and C. H. Lee; leechinghao@upm.edu.my

Received 25 October 2021; Revised 25 May 2022; Accepted 8 July 2022; Published 23 November 2022

Academic Editor: Karthik Reddy Peddireddy

7000 years ago, miswak fiber (MF) was used as a toothbrush for oral care. However, since the emergence of plastic materials, it monopolized the oral care industry. The increment of plastic products also promotes accumulation of plastic wastes after its disposal. Thus, many researchers have turn to biodegradable products to reduce this problem. The aim of this study is to investigate the chemical, physical, and mechanical properties of MF as reinforcement in composites that are suitable to replace the toothbrush materials. The MF was reinforced in PLA composite with different weight percentage (0%, 10%, 20%, and 30%) and undergoes several types of testing. The chemical results show that there were high presence of cellulose in the fiber which could act as medium to transfer stress load equally from fiber to matrix. However, the results show low cellulosic contents in MF that affects the poor interfacial bonding between fiber and matrix. Physical properties shows a positive indication to be used as a toothbrush handle. As the fiber content increases, the density also increased. SEM micrographic illustrated the presence of voids as the cause for reduction in mechanical properties of composites. The mechanical results show the proposed material is comparable to the materials used in commercial applications. As for the thermal result, the TGA test melting point of the proposed composite material was comparable to the pure PLA, which means the proposed material can use similar processing temperature as PLA. DSC shows that Tg of PLA/MF composite is found to be similar to Tg in loss modulus of composites. DMA finding found that PLA/MF30 have the highest storage modulus 2062 MPa and the lowest tan δ 0.6 among PLA/MF composites. This concludes that there is a possibility of using these materials as an alternative in composites and increase the fiber strength by using pretreatments and/or compatibilizer.

1. Introduction

In the past decades, natural materials have been used to manufacture personal hygiene products. In the early 1900s, chemists had found that the substance known as "celluloid" could be shaped into practical shapes, which are suitable for toothbrush handles. In the early twentieth century, manufacturers started to make use of nylon and other plastics to replace celluloid materials when plastic was invented [1]. Due to its 100% waterproof property, nylon had gain higher attraction and replaces celluloid in 1938 [2, 3]. Since then, plastic has dominated the hygiene industry and was commonly used to manufacture toothbrushes as shown in Figure 1. However, plastics are well known as a nonbiodegradable material, which promotes landfills after its disposal. Every single toothbrush that was manufactured decades ago

Figure 1: Conventional toothbrush.

could still be found around us as a piece of trash, somewhere on the planet [2, 3]. Furthermore, the American Dental Association stated that everyone should change their toothbrushes every three to four months. Hence, this had further increased the amount of wastes produced from the toothbrush disposal, where approximately 23 billion toothbrushes were annually discarded [3, 4]. Many toothbrushes were nonrecyclable due to the materials used during production. Biodegradable or biobased plastics were not always better for the environment than traditional plastics, either because they do not break down as well or because they have their own complicated environmental footprints [3, 5]. However, any alternative that decreases the overall amount of material and packaging used is a positive move. An alternative action is to incorporate natural fiber into polymer matrix to produce composite material for toothbrush handles.

The development of biodegradable materials has attracted many interests of researchers globally. Recently, a new toothbrush that uses biodegradable bamboo toothbrushes with PLA-based compostable bristles has been produced and available in the market [6]. This had arisen the need of toothbrush waste reduces in our environment. The biodegradable and renewable aliphatic polyesters are one of the most promising biodegradable plastic materials. Polylactic acid (PLA) polymer is one of the most intensively developed and commercially available due to its biodegradability, renewability, and high strength to weight ratio. There were many studies that had extensively used PLA as the polymer matrix for composite material for numerous applications and purposes [7]. In addition, PLA were also used for food packaging, tissue engineering, household engineering, and drug delivery application [8], and it was commonly used for biomedical applications due to its biocompatibility, biodegradability, and nontoxic features [9].

In the midst of competitive materials and processing cost of biopolymer, PLA polymer exhibits attractive physical and mechanical properties such as good clarity, barrier properties, superior modulus, and strength performances [10]. However, the cost of the raw material of PLA is relatively higher compared to conventional synthetic materials, thus demoted the willingness of industrialists to use it. PLA also exhibits drawbacks such as sensitive to heat distortion temperature and moisture, as well as low resistance to hydrolysis and flexibility, which makes it harder to use PLA as the composite's matrix [11].

Fiber reinforcements are also one of the factors that could increase the composite's mechanical strength. Several experimental studies had combined PLA with a variety of natural fibers such as flax, kenaf, hemp, and bamboo, in order to create biodegradable composites [12–17]. From these studies, it was found that natural fiber reinforcement in polymer composites was able to reduce the production cost while still retaining its biodegradability [18]. There was one study made by Bajpai et al., which had developed new tribological material and better wear behavior of the composites by incorporating 20 wt. % of sisal, nettle, and Grewia optiva fibers into the polymer composite [19]. Oksman et al. [20] study had shown that flax fiber-reinforced PLA composite has 50% higher tensile strength as compared with flax/polypropylene composite [20]. Meanwhile, in Nishino's study, it was found that kenaf fiber reinforcement of up to 70 wt. % resulted in high strength of biodegradable composite [21]. All of these studies show that natural fiber reinforcements in composites could potentially increases the mechanical performance of the polymer composites.

In this technologically advanced era, the conventional toothbrush was deemed to be more expensive compared to the cost of miswak, especially in regions where miswak tree was grown locally. Figure 2 shows the processing of the miswak tree to fibers which could be used as a reinforcement material. 7000 years ago, Babylonians (the Greeks and Romans) used chewing sticks as a toothbrush as shown in Figure 3, which then gradually changes to the current plastic toothbrush [22].

Miswak is becoming more popular in Muslim countries, particularly in various African and Arab nations. It was also known as the natural toothbrush. The World Health Organization has also suggested of using miswak for oral hygiene due to its antibacterial effect [23]. There are more than 180 plant species that can be used as a natural toothbrush. These species differ from each other on the basis of appearance, scent, texture, and taste. The plant sources vary around the world, with neem (Azadirachta indica) being the most widely used in India; lime tree (Citrus aurantifolia) and orange tree citrus (Citrus sinensis) being used in West Africa; Senna (Cassia vennea) being used in other parts of Africa; and Arak (Salvadora persica) being used in the Middle East [24]. Furthermore, neem is a native plant of India, and Arak (S. persica) is widely used in Saudi Arabia; miswak could be found in Indonesia, Malaysia, Australia, Sri Lanka, Burma, Pakistan, and Africa [25]. Miswak is popular for a variety of reasons, including its inexpensive cost of production and easy access to the source [26] and most importantly its antibacterial effects. *Salvadora persica* or miswak fiber (MF) could be used as an alternative fiber reinforcement for polymer composites. The miswak has been used for

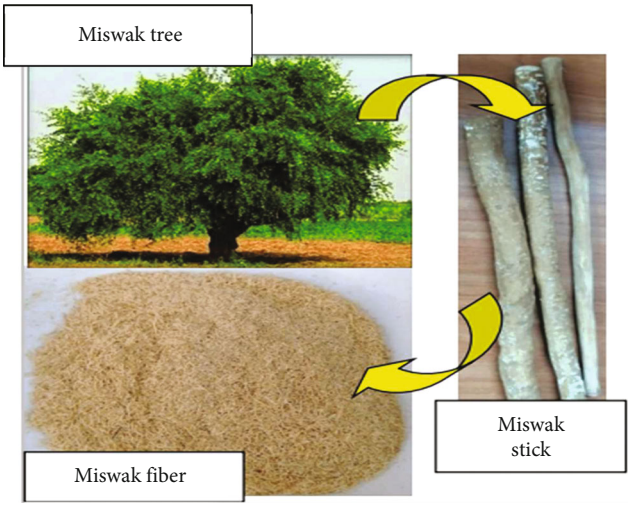

Figure 2: Miswak fiber obtained from miswak stick that originated from miswak tree.

Figure 3: Frayed miswak stick.

centuries, and there is an Islamic etiquette in using miswak as stated in past studies [27]. Cleansing effects and oral health protection provided by the miswak fibers during mechanical cleaning and releases of beneficial chemicals from fibers, respectively, have proven its high value as a composite fiber reinforcement with antibacterial properties [28]. Miswak fibers have been reported having more than one type of antimicrobial agents that inhibit positive and negative bacteria that help enhance in plaque removal [29]. Despite the fact that there have been several articles on PLA and natural fiber composites, there was no study which discusses on the effect of miswak (*Salvadora persica*) fiber as a reinforcement fiber in PLA matrix. Natural fiber not only reduces the cost of the material, but they also encourage disintegration and biodegradation, with the added benefit of antibacterial characteristics. This advantage is potentially useful for a wide range of application, especially in dental care. Therefore, the aim of this study was to characterize the mechanical, physical, and thermal properties of the miswak fiber-reinforced polymer composites.

2. Experimental Details

2.1. Materials. Polylactic acid (PLA) (grade 2003D) produced by Nature Works, USA, was used and purchased at Polycomposite Sdn Bhd. The density, melting temperature, and glass transition temperature of PLA were 1.24 g/cm^3, 160°C, and 55-60°C, respectively. Miswak stick was bought from Al-Khair Natural Products, Malaysia.

2.2. Biocomposite Preparation. Miswak fiber (MF) was prepared by chopping the stick into smaller pieces and then crushed the pieces into short fibers. The short fibers were then grind into powder and then dried in an oven to remove moisture. The dried MF was then sieved to get fibers below mesh 30. PLA pallets and MF were mixed by using Brabender Internal Mixer to obtain the composite blends. The temperature and rotor speed were fixed at 160°C and 50 rpm, respectively. The composite was prepared with varying weight composition ranging from 0 to 30 wt. % of MF content as shown in Table 1.

The composite blends were preheated for 4 minutes at 160°C before going to full-press. It was then hot pressed for four minutes at 160°C using a Vechno Vation 40 tonne compression molding. The 30 cm × 30 cm composite plate was then placed in a cold press between two steel plates, where it was cooled for 4 minutes at 25°C. Figure 4 depicts the compression molding machine. Finally, the composite plate was cut into smaller samples suitable for testing based on the ASTM Standard.

2.3. Materials Characterization Process

2.3.1. Board Density. The composite samples were weighed in air using digital weighing scale and in water using the densimeter, MD-200S Mirage. The difference in weight of the samples in two different mediums will give the weight of water displaced by the samples, and this weight in gm was converted to volume in cm^3. Ten samples were cut into square shape with the dimension of (10 × 10 × 3) mm. The solid square piece was then polished with 1200 grade sandpaper in order to make smooth and shiny surface. The density test was performed according to ASTM D4018 by using a weighing scale, and the dimensions were measured using Mitutoyo Digital Vernier calipers. The volume was calculated from the measured dimension. The density was then recorded for all samples and presented in Table 2 under Section 3.1 Density of composite.

The density was calculated using the equation

$$\text{Density}\left(\text{g/cm}^3\right) = \frac{\text{Mass}}{\text{Volume}}. \quad (1)$$

2.3.2. Chemical Analysis Test. Preliminary chemical analysis was performed by means of solvent extraction as well as weighing procedure after 2 hours of heating at 105°C for water content. The test used TAPPI standard procedure to determine the extractive (T204), cellulose (T203), holocellulose [30], and lignin (T222) content of the fiber composition.

Table 1: Formulation of PLA/MF composites.

Sample code	Matrix PLA (wt. %)	Reinforcement MF (wt. %)
PLA	100	0
PLA/MF10	90	10
PLA/MF20	80	20
PLA/MF30	70	30

Figure 4: Compression molding.

Table 2: Properties of PLA/MF composites density.

Specimens	Density (g/cm^3)	Density increment, %
PLA	1.240	—
PLA/MF10	1.255	1.21%
PLA/MF20	1.283	2.23%
PLA/MF30	1.308	1.95%

2.3.3. Water Absorption. Ten composite samples with the dimensions of $(10 \times 10 \times 3)$ mm were prepared according to ASTM D570 for each different composites composition. All samples were oven dried at 60°C for 24 hours. After oven drying, the samples were cooled in desiccators over granulated silica gel before water absorption test was conducted. The test was conducted by submerging the specimens in distilled water for 72 hours and measured the increase in weight in every one hour as compared to the original oven dry weight of the specimen. Two specimens of each type formulations were tested in an adjusted room temperature of 27°C, and the average result was recorded. Water absorption was calculated as

$$\text{Water absorption } (\%) = \frac{(W_1 - W_0)}{W_0} \times 100, \quad (2)$$

where W_0 is the weight of specimens before immersion and W_1 is the weight of specimens after 72 hours of immersion in distilled water.

2.3.4. Thickness Swelling. Ten specimens of $(10 \times 10 \times 3)$ mm3 samples of each composite's formulations were prepared according to ASTM D570 for the testing of thickness swelling. The samples were measured before as T_o and T_t as after by using Digital Vernier calipers (Mitutoyo) with 0.01 cm accuracy. The thickness swelling was calculated according to the Equation (3):

$$\text{Thickness swelling } (\%) = \frac{(T_{1-}T_0)}{T_0} \times 100, \quad (3)$$

where T_0 is the thickness of specimens before immersion and T_1 is the thickness of specimens after 72 hours of immersion in distilled water.

2.3.5. Scanning Electron Microscope (SEM). Scanning electron microscope (Hitachi S-3400 N) equipped with energy dispersive X-ray under an accelerating voltage of 15 kV at an emission current of 58 μA was used to observe the fracture surface after the tensile test. The fracture ends of the samples were mounted on an aluminum stub and coated with a thin layer of gold to avoid electrostatic charging during examination.

2.3.6. Tensile Properties. The tensile testing of the composite was conducted using 5kN Bluehill INSTRON Universal Testing Machine. The test was carried out according to ASTM D638-14. The samples were cut into dog bone shape by a plastic molder machine with the specifications of length of 165 mm, width of 13 mm, and thickness of 3 mm, respectively. The crosshead speed was set at 2.0 mm/min, and the composites were gripped at a 30-mm gauge length. Five samples were kept in a conditioning room, and the test was run at 20.5°C with the relative humidity (RH) at 48%.

2.3.7. Flexural Properties. Flexural test of the composite was performed using 5kN Bluehill INSTRON Universal Testing Machine. The test was carried out according to ASTM D790-17 three-point bending test. The samples were cut with the specifications of length of 127 mm, width of 12.7 mm, and thickness of 3 mm, respectively. The crosshead speed was set at 2 mm/min with a support span-to-depth ratio of 16 : 1. Five samples were kept in a conditioning room, and the test was run at 20.5°C with the relative humidity (RH) at 48%.

2.3.8. Fourier Transform Infrared Spectrometry (FTIR). Using an FTIR (Nicolet iS10 Thermo Scientific) analyzer, the chemical functional group contained in the MF was discovered. The infrared (IR) spectra were analyzed using

OMNIC software and the attenuated total reflectance (ATR) technique. The sample was prepared as a powder and scanned 32 times with a resolution of 2 cm^{-1} over a wavenumber range of 500 cm^{-1} to 4000cm^{-1}.

2.3.9. Thermogravimetric Analysis (TGA). The samples were analyzed (TGA) on a Mettler Toledo TGA/DSC 1HT Stare System (Switzerland) from 30 to 600°C at a heating rate of 10°C/min and nitrogen gas as its medium. TGA is a method for determining a material's thermal stability and volatile component fraction by measuring the weight change as the sample is heated at a constant rate.

2.3.10. Differential Scanning Calorimetry (DSC). The heat capacity of the composites was measured using differential scanning calorimetry. The specimens were examined to differential scanning calorimetry on a Mettler Toledo TGA/DSC 1HT Stare System (Switzerland) from 30 to 200°C at a heating rate of 10°C/min in nitrogen gas.

2.3.11. Dynamic Mechanical Analysis (DMA). TA Instrument Q800 was used to perform dynamic mechanical analysis (DMA) in accordance with ASTM D4065. In a nitrogen environment, samples of 60 mm × 12 mm for each composite structure were placed in 3-point bending mode at a frequency of 1 Hz and an amplitude of 15 μm at 25-105°C with a continuous heating rate of 5°C/min.

3. Results and Discussion

3.1. Density of PLA/MF Composites. Table 2 shows that density of PLA/MF composites, and it found density increment with increases of MF contents; this is found aligned with previous study [31]. It was found that the MF30 sample has the highest density value. This was expected since there was a higher portion of relatively high-density MF that replaced the PLA matrix [32]. However, nonlinear response on density increment was found in this study. This can be foreseen by high porosities in the composites due to poor interfacial bonding between fiber and matrix. The voids, as a result from ineffective fiber wetting, make the composite have a lower density than it should be. Hence, there will be a high reduction of strength properties shown on the MF30 specimen.

3.2. Analysis of Chemical Composition of Miswak Fiber. Table 3 shows the chemical composition of various natural fiber from previous studies, as well as the results of a preliminary chemical study of the MF. It was reported that agricultural lignocellulosic biomass typically contains between 10% and 25% of lignin, 20% to 30% of hemicellulose, and 40% to 50% of cellulose [33]. Carbohydrates (cellulose and hemicellulose) constitute the majority of the chemical components of wood, with cellulose accounting for 40% to 50% of the dry weight and hemicelluloses for 25% to 35%. Additionally, hardwood lignin make up between 10% and 20% of the overall lignin composition [34].

According to the chemical analysis, this miswak fiber comprises 5.09% lignin, 28.12% hemicellulose, and 21.81% cellulose. The test also indicated extractives as a component. Other than cellulose, hemicellulose, and lignin, the extraneous components in wood include extractives and ash. Extractives are the extraneous material that is soluble in neutral solvents and amounts from 4 to 10% of the dry weight of typical wood in temperate climate species. However, extractives may make up as much as 20% of the dry weight of wood from tropical species [34]. Miswak fiber comprises 20.1% of the extractives composition, according to the results of lignocellulosic biomass composition testing using the TAPPI T204 standard. It suggests that miswak fiber can be classified as tropical series wood. Miswak fiber, or S. persica as it is known scientifically, is a well-established plant with high drought resilience that grows in dry to arid regions of the tropics and subtropics [35].

Natural fiber's main composition has a significant impact on how well composites perform. To examine and ascertain the impact of miswak fiber on polylactic acid polymer, however, substantial experiments are required. To better comprehend the impact of fiber composition on the mechanical and thermal characteristics of composite, tests like X-diffraction to detect the crystalline structure may be helpful. To date, it has been shown that miswak fiber has a lower cellulose concentration than other natural fibers; however, Pettersen [34] noted that cellulose from wood is difficult to separate in pure form because it is closely linked to lignin and hemicellulose. However, according to TAPPI T203 or ASTM Standard D 1103, the majority of alpha cellulose is produced after the holocellulose is treated with 17.5 percent NaOH [34, 36]. On the other hand, hemicellulose can be found mostly in the primary wall of the fiber, and lignin is an amorphous in nature incorporated into cellulose structure to enhance the strength of the wood [37]. MF has the highest hemicellulose contents as compared to other natural fiber and the hemicellulose binding microfibrils in the fiber, which provides structural reinforcement [38]. Lignin acts as glue between individual cells in the cell wall, and it provides flexibility, properties, or structure of the fiber [38].

The main component that gives fibers their stiffness, strength, and favorable thermal qualities is cellulose. However, a number of factors, including fiber particle size, fiber orientation, and fiber processing conditions, may have an impact on composite characteristics. To learn more about the qualities of composite materials, greater research on the impact of fiber sizes, orientation, and processing conditions on those attributes is required. Table 3 shows the comparison of chemical composition of miswak with other type of fibers.

3.3. Water Absorption and Thickness Swelling of PLA/MF Composites. Figure 5 shows the level of water absorption of PLA/MF composites. The aim of this study was to investigate the water absorption characteristic of the PLA/MF composites. It is significant to understand the behaviors of the composites in moist surrounding. This is also because natural fibers are sensitive to water; thus, this characteristic will definitely affect the strength of the composite when it is highly exposed to water. Other factors that could affect the composite physical properties were voids/pores, volume fraction of fibers, humidity, viscosity of matrix, and temperature [43].

Table 3: Constituents of miswak fiber and other natural fibers.

Fiber	Cellulose (wt. %)	Hemicellulose (wt. %)	Lignin (wt. %)	Reference
Miswak	21.81	28.12	5.09	Present study
Kenaf	70	19	3	[39]
Sugar palm	37.3	4.71	17.93	[40]
EFB	45	21	23	[41]
Hemp	70.2-74.4	17.9-22.4	3.7-5.7	[37]
Flax	71	18.6-20.6	2.2	[37]
Jute	61-71.5	13.6-20.6	12-13	[37]
Sisal	45	14.2	20.5	[42]

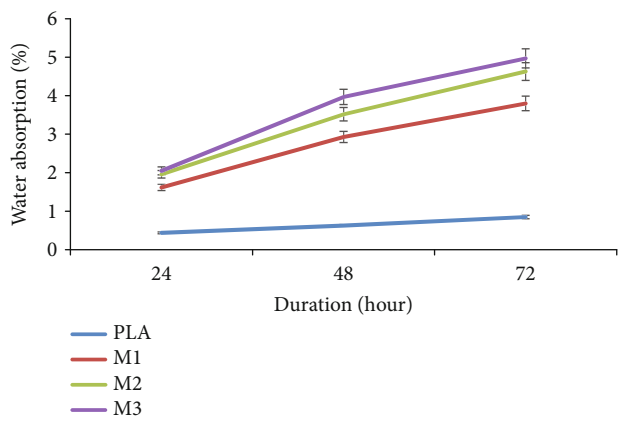

Figure 5: Water absorption level of PLA/MF composites.

In Figure 5, the level of water absorbs by sample for PLA, PLA/MF10, and PLA/MF20/PLA/MF30 are 0.93%, 1.34%, 1.36%, and 1.42%. Neat PLA was expected to record the lowest water absorption due to its hydrophobic nature. This was expected since PLA/MF30 had the highest cellulose content in the miswak fiber, which increases the penetration of water by capillary mechanism [44]. The increase in water absorption for hydrophilic fiber in composite samples was predicted since the PLA/MF molten flow fills the mold before it crystallizes during composite processing. When this happened, some air was retained, resulting in water penetration into the voids of the samples [45].

In Figure 6, the thickness swelling for PLA, PLA/MF10, PLA/MF20, and PLA/MF30 are 0.08%, 0.75%, 0.76%, and 0.80%. The slight increasing thickness of the neat PLA samples proofs that water diffuses into the samples. PLA/MF30 composite had the highest thickness swelling due to its high fiber content. The increase in swelling of the specimens was resulted due to the presence of voids and the hydrophilic nature of the fibers that attracts water. Similar findings was reported by [46], where his study found that there was an increase in the level of swelling of the PP/miswak powder samples as the fiber content increases.

3.4. Scanning Electron Microscope of PLA/MF Composites. Figures 7(a)–7(c) show the SEM micrographics for different MF ratio (10-30 wt. %) reinforcement in PLA composite. In the 10 wt. % of MF reinforcement composite (Figure 7(a)), ineffective mixing of fibers and matrix causes the formulation of voids. Multiple variables, including manufacturing and processing conditions, fiber volume percentage, and fiber length, can lead to void development in polymer composites. Further elements that may impact void content include matrix material, moisture content, and processing conditions [43, 46, 47]. The appearance of MF has disturbed the homogeneous flow of molten resin, creating meso- and microvoids. Nonhomogeneous air permeability of natural MF entrapped more air and reduced matrix bonding strength. The voids act as a stress concentration spot and lead to earlier failure during loading.

On the other hand, presences of void between fiber and matrix (Figure 7(b)) show ineffective interfacial bonding between hydrophilic matrix and hydrophobic natural fiber. Besides, poor fiber wetting due to poor matrix adhesion on impurities-riches fiber's surface shall be visible. This resulted a full detachment of matrix from fibers during applied tensile forces.

In Figure 7(c), there was a presence of fiber fracture and fiber pull-out. The micrographs showed that the composite breaks due to fiber-to-fiber interaction in the composite matrix. This observation was similar to the previous study [48]. From this analysis, PLA/MF composites were expected to have low mechanical properties due to conditions such as improper fiber handling, poor fiber-matrix interaction, and matrix detachment.

3.5. Tensile Properties of PLA/MF Composites. Table 4 and Figure 8 shows the tensile properties of PLA/MF samples. PLA with MF10 showed the highest tensile strength and Young's modulus values of 33.7 MPa and 2.9GPa, respectively. The lowest tensile strength and Young's modulus values were observed from PLA with 30 wt. % fiber content as shown in Table 4.

Tensile strength was found to have dropped by 35% as a result of the addition of 10% MF to polymer. The absence of adequate polymer reinforcement provided by the MF, as seen in Figure 7(a), is what causes the composite's decreased tensile strength. The parameters used in composite fabrication led to the occurrence of voids. When fibers are incorporated into a composite material, air or volatile substances may get trapped in the material. As a result, the fiber spacing between resin-rich regions can cause microvoids to form in the composite along the individual fibers, which has a

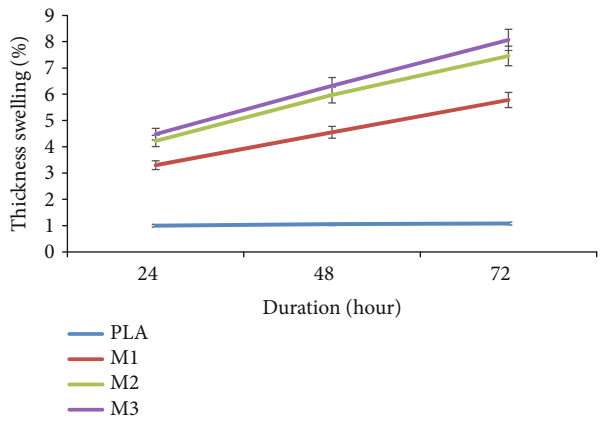

Figure 6: Thickness swelling level of PLA/MF composites.

negative impact on the tensile properties of the composites. The adherence of the fibers to the matrix is another element that lowers the tensile strength of PLA/MF composite.

When fibers were added to a matrix, it was anticipated that the resulting fiber-reinforced composite will be stiffer than a pure polymer; thus, it could carry the load applied to the composite. However, as shown by SEM in Figures 7(b) and 7(c), the condition of poor adhesion between the fiber and the matrix had led to a reduction in tensile characteristics. According to study made by Mazur et al., PLA composites made with natural particles (Wood, Bamboo, and Cork), inadequate fiber/matrix adhesion, and empty spaces in the material had a detrimental impact on the material's mechanical characteristics [49]. Pongtanayut et al. discovered that the insertion of soft phase rubber reduced the tensile strength of PLA matrix, suppressing PLA crystallinity and resulting in decreased tensile strength [50]. However, by adding 10 wt. % MF to polymers results in increased Young's modulus values. The MF reinforcements, regardless of the amount of fiber content, have shown better strength but small increment (<5%) on the tensile modulus. All of the blends had similar Young's modulus values to the pure PLA as the modulus improvement is only ranging from 1.05% to 3.19%. It is widely known that adding any mineral or filler to a composite will improve its stiffness or modulus.

Studies on the enhancement in Young's modulus brought on by adding wood flour (WF) materials up to 7 wt. % were discovered by Zhang et al. in [51] with 2wt. % WF/resin recording the highest Young's modulus at 323.8 MPa [51]. Similar increment in tensile modulus of composite was found by Sherwani et al. [52] in which untreated sugar palm fiber/glass fiber-reinforced PLA hybrid composite tensile modulus increased with the addition of GF [52]. Table 4 displays the elongation at break as a function of MF content. The abrupt decrease in elongation upon break is a result of miswak fiber's stiffening action. Similar behavior is consistent with studies conducted by Morreale et al. [53] that discovered the addition of WF into biodegradable polyester will decrease the elongation at break of the samples [53].

In this research, the Brabender internal mixer screw speed was maintained at 50 rpm to blend PLA pallets with MF. According to [54], increasing the microscrew compounder's speed had a negative influence on the tensile and impact parameters of all composite materials. When PEG was added to virgin PLA at a screw speed of 200 rpm, it was discovered that the yield strength and modulus value decreased. Sample PLA/PEG/POSS composite compounded at a screw speed of 100 rpm, however, showed higher tensile and impact results. As it was discovered, PLA/kenaf bast and PLA/kenaf core exhibit improved results on flexural strength of 60 rpm rotation speed, and impact strength higher value was measured with PLA/kenaf bast and PLA/kenaf core at 70 rpm rotation speed. Jaafar et al. [55] investigated the varying speeds of extrusion (60, 70, and 80 rpm) and showed various behavior of fiber dispersion. The effect of screw speeds of 40, 80, and 140 rpm extrude on the mechanical characteristics of PLA/HNT composite has been examined by Venkatesh et al. [56]. The PLA/HNT 5 wt. % nanocomposite compounded at 140 rpm showed improved HNT dispersion in the PLA matrix, leading to higher mechanical characteristics. Whereas processing speed does not significantly affect the tensile characteristics of virgin PLA, Galvez et al. [57] have found that adding ATBC 10 wt. % causes a reduction in tensile values of 36% for 60 rpm speed and 50 percent for 150 rpm speed. Tensile modulus was reduced by 36% and 44% at 60 and 70 rpm, respectively. Nevertheless, it should be highlighted that the bra-bender's screw speed had a detrimental effect on the mechanical characteristics of the PLA/MF composite.

The technique used to manufacture composites has an influence on the performance of natural fiber-reinforced polymer composites. The settings used during the compression molding process to create short natural fiber composites have a big impact on the composite's mechanical characteristics. When creating composites via compression molding, studied the compounding process between polymer and short natural fiber. According to research, compression molding holds materials for an average of 4 to 15 minutes. To produce superior mechanical characteristics of natural fiber composites, it is vital to choose the right molding pressure, temperature, and holding time. The impact of manufacturing factors on the strength of biodegradable composite was researched by Rubio-Lopez et al. [58]. Studies have shown that a large reduction in production time may result in a decrease in the manufacturing cost of composite materials. Compression molding preheating time of 2 minutes and heating under pressure for 3 minutes produced tensile strengths more than 100 MPa. The mechanical characteristics of kenaf fiber polymer composite were studied by Bernard et al. [59] to see how temperature and speed of compression molding affected such qualities. Tensile strength increased with the addition of 10 weight percent unidirectional kenaf fiber, and impact characteristics were shown to worsen with compression at 230°C and 10 minutes of holding. In this PLA/MF studies, the compression molding parameter was discovered after 4 min of preheating, complete pressing, and cooling at 160°C. The parameter was discovered by analyzing the state of the extracted

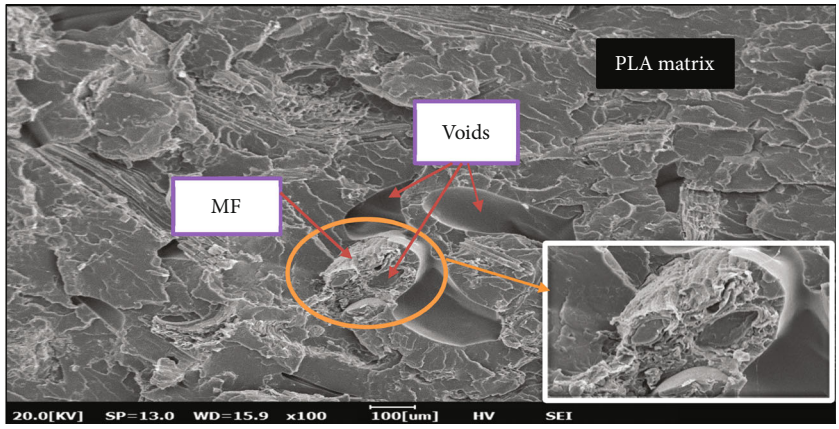

(a) PLA/MF10

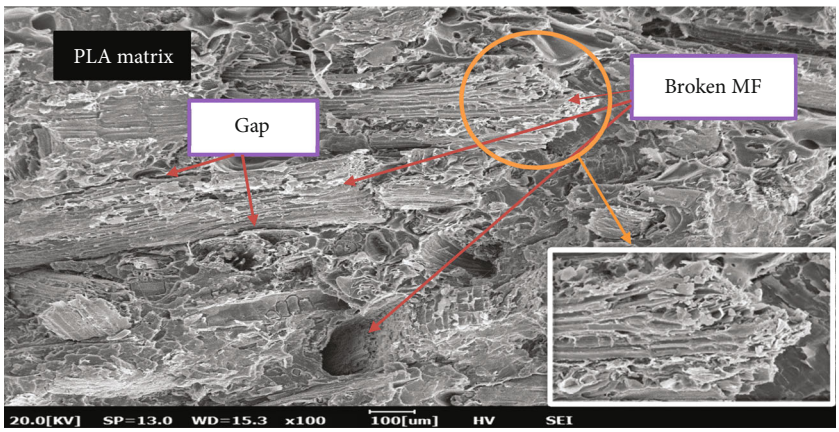

(b) PLA/MF20

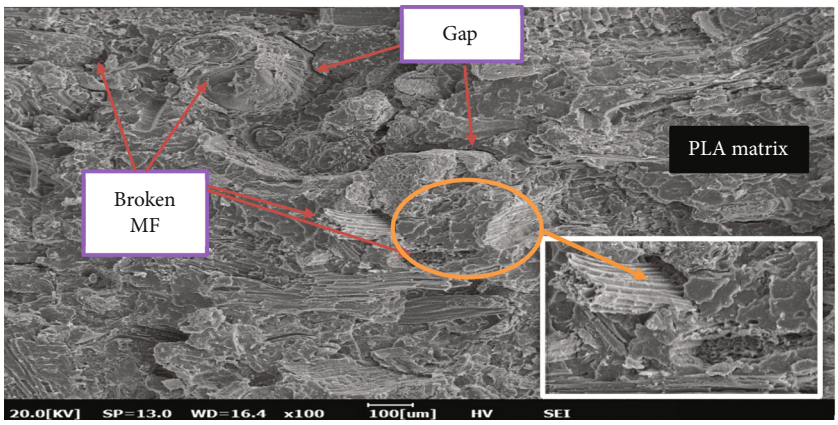

(c) PLA/MF30

Figure 7: SEM micrograph of PLA/MF tensile fractured surfaces of different loading (a) PLA/MF10 wt. %, (b) PLA/MF20 wt. %, and (c) PLA/MF30 wt. % with 100 magnifications.

sample, which had a well melted flat surface and no evidence of trapped air.

3.6. Flexural Properties of PLA/MF Composites. An INSTRON universal testing machine was used to determine the flexural strengths of PLA/MF, and the results are shown in Table 5. The link between the flexural characteristics of the polymers and the miswak fiber was shown in Figure 9. For neat PLA, the maximum flexural strength and modulus were displayed as 95.6 MPa and 3.4 GPa, respectively. The maximum flexural strength and modulus with 10 wt. % MF were 66.1 MPa and 3.2GPa, respectively. It was discovered that PLA with MF offered noticeably weaker flexural characteristics. Pure PLA was stiffer and more brittle than PLA/MF composite. The flexural characteristics of the composites were influenced by the polymers' inherent strengths [60]. According to Doh et al. [60], the inclusion of 10% liquefied wood in liquefied wood polymer composites (LWPC)

Table 4: Tensile properties of the composite's samples.

Sample	Tensile Strength (MPa)	Tensile Young modulus (GPa)	Elongation at break (%)
PLA	52.1	2.85	2.64
PLA/MF10	33.7	2.94	1.69
PLA/MF20	28.4	2.88	1.74
PLA/MF30	24.1	2.89	1.49

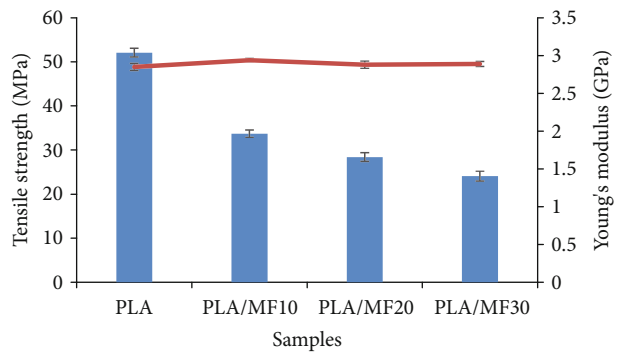

Figure 8: Tensile strength and modulus of PLA/MF composites.

Table 5: Flexural properties of composite samples.

Sample	Flexural Strength (MPa)	Flexural Young's modulus (GPa)
PLA	95.6	3.4
PLA/MF10	66.1	3.2
PLA/MF20	57.1	2.8
PLA/MF30	49.5	2.9

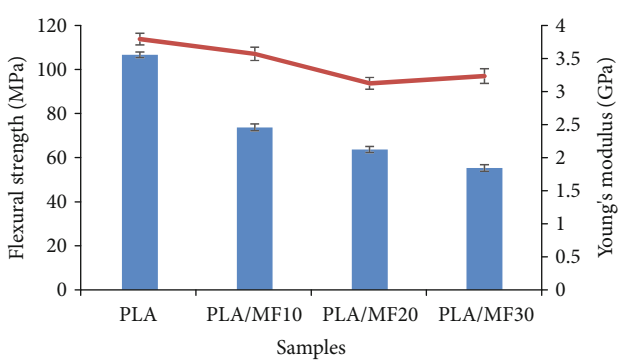

Figure 9: flexural strength and the flexural modulus of PLA/MF composites.

increased the flexural MOE and MOR of polymer with higher melt index. This is because the high flow value of the polymer helps in blending the polymer and the liquid wood powder during the compounding process at a specific temperature, increasing the flexural characteristics [60].

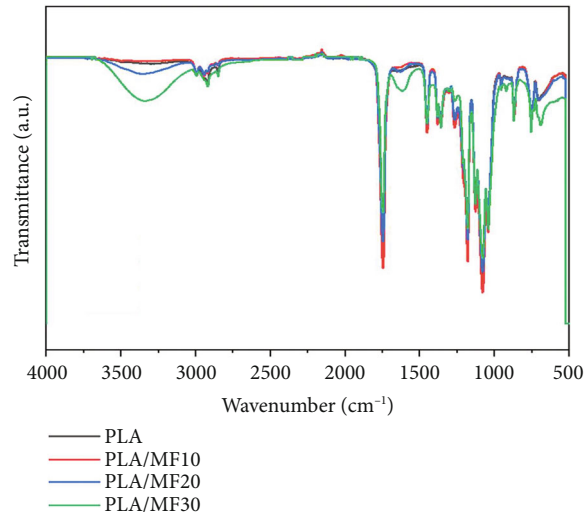

Figure 10: IR spectra of PLA/MF composites.

Fiber orientation is another aspect that impacts the flexural characteristics. As the fiber orientation becomes more parallel to the direction of the load applied, the greater the flexural qualities since the phenomena happening during the flexural test depend on the location, with the top layer being subjected to compression and the lower layer to tension [49]. However, Golmakani et al. [61] discovered the opposite conclusion in their investigation into the impact of wood powder and nanoclay particle content on polyethylene matrix. They discovered that when wood floor was added in amounts of 40 wt. % and 50 wt. % in composites without nanoclay, the flexural strength values were 40.78 MPa and 45.87 MPa, respectively, which may be regarded as having strong flexural qualities [61].

Flexural strength and modulus were decreased for composite materials when fiber content was increased by 10%, 20%, and 30%. When compared to plain PLA, PLA/MF10, PLA/MF20, and PLA/MF30, all decreased by roughly 30.8%, 40.2%, and 48.2% as compared to neat PLA, respectively. As shown in (Figures 7(a)–7(c)), the increase in porosity of the composites brought on by insufficient interfacial bonding is what leads to the drop in characteristics. The outcomes match those of the PLA composite with natural fibers work as determined by SEM [49]. Yusoff et al. [62] found that while the flexural strength of kenaf-coir/PLA was lower than kenaf-bamboo-coir/PLA and bamboo-coir/PLA, it had the highest flexural modulus, which was 70% higher than the other combinations, as the impurities in bamboo fiber caused fiber-matrix interfacial failure and decreased the stiffness of the composites [62].

3.7. Fourier Transform Infrared Spectrometry (FTIR) of PLA/MF Composites. Figure 10 shows the IR spectra of PLA polymer and PLA/MF. The sample's primary absorbance was found in low-wave number areas, particularly 500 cm^{-1} to 1800cm^{-1}. In a previous study, similar findings were reported [63]. The spectra of three different types of fiber loading in matrix were almost identical, as shown in Figure 9. The information about the functional groups in

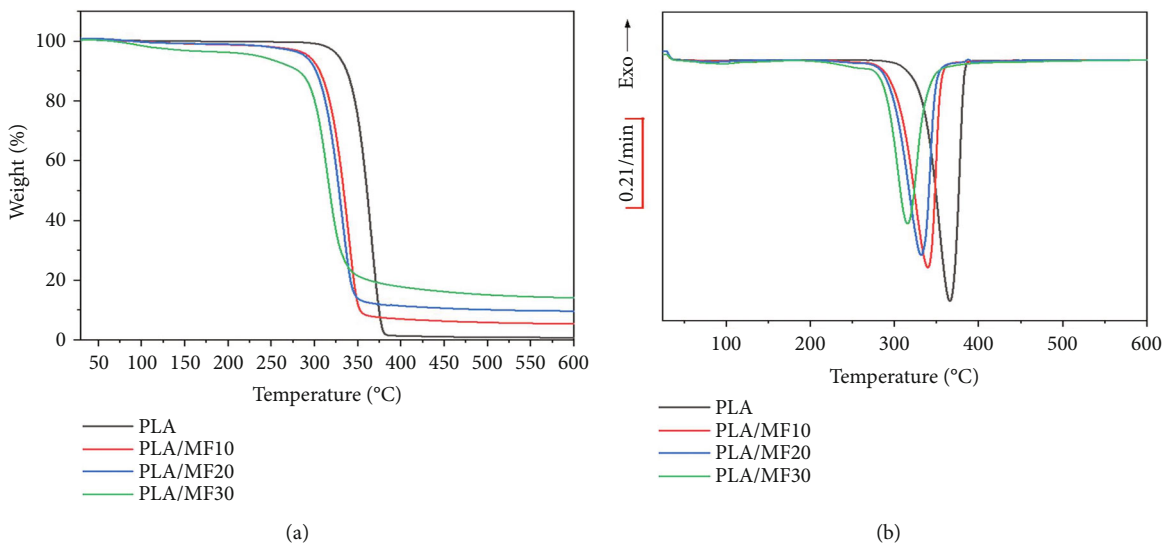

Figure 11: (a) TGA curve of PLA/MF composite. (b) DTG curve of PLA/MF composite.

Table 6: Thermal degradation temperature of PLA/MF composites.

Sample	Initial degradation, (°C)	Final degradation, (°C)	Residue (wt. %)
PLA	336.38	367.32	0.86
PLA/MF10	292.42	341.64	5.52
PLA/MF20	265.77	333.36	9.78
PLA/MF30	266.98	317.27	14.23

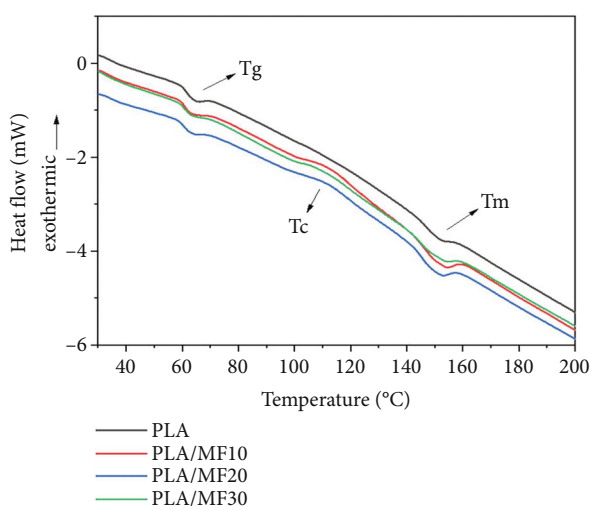

Figure 12: DSC curve of PLA/MF composite.

the sample is revealed by FTIR spectra. The PLA characteristic peaks, on the other hand, were found ranging in between 2800 cm^{-1} and 3000cm^{-1}, as show in Figure 9. The peaks at 2994 cm^{-1} correspond on O-H stretching to the carboxylic acid and 2944 cm^{-1} to the alkane's C-H stretching. The spectrum of the PLA/MF composite resembled that of Wisam et al. [64], with primary peaks almost identical in wavenumbers (2995 cm^{-1}, 2944 cm^{-1}, 1749 cm^{-1}, and 1184 cm^{-1}) [64].

The peak at 1746 cm^{-1} corresponds to the C=O stretching of lignin esters or lactone groups [65, 66], the peak at 1451 cm^{-1} corresponds to the C-H bending of cellulose and hemicellulose alkane or methyl groups, and the peak at 1180 cm^{-1} corresponds to the C-O stretching of aliphatic ether groups of hemicelluloses. The peak at 1042 cm^{-1} corresponds to the sulfoxide group's S=O stretching, while the peak at 755 cm^{-1} corresponds to the 1, 2-disubstituted group's C-H bending. The interaction between the PLA/MF in this study was primarily physical, as no significant peaks or obvious shifting were observed when compared to the neat PLA spectrum [67]. The major peaks of MF fiber were not observed in the fiber-reinforced PLA composites, possibly because they were covered by other strong PLA peaks, given that the amount of fiber was small in comparison to the PLA polymer matrix. The presence of these peaks at 1746 cm^{-1}, 1451 cm^{-1}, 1381 cm^{-1}, 1359 cm^{-1}, 1266cm^{-1}, 1180 cm^{-1}, 1127cm^{-1}, 1042 cm^{-1}, and 755 cm^{-1} indicated that the fiber had been introduced into the polymer matrix.

3.8. Thermogravimetric Analysis (TGA). TGA testing was used to investigate the thermal degradation of the PLA/MF composite. Figures 11(a) and 11(b) shows the mass lost at each stage as a function of temperature, with the residual mass at 600°C and its derivative mass analysis.

The first degradation showed a mild weight loss at less than 100°C for each sample due to moisture loss, as shown in Figure 10(b) [15, 70]. According to the FTIR results, as shown in Figures 11(a) and 11(b), the thermal degradation of the PLA/MF composite included complex reactions such as the breakage of C-H and C-O bonds [69].

Figure 11(a) illustrates a single step of transition occurred for plain PLA and PLA/MF composites. The single step was described as the decomposition of cellulose in PLA/

Table 7: DSC analysis of PLA/MF composites.

Samples	Tg (°C)	Tc (°C)	Tm (°C)
PLA	57.27	—	138.91
PLA/MF10	56.57	95.84	139.19
PLA/MF20	56.09	91.19	139.75
PLA/MF30	56.39	94.55	138.42

MF composite; a sharp transition occurred over a temperature range of 300°C to 400°C [40, 70]. The decomposition of PLA was a shift that occurred at the initial temperature of 330°C-360°C. As can be seen in Figure 11(a), the miswak fiber has an effect on the thermal stability of the composites as the step mainly occurred over a temperature range of 325°C to 350°C. Hence, the use of MF has resulted in a lower thermal degradation temperature and increase in residual value as shown in Table 6.

Maximum degradation is illustrated in Figure 11(b) and as final degradation temperature in Table 6. The composite decomposed quickly at 300°C to 400°C, as shown in Figure 11(b). Figure 11(b) also shows the thermal degradation on the PLA molecular chain caused the maximum decomposition rate peak around 360°C. Moreover, it was observed that there was no more mass loss after 400°C, indicating that the molecular chain had begun to carbonize at this point [68]. All PLA/MF composite maximum decomposition rate peak occurred around 300°C to 350°C. For the composition with high MF contents (30 wt. %), it seems obvious that the degradation is shifted to lower temperature. It indicates that the addition of MF had reduced the composite thermal stability as it was also found that MF's thermal degradation temperature (166°C) was found to be lower than PLA's (336°C) and could be one of the causes for lower thermal degradation temperature. The finding revealed that the addition of natural fiber affects the matrix by accelerating the thermal degradation of PLA as fiber contains a carbonyl group as observed in the FTIR test [71–73]. All of these observations further proved that the MF shows an effect on the thermal stability of the PLA matrix.

In addition to MF, the composites' initial degradation temperature has decreased slightly, and the composites' final thermal decomposition solid residue has increased, as shown in Table 6. The much high solid residue generated from hemicellulose and lignin contain in MF can be attributed to the charring, while the full decomposition of cellulose may be attributed to quick devolatilization reaction that led to very few solid residues left as such in PLA/MF10 [74]. Furthermore, the MF thermal decomposition solid residue was found to be 37% higher than PLA (0.86%). As a result, the thermal decomposition solid residue has increased, while the composite initial decomposition temperature decreased.

3.9. Differential Scanning Calorimetry (DSC). The thermal characteristics of plain PLA and PLA-based composites were characterized using DSC measurements. The thermograms that are produced are shown in Figure 12, and the numerical values are listed in Table 7. A melt-peak in the thermograms suggests the presence of crystalline domains.

All composites had comparable glass temperatures (Tg); however, they were somewhat lower than plain PLA. Molecular properties, compatibility, and composition all impact the glass transition temperature [75]. Glass transition temperature can also be influenced by poor compatibility with additional fiber [68]. As a result of the poor compatibility between the MF and PLA, the glass transition temperature was decreased. Tg of particulate packed polymers did not alter much as a result of the creation of a hard interphase because the surface area of micron-sized fiber particles is too small to induce large quantities of interphase to occur [76, 77].

In the DSC heating scans, all the PLA-based composites showed faint exothermic peaks just before the endotherm peak associated with melting is attributed to the crystallization [78]. However, no obvious crystallization peak was found for plain PLA. This indicates that the crystallization rate of PLA was very slow and temperature 90°C was too low to induce PLA crystallization within a short time due to low chain mobility. The MF/PLA composites however observed a faint exothermal peak from 90°C to 120°C as addition of fiber slightly induce PLA crystallization in composite.

Melting temperatures for PLA-based composites increased somewhat, suggesting that crystal sizes grew in the sequence MF30 < MF10 < MF20, as bigger crystals melt at higher temperatures than smaller crystallites [79]. Table 7 shows that the melting temperatures of pure PLA and PLA/MF composites are 138°C to 140°C, as illustrated in Figure 12. Spiridon et al. [79] discovered exothermic peaks in cellulose fiber/PLA samples using a similar DSC heating scan [79].

3.10. Dynamic Mechanical Analysis (DMA). The effect of MF loading on the viscoelastic properties of PLA composites was investigated using DMA. Figure 13 depicts the temperature dependence of dynamic mechanical properties, storage modulus in Figure 13(a), loss modulus in Figure 13(b), and tan δ in Figure 13(c) of PLA and MF/PLA composites.

The storage modulus, loss modulus, and tan delta curves as a function of temperature were examined using a dynamic mechanical analyzer at elevated temperatures. The viscoelastic behavior of materials can disclose the polymeric system's structure. PLA and all composite samples have a typical storage modulus curve illustrated in Figure 13(a), as found in semicrystalline polymers, with high storage modulus at low temperatures and a sharp decline at glass transition temperature, reaching the second plateau, which corresponds to the rubbery state. The storage modulus of all samples is provided in Table 8 at two distinct temperatures (above and below the glass transition temperature). PLA-based composites had a greater storage modulus in glassy areas than plain PLA, which is especially noticeable in composites with MF30 with 30 wt. % fiber content. Only MF30 had a slightly greater storage modulus in the rubbery state than pure PLA, indicating that PLA/MF composites had improved thermal-mechanical stability at extreme temperatures [80]. The improvement in storage modulus was characterized by the restricted polymer chain mobility because of the addition of lignocellulosic fiber. Similar behavior for PLA-based composites has been reported due to the incorporation of

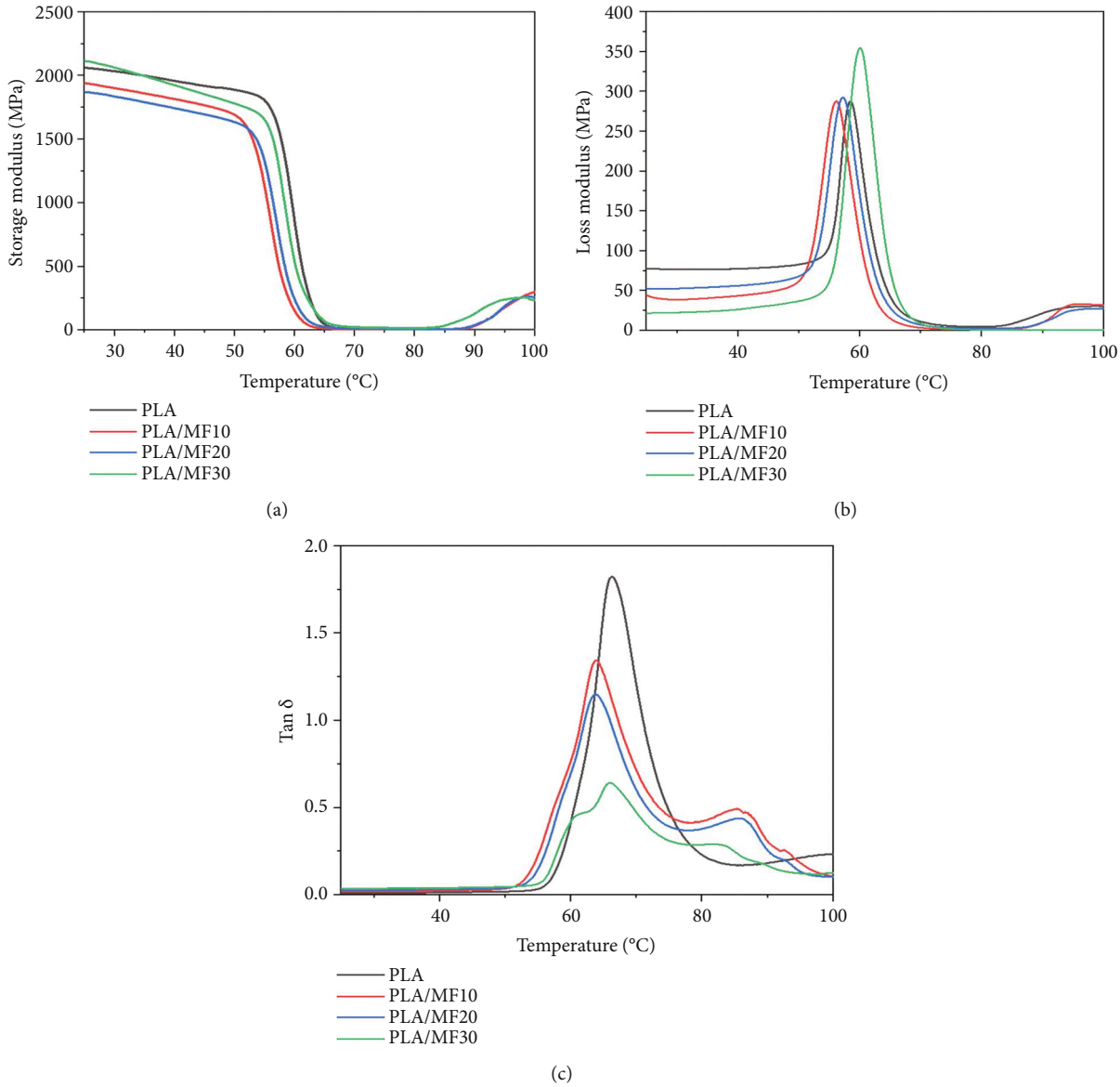

Figure 13: (a) Storage modulus curve of PLA/MF composites with different fiber loading (10 wt. %-30 wt. %). (b) Loss modulus curve of PLA/MF composites with different fiber loading (10 wt. %-30 wt. %). (c) Tan Delta curve of PLA/MF composites with different fiber loading (10 wt. %-30 wt. %).

Table 8: Storage modulus, loss modulus, and tan δ of PLA/MF composites.

Composites	Storage modulus (MPa)		Peak height of tan δ curve	Tg (°C) from tan δ curve	Tg (°C) from loss modulus curve
	30 °C	100 °C			
PLA	2034	4.35	1.8	66	60
MF10	1901	302.93	1.3	63	56
MF20	1835	260.08	1.1	63	57
MF30	2062	236.32	0.6	65	58

different concentration of lignocellulosic fiber into PLA matrix [80]. In glass transition region, it was observed that the E″ peak of PLA composite was higher than PLA/MF composites illustrated in Figure 13(b). The PLA/MF composites all had a similar level of E″ peak, showing that adding fiber into the polymer chain disrupts PLA chain movement, which is linked to the matrix chains' reduced mobility.

Table 9: Comparison mechanical properties of PLA/MF with thermoplastic based material.

Type of material	Tensile strength (MPa)	Young's modulus (GPa)	Flexural strength (MPa)	Flexural modulus (GPa)	Fabrications	Characteristics	Reference
PLA/MF	24-34	2-3	49-66	2-3.2	Melt mixing, compression molding	(i) High stiffness (ii) High flexural strength (iii) Lightweight	Present study
PLA	45-62	1.-2.8	63-79	2.8-3.7	Extrusion, injection molding	(i) High strength (ii) High stiffness (iii) Biodegradable	[99–101]
Recycled PLA	52-64	0.012-0.014	0.001-0.004	NA	Extrusion, 3D printing	(i) Drastic decrease in tensile after 9th recycle (ii) Good phase shape (iii) Low processing temperature	[102, 103]
PP	30-45	2-3	20-35	1-4	Rotating twin screw extruder	(i) Flexible (ii) Lightweight (iii) Toughness	[104–106]
Recycled PP	25-40	0.6-0.8	30-40	3-4	Rotating twin screw extruder	(i) Stiffer (ii) Brittle (iii) High bending	[105, 106]
Bamboo/PP	10-15	2-4	45-50	2-3.5	Melt mixing and compression molding	(i) Lightweight (ii) High flexural strength (iii) Hybrid has better tensile strength	[107, 108]
PE	15-17	2-3	19-20	1-2	Rotating twin screw extruder	(i) Chemical resistant (ii) Impact resistance (iii) Resist wear and fatigue	[107]
LDPE	10-15	0-1	20-30	0.3-0.4	Rotating twin screw extruder	(i) Toughness (ii) Flexible (iii) Lightweight	[83, 107]

The placement of the tan delta curve's peak value as the glass transition temperature of samples suggests that DSC measurements yielded similar glass transition temperatures. In Figure 13(b) after 60°C, the composite softened, the modulus began to decrease, and after 70°C, the composite was in a constant state due to α-relaxation of the amorphous regions in PLA [81]. Furthermore, the amplitude of the tan delta peak indicates the energy dissipation caused by the chain mobility of the polymer segments at the corresponding temperature as illustrated in Figure 13(c). The tan delta peak value was reduced when fillers were added to PLA, indicating stiffening action of fillers in composites. The peak value of tan delta in composites decreased as the fiber content of the composite increased. The lower tan delta peak values for PLA/MF30 composites compared to PLA/MF10 composites can be attributed to a greater interfacial connection between the MF and PLA matrix due to more uniform fiber dispersion as better fiber-matrix contact can constrain polymer chains, resulting in less energy loss [82]. This finding matches that of Shojaeiarani et al., who found decreased tan delta intensity in PLA-based composites reinforced with cellulose crystal [80].

4. Comparison of the Mechanical Characteristics of MF/PLA Composite with Thermoplastic-Based Materials

Most researchers utilize the ASTM D638 standard to assess the tensile characteristics and the ASTM D790 standard to determine the stiffness for the material used for dental applications like toothbrushes or biomedical applications like implants [46, 83–89].

The mechanical characteristics of PLA/MF composite are compared in Table 9 to materials that are often used to make biomedical, dental, or packaging products, such as PP, PE, TPE, recycled polymer, and bamboo-based PP composite material [88–95].

The table demonstrates that the majority of the tensile and flexural characteristics of PLA/MF are within the specified application's range. This demonstrates that adding MF to PLA polymer will not reduce the initial strength of the commercial polymer or PLA based composite; rather, it will only cause a decrease in PLA's properties, which could be brought on by a number of factors, including the strength of the fiber reinforcement, the processing environment, and the interfacial adhesion between the fiber and matrix.

Table 10: Challenge injection molders deals with PLA polymer.

Material	Challenge	Causes	Solution suggestion
PLA	Flow lines (patterns or lines appear on parts)	(i) Issue in varying flow rates as molten polymer moves through mold (ii) Changes in the thickness of the molds walls (iii) Injection speed to slow that cause molten polymer to solidify at different rates	✓ Increase the injection pressure and speeds to ensure cavities are filled evenly ✓ Increase temperature of the molten polymer or mold preventing polymer from quick cooling
	Sink marks (small depression in thicker areas of the injection molding after there is shrinkage in the finished product)	(i) Issue with pressure inside cavity (ii) Incorrect mechanism or cooling time	✓ Decrease mold temperature ✓ Allow polymer to cool and cure longer inside the mold
	Vacuum voids (air pockets trapped inside an injection molded part)	(i) Insufficient holding pressure that led to molten plastic to condense inside the mold	✓ Use less viscous polymer to avoid trapping gas ✓ Increase holding pressure and time
	Warping (finished part are uneven in areas)	(i) Nonuniform cooling or varying cooling rates inside mold	✓ Cooling process are not rushed in term of time and speed

∗ Source from http://www.iconnsystems.com and http://www.rtpcompany.com/technical-info.

Owing to the near resemblances in strength and stiffness as shown in Table 9, it is evident that employing MF might be more advantageous than using a conventional polymer, but modifications and more study are required to attain the necessary features and characteristics.

Additionally, PLA is one of the least expensive materials available for composite materials of biomedical or packaging, and it also has some of the finest tensile and flexural qualities among other thermoplastics [94, 96, 97]. There is a good likelihood that the material will come into contact with moisture and water while the toothbrush is being made. Injection molding is often used in the production of toothbrushes. This procedure entailed creating a mold in the shape of a toothbrush, injecting molten plastic into the mold using a hot channel nozzle, cooling the plastic, and ejecting it from the mold [98].

Currently, this procedure requires comprehension of the fundamentals of injection molding, where material choice is frequently reliant on knowledge of the maximum short-use temperature, the melt flow, and the relation between stress and temperature [109]. Therefore, in order to use the injection molding method, it is crucial to comprehend not only the mechanical side of the material but also its thermal stability. Thermoplastic materials including PP, PE, ABS, PA, and PMMA are often utilized in injection molding [109].

Bioplastic has previously caused problems for injection molders since the materials were pricey and incompatible with existing machinery. However, PLA's characteristics might make it well suited for some applications while necessitating changes for others [92, 110].

4.1. Injection Molding and PLA. We compared the mechanical properties of the current PLA/MF composites with those of a commercial material that is currently widely used in making toothbrush handles as shown in Table 9 because one of the objectives of this study was to develop composite materials containing miswak, which is renowned for its antibacterial properties, to be potentially feasible for application similar to toothbrush handle. Understanding the optimal injection molding settings for polylactic acid (PLA)-based compounds is crucial to obtaining the best performance out of the materials [109]. PLA is a semicrystalline polyester thermoplastic. Since polyester is prone to hydrolysis, molders must take special care to ensure that the material is dry before molding. By adjusting the molding conditions, PLA may be molded similarly to other semicrystalline polyester. Thermoplastic PLA rapidly absorbs water from the atmosphere because it is hygroscopic. Even a minor quantity of moisture will hydrolyze PLA in the melt phase, causing molecular weight to drop and characteristics to be lost [79, 89, 111]. Table 10 shows factor or challenge that occurs when polymers are molded using the injection process.

Since PLA is costly, has inferior water barrier qualities to more common thermoplastics like PP, and has low heat stability, it is not utilized to produce toothbrushes [71, 110, 112–114]. However, great attempts have been made to alter PLA's performance to increase its temperature tolerance and mechanical strength as well as to adapt it to increase its uses in high-end markets [72, 110, 114–118].

The slower PLA crystallization time, which is reflected in longer molding cycles compared to commercial fossil-based polymers, is a disadvantage for the PLA injection molding application. PLA could not be injected into molds at ambient temperature, which is the norm for fossil-based polymers, since the resultant material is amorphous and has a poor storage modulus, especially at temperatures higher than its glass transition temperature. This complicates the PLA injection molding process [119, 120]. The proper mold temperature and cycle duration must be attained in order to crystallize PLA during injection molding. However, the PLA crystallization rate must be hastened throughout the process to decrease the additional cost brought on by the usage of hot molds and the lengthened time cycle. In the past, studies have looked at a variety of methods, including plasticization, nucleation, and physical blending with other polymers, in order to quickly obtain high PLA crystallinity [119,

Table 11: Characteristic of PLA based material by using injection molding.

Material	Approach	Application	Fabrication	Characteristics	Ref
PLA/sisal fiber	Reinforcement fiber	Bio composites material	Direct- injection molding	✓ High tensile modulus ✓ High flexural modulus ✓ Better impact properties	[126]
PLA/nucleating agents (LAK, talc, calcium carbonate)	Nucleating agents	Commercial application	Extrusion and injection molding	✓ Improving heat deflection ✓ Temperature with crystallinity ✓ Percentage above 50%. ✓ Increase flexural modulus ✓ Lower impact resistance	[127]
PLA/nucleating agents (talc, ethylenebis-stearamide (EBS))	Nucleating agents		Extrusion and injection molding	✓ Improve strength and modulus ✓ Increase heat distortion temperature ✓ Decreased processing time increase crystallinity level	[121]
PLA-based bone screws	Reinforcement nanoparticles	Biomedical application	Injection molding	✓ High loads resistance ✓ Increase shrinkage with melt temperature increase ✓ Increase warpage with packing time decrease	[128]
PLA/TPU	Hybrid polymer		Extrusion and injection molding	✓ Large range of mechanical properties ✓ Improve microstructure ✓ Improve surface roughness	[129]
PLA/hydroxyapatite (HA)	Surface modification of HA	Good load bearing applications	Extrusion and injection molding	✓ Improved thermal properties ✓ Improved tensile and impact properties ✓ Reduction damping factor	[130]
PLA/jute	Reinforcement fiber	Fully environmentally friendly material (FEFM)	Pultrusion process and injection molding	✓ Increase deflection temperature under load ✓ Increase tensile modulus ✓ Increase Izod strength	[131]

121–124]. The nucleation method is particularly appealing since it may reduce the injection molding time while barely impacting PLA stiffness and strength. Additionally, it was claimed that the nucleation technique is adaptable since it is simple to apply during extrusion and that a variety of nucleating chemicals are readily available [125]. The method for enhancing PLA characteristics by injection molding is shown in Table 11.

PLA is by far the most significant and promising bio-based and biodegradable plastic for solid applications. Even though PLA has received a lot of scientific attention, it has mostly been used in biomedical and packaging applications. The manufacturing cost of PLA will drop dramatically at industrial sizes due to a growing awareness of environmental contamination and advancements in production technology, and PLA-based composites will hold great promise for the future of the material business.

5. Conclusion and Future Scopes

Miswak fiber (MF)-reinforced PLA composites with different fiber loading were successfully prepared by melt blending. These studies have looked into how MF affects morphologies, physical characteristics, mechanical properties, and thermal attributes. The research has proved that increasing the amount of MF slightly lowered the tensile and flexural strength and modulus of PLA/MF composites. The results might have been impacted by void presence, porosity, fiber orientation, and inadequate interfacial adhesion between the fiber and matrix composite. In addition, fiber's low adhesion profile—caused by a smaller proportion of cellulosic components and a higher proportion of hemicellulose and extractives on the fiber surface—prevents it from effectively binding with the matrix. This study discovered a nonlinear response to density increments of 10 wt. % fibers. The addition of MF increases the storage modulus in the low temperature region, which is associated with lower α-relaxation, as compared to PLA. According to DSC's TGA study, the composites' initial thermal degradation temperature has dropped considerably, while their final thermal decomposition residual ratio has risen steadily. This is as a result of MF's lower thermal decomposition temperature compared to PLA's. Also, with fabrication of the PLA/MF composite, the study's objective was accomplished, and the material's characteristics in terms of its physical, mechanical, and thermal capabilities were investigated. In the future, the

studies intend to examine the whole range of how various processing conditions—including those related to time and temperature—affect the mechanical and thermal characteristics of composite materials. Additionally, fiber processing parameters, fiber orientation, and fiber particle size can all be taken into account as variables that affect the features of the composite. In addition, fiber treatment or compatibilizing agents are considered in the endeavor to enhance the qualities of PLA/MF composites, as their effect on antibacterial and biocompatibility of the composites is still needed for research as to utilize and explored the efficacy and usefulness of miswak plant for diverse application.

Data Availability

The analysis data used to support the findings of this study are included within the article.

Conflicts of Interest

The authors declare no conflict of interest.

Authors' Contributions

Conceptualization was performed by Khalina A.; methodology was contributed by Nur Diyana A.F.; validation was performed by Sapuan M.S.; formal analysis was performed by Nurazzi M.N.; investigation was performed by Aisyah H.A.; resources was contributed by Nur Diyana A.F.; data curation was performed by Nur Diyana A.F.; writing—original draft preparation was contributed by Nur Diyana A.F.; writing—review and editing was contributed by Lee C.H.; supervision was performed by Khalina A. All authors have read and agreed to the published version of the manuscript.

Acknowledgments

The authors extend their gratitude to the Ministry of Higher Education for providing HICOE Grant No: 6369109 to INTROP, Universiti Putra Malaysia (UPM) and for supporting this research work.

References

[1] M. A. P. de Carvalho, F. M. Flório, S. A. dos Santos Pereira, A. C. A. Martin, E. J. C. Silveira, and E. Saba-Chujfi, "Efficacy of two different toothbrushes on plaque control: a randomized clinical study," *PesquisaBrasileira em Odontopediatria e Clínica Integrada*, vol. 19, no. 1, article e4305, pp. 1–12, 2019.

[2] S. Akifusa, A. Isobe, K. Kibata et al., "Comparison of dental plaque reduction after use of electric toothbrushes with and without QLF-D-applied plaque visualization: a 1-week randomized controlled trial," *BMC Oral Health*, vol. 20, no. 1, p. 4, 2020.

[3] B. Alejandra, "How your toothbrush became a part of the plastic crisis," *National Geographic*, 2019, http://www.nationalgeographic.com/environment/article/story-of-plastic-toothbrushes.

[4] A. Moeintaghavi, N. Sargolzaie, M. Rostampour, S. Sarvari, S. Kargozar, and S. Gharaei, "Comparison of three types of tooth brushes on plaque and gingival indices: a randomized clinical trial," *The Open Dentistry Journal*, vol. 11, no. 1, pp. 126–132, 2017.

[5] N. Aggarwal, S. Gupta, R. Grover, G. Sadana, and K. Bansal, "Plaque removal efficacy of different toothbrushes: a comparative study," *International Journal of Clinical Pediatric Dentistry*, vol. 12, no. 5, pp. 385–390, 2019.

[6] L. Tammy, "Finally a toothbrush with plant-based," 2018, http://gippslandunwrapped.com/2018/06/24/finally-a-toothbrush-with-plant-based-biodegradable-bristles/.

[7] S. Farah, D. G. Anderson, and R. Langer, "Physical and mechanical properties of PLA, and their functions in widespread applications — a comprehensive review," *Advanced Drug Delivery Reviews*, vol. 107, pp. 367–392, 2016.

[8] Y. Huang, T. Wang, X. Zhao et al., "Poly(lactic acid)/graphene oxide-ZnO nanocomposite films with good mechanical, dynamic mechanical, anti-UV and antibacterial properties," *Journal of Chemical Technology & Biotechnology*, vol. 90, no. 9, pp. 1677–1684, 2015.

[9] P. Saini, M. Arora, and M. N. V. R. Kumar, "Poly(lactic acid) blends in biomedical applications," *Advanced Drug Delivery Reviews*, vol. 107, pp. 47–59, 2016.

[10] M. Nofar, D. Sacligil, P. J. Carreau, M. R. Kamal, and M.-C. Heuzey, "Poly (lactic acid) blends: processing, properties and applications," *International Journal of Biological Macromolecules*, vol. 125, pp. 307–360, 2019.

[11] J.-M. Raquez, Y. Habibi, M. Murariu, and P. Dubois, "Polylactide (PLA)-based nanocomposites," *Progress in Polymer Science*, vol. 38, no. 10-11, pp. 1504–1542, 2013.

[12] H. A. Aisyah, M. T. Paridah, A. Khalina et al., "Effects of fabric counts and weave designs on the properties of laminated woven kenaf/carbon fibre reinforced epoxy hybrid composites," *Polymers*, vol. 10, no. 12, p. 1320, 2018.

[13] C. H. Lee, M. S. Salit, and M. R. Hassan, "A review of the flammability factors of kenaf and allied fiber reinforced polymer composites," *Advances in Materials Science and Engineering*, vol. 2014, Article ID 514036, 8 pages, 2014.

[14] C. H. Lee, S. M. Sapuan, and M. R. Hassan, "Mechanical and thermal properties of kenaf fiber reinforced polypropylene/magnesium hydroxide composites," *Journal of Engineered Fibers and Fabrics*, vol. 12, no. 2, p. 155892501701200, 2017.

[15] C. H. Lee, S. M. Sapuan, and M. R. Hassan, "Thermal analysis of kenaf fiber reinforced floreon biocomposites with magnesium hydroxide flame retardant filler," *Polymer Composites*, vol. 39, no. 3, pp. 869–875, 2018.

[16] C. H. Lee, S. M. Sapuan, J. H. Lee, and M. R. Hassan, "Melt volume flow rate and melt flow rate of kenaf fibre reinforced Floreon/magnesium hydroxide biocomposites," *Springerplus*, vol. 5, no. 1, p. 1680, 2016.

[17] M. Murariu and P. Dubois, "PLA composites: from production to properties," *Advanced Drug Delivery Reviews*, vol. 107, pp. 17–46, 2016.

[18] M. R. Manshor, H. Anuar, M. N. Aimi et al., "Mechanical, thermal and morphological properties of durian skin fibre reinforced PLA biocomposites," *Materials & Design*, vol. 59, pp. 279–286, 2014.

[19] P. Bajpai, I. Singh, and J. Madaan, "Tribological behavior of natural fiber reinforced PLA Composites," *Wear*, vol. 297, no. 1-2, pp. 829–840, 2013.

[20] K. Oksman, M. Skrifvars, and J. F. Selin, "Natural fibres as reinforcement in polylactic acid (PLA) composites,"

Composites Science and Technology, vol. 63, no. 9, pp. 1317–1324, 2003.

[21] T. Nishino, K. Hirao, M. Kotera, K. Nakamae, and H. Inagaki, "Kenaf reinforced biodegradable composite," *Composites Science and Technology*, vol. 63, no. 9, pp. 1281–1286, 2003.

[22] C. Wu, I. Darout, and N. Skaug, "Chewing sticks: timeless natural toothbrushes for oral cleansing," *Journal of Periodontal Research*, vol. 36, no. 5, pp. 275–284, 2001.

[23] R. Bairwa, P. Gupta, V. K. Gupta, and B. Srivastava, "Traditional medicinal plants: use in oral hygiene," *International Journal of Pharmacy and Pharmaceutical Sciences*, vol. 1, no. 4, pp. 1529–1538, 2012.

[24] I. A. S. Ra'ed and A. M. Khalid, "Miswak [chewing stick]: a cultural and scientific Heritage," 1999.

[25] F. Niazi, M. Naseem, Z. Khurshid, M. S. Zafar, and K. Almas, "Role of Salvadora persica chewing stick (miswak): a natural toothbrush for holistic oral health," *European Journal of Dentistry*, vol. 10, no. 2, pp. 301–308, 2016.

[26] H. Ramli, T. N. Mohd-Dom, and S. Mohd-Said, "Clinical benefits and adverse effects of siwak (S. persica) use on periodontal health: a scoping review of literature," *BMC Oral Health*, vol. 21, no. 1, p. 618, 2021.

[27] M. Aumeeruddy, G. Zengin, and F. Mahomoodally, "A review of the traditional and modern uses of Salvadora persica L. (Miswak): toothbrush tree of Prophet Muhammad," *Journal of Ethnopharmacology*, vol. 213, pp. 409–444, 2017.

[28] T. Al-Khateeb, D. M. O'mullane, H. Whelton, and M. I. Sulaiman, "Periodontal treatment needs among Saudi Arabian adults and their relationship to the use of the miswak," *Community Dental Health*, vol. 8, no. 4, pp. 323–328, 1991.

[29] M. Abhary and A.-A. Al-Hazmi, "Antibacterial activity of Miswak (Salvadora persica L.) extracts on oral hygiene," *Journal of Taibah University for Science*, vol. 10, no. 4, pp. 513–520, 2016.

[30] L. E. Wise, M. Murphy, and A. D'Addieco, "Chlorite holocellulose, its fractionation and bearing on summative wood analysis and studies on the hemicelluloses," *Paper Trade Journal*, vol. 122, pp. 35–43, 1946.

[31] I. Tawakkal, R. A. Talib, K. Abdan, and C. N. Ling, "Mechanical and physical properties of kenaf-derived cellulose (KDC)-filled polylactic acid (PLA) composites," *BioResources*, vol. 7, no. 2, pp. 1643–1655, 2012.

[32] R. Siakeng, M. Jawaid, H. Ariffin, S. Sapuan, M. Asim, and N. Saba, "Natural fibre reinforced polylactic acid composites: a review," *Polymer Composites*, vol. 40, 2018.

[33] T. Shahzadi, S. Mehmood, M. Irshad et al., "Advances in lignocellulosic biotechnology: a brief review on lignocellulosic biomass and cellulases," *Advances in Bioscience and Biotechnology*, vol. 5, no. 3, pp. 246–251, 2014.

[34] R. C. Pettersen, "The chemical composition of wood," *Advances in Chemistry*, vol. 207, 126 pages, 1984.

[35] C. K. Ruffo, A. Birnie, and B. Tengnas, "Edible wild plants of Tanzania," 2002, http://tropical.theferns.info/viewtropical.php?id=Salvadora+persica (regional land management unit; Nairobi).

[36] ASTMD1103, *Method of Test for Alpha-Cellulose in Wood*, ASTM International (ASTM), 60th Edition edition, 1977.

[37] M. Sood and G. Dwivedi, "Effect of fiber treatment on flexural properties of natural fiber reinforced composites: a review," *Egyptian Journal of Petroleum*, vol. 27, no. 4, pp. 775–783, 2018.

[38] M. H. Mohd Roslim, S. Sapuan, Z. Leman, and M. Ishak, "Comparative study on chemical composition, physical, tensile, and thermal properties of sugar palm fiber (Arenga pinnata) obtained from different geographical locations," *BioResources*, vol. 12, pp. 9366–9382, 2017.

[39] Y. Millogo, J.-E. Aubert, A. D. Séré, A. Fabbri, and J.-C. Morel, "Earth blocks stabilized by cow-dung," *Materials and Structures*, vol. 49, no. 11, pp. 4583–4594, 2016.

[40] M. R. Ishak, S. M. Sapuan, Z. Leman, M. Z. A. Rahman, and U. M. K. Anwar, "Characterization of sugar palm (Arenga pinnata) fibres," *Journal of Thermal Analysis and Calorimetry*, vol. 109, no. 2, pp. 981–989, 2012.

[41] R. S. Ayu, A. Khalina, A. S. Harmaen et al., "Effect of Empty Fruit Brunch reinforcement in PolyButylene- Succinate/Modified Tapioca Starch blend for Agricultural Mulch Films," *Scientific Reports*, vol. 10, no. 1, p. 1166, 2020.

[42] R. Haque, M. Saxena, S. C. Shit, and P. Asokan, "Fibre-matrix adhesion and properties evaluation of sisal polymer composite," *Fibers and Polymers*, vol. 16, no. 1, pp. 146–152, 2015.

[43] A. M. Radzi, S. Sapuan, M. Jawaid, and M. R. Mansor, "Water absorption, thickness swelling and thermal properties of roselle/sugar palm fibre reinforced thermoplastic polyurethane hybrid composites," *Journal of Materials Research and Technology*, vol. 8, no. 5, pp. 3988–3994, 2019.

[44] S. Savaş, "Structural properties and mechanical performance of Salvadora persica L. (Miswak) reinforced polypropylene composites," *Polymer Composites*, vol. 40, 2018.

[45] T. Alomayri, H. Assaedi, F. U. A. Shaikh, and I. M. Low, "Effect of water absorption on the mechanical properties of cotton fabric-reinforced geopolymer composites," *Journal of Asian Ceramic Societies*, vol. 2, no. 3, pp. 223–230, 2014.

[46] M. Mehdikhani, L. Gorbatikh, I. Verpoest, and S. V. Lomov, "Voids in fiber-reinforced polymer composites: a review on their formation, characteristics, and effects on mechanical performance," *Journal of Composite Materials*, vol. 53, no. 12, pp. 1579–1669, 2018.

[47] N. Z. Zuhudi, A. F. Zulkifli, M. Zulkifli, A. N. Yahaya, N. M. Nur, and K. D. Aris, "Void and moisture content of fiber reinforced composites," *Journal of Advanced Research in Fluid Mechanics and Thermal Sciences*, vol. 87, no. 3, pp. 78–93, 2021.

[48] A. Atiqah, M. Jawaid, S. M. Sapuan, M. R. Ishak, M. N. M. Ansari, and R. A. Ilyas, "Physical and thermal properties of treated sugar palm/glass fibre reinforced thermoplastic polyurethane hybrid composites," *Journal of Materials Research and Technology*, vol. 8, no. 5, pp. 3726–3732, 2019.

[49] K. E. Mazur, A. Borucka, P. Kaczor et al., "Mechanical, thermal and microstructural characteristic of 3D printed polylactide composites with natural fibers: wood, bamboo and cork," *Journal of Polymers and the Environment*, vol. 30, no. 6, pp. 2341–2354, 2021.

[50] K. Pongtanayut, C. Thongpin, and O. Santawitee, "The effect of rubber on morphology, thermal properties and mechanical properties of PLA/NR and PLA/ENR blends," *Energy Procedia*, vol. 34, pp. 888–897, 2013.

[51] S. Zhang, S. Bhagia, M. Li, X. Meng, and A. J. Ragauskas, "Wood-reinforced composites by stereolithography with the stress whitening behavior," *Materials & Design*, vol. 206, 2021.

[52] S. F. K. Sherwani, E. S. Zainudin, S. M. Sapuan, Z. Leman, and A. Khalina, "Physical, mechanical, and morphological

properties of treated sugar palm/glass reinforced poly(lactic acid) hybrid composites," *Polymers*, vol. 13, no. 21, 2021.

[53] M. Morreale, R. Scaffaro, A. Maio, and F. P. La Mantia, "Effect of adding wood flour to the physical properties of a biodegradable polymer," *Composites Part A: Applied Science and Manufacturing*, vol. 39, no. 3, pp. 503–513, 2008.

[54] M. Kodal, H. Sirin, and G. Ozkoc, "Effects of reactive and nonreactive POSS types on the mechanical, thermal, and morphological properties of plasticized poly(lactic acid)," *Polymer Engineering & Science*, vol. 54, pp. 264–275, 2014.

[55] W. N. R. W. Jaafar, S. N. Surip, and N. N. Azmi, "Effect of Screw Rotation Speed on Mechanical Properties of Extruded PLA/Kenaf Nanocomposites," *Advanced Materials Research*, vol. 748, pp. 61–64, 2013.

[56] C. Venkatesh, E. Fuenmayor, P. Doran, I. Major, J. Lyons, and D. Devine, "Additive manufacturing of PLA/HNT nanocomposites for biomedical applications," *Procedia Manufacturing*, vol. 38, pp. 17–24, 2019.

[57] J. Gálvez, J. P. Correa Aguirre, M. A. Hidalgo Salazar, B. Vera Mondragón, E. Wagner, and C. Caicedo, "Effect of Extrusion Screw Speed and Plasticizer Proportions on the Rheological, Thermal, Mechanical, Morphological and Superficial Properties of PLA," *Polymers*, vol. 12, p. 2111, 2020.

[58] A. Rubio-Lopez, A. Olmedo, A. Díaz-Álvarez, and C. Santiuste, "Manufacture of compression moulded PLA based biocomposites: A parametric study," *Composite Structures*, vol. 131, pp. 995–1000, 2015.

[59] M. Bernard, A. Khalina, A. Ali et al., "The effect of processing parameters on the mechanical properties of kenaf fibre plastic composite," *Materials & Design*, vol. 32, pp. 1039–1043, 2011.

[60] G.-H. Doh, I.-A. Kang, S.-Y. Lee, Y.-T. Kong, C.-S. Jeong, and B.-S. Lim, "Mechanical properties and creep behavior of liquefied wood polymer composites (LWPC)," *Composite Structures*, vol. 68, no. 2, pp. 225–233, 2005.

[61] M. E. Golmakani, T. Wiczenbach, M. Malikan, S. M. Mahoori, and V. A. Eremeyev, "Experimental and numerical investigation of tensile and flexural behavior of nanoclay wood-plastic composite," *Materials*, vol. 14, no. 11, p. 2773, 2021.

[62] R. B. Yusoff, H. Takagi, and A. N. Nakagaito, "Tensile and flexural properties of polylactic acid-based hybrid green composites reinforced by kenaf, bamboo and coir fibers," *Industrial Crops and Products*, vol. 94, pp. 562–573, 2016.

[63] Y. Yee, C. Yern Chee, S. Rozali, N. Hashim, and R. Singh, "Preparation and characterization of poly(lactic acid)-based composite reinforced with oil palm empty fruit bunch fiber and nanosilica," *BioResources*, vol. 11, 2016.

[64] W. H. Hoidy, M. B. Ahmad, E. A. Jaffar Al-Mulla, and N. A. B. Ibrahim, "Preparation and characterization of polylactic acid/polycaprolactone clay nanocomposites," *Journal of Applied Sciences*, vol. 10, no. 2, pp. 97–106, 2010.

[65] Y. C. Ching, A. Rahman, K. Y. Ching, N. L. Sukiman, and H. C. Cheng, "Preparation and characterization of polyvinyl alcohol-based composite reinforced with nanocellulose and nanosilica," *BioResources*, vol. 10, no. 2, pp. 3364–3377, 2015.

[66] T. S. Ng, Y. C. Ching, N. Awanis, N. Ishenny, and M. R. Rahman, "Effect of bleaching condition on thermal properties and UV transmittance of PVA/cellulose biocomposites," *Materials Research Innovations*, vol. 18, no. sup6, pp. S6-400–S6-404, 2014.

[67] P. Qu, H. Tang, Y. Gao, L. Zhang, and S. Wang, "Polyethersulfone composite membrane blended with cellulose fibrils," *BioResources*, vol. 5, no. 4, pp. 2323–2336, 2010.

[68] S. Lee, I. Kang, G. Doh, H. Yoon, B. Park, and W. Qinglin, "Thermal and mechanical properties of wood flour/talc-filled polylactic acid composites: effect of filler content and coupling treatment," *Journal of Thermoplastic Composite Materials*, vol. 21, no. 3, pp. 209–223, 2008.

[69] R. S. Ayu, A. Khalina, A. S. Harmaen, K. Zaman, M. Jawaid, and C. H. Lee, "Effect of modified tapioca starch on mechanical, thermal, and morphological properties of pbs blends for food packaging," *Polymers*, vol. 10, no. 11, p. 1187, 2018.

[70] J. M. F. de Paiva and E. Frollini, "Unmodified and modified surface sisal fibers as reinforcement of phenolic and lignophenolic matrices composites: thermal analyses of fibers and composites," *Macromolecular Materials and Engineering*, vol. 291, no. 4, pp. 405–417, 2006.

[71] A. A. Cuadri and J. E. Martin-Alfonso, "Thermal, thermo-oxidative and thermomechanical degradation of PLA: a comparative study based on rheological, chemical and thermal properties," *Polymer Degradation and Stability*, vol. 150, pp. 37–45, 2018.

[72] G. Wang, D. Zhang, G. Wan, B. Li, and G. Zhao, "Glass fiber reinforced PLA composite with enhanced mechanical properties, thermal behavior, and foaming ability," *Polymer*, vol. 181, p. 121803, 2019.

[73] M. Oliveira, E. Santos, A. Araújo, G. J. M. Fechine, A. V. Machado, and G. Botelho, "The role of shear and stabilizer on PLA degradation," *Polymer Testing*, vol. 51, pp. 109–116, 2016.

[74] H. Yang, R. Yan, H. Chen, D. H. Lee, and C. Zheng, "Characteristics of hemicellulose, cellulose and lignin pyrolysis," *Fuel*, vol. 86, no. 12-13, pp. 1781–1788, 2007.

[75] H. J. Chung, E. J. Lee, and S. T. Lim, "Comparison in glass transition and enthalpy relaxation between native and gelatinized rice starches," *Carbohydrate Polymers*, vol. 48, no. 3, pp. 287–298, 2002.

[76] C. DeArmitt, "23 - functional fillers for plastics," in *Applied Plastics Engineering Handbook (Second Edition)*, M. Kutz, Ed., pp. 517–532, William Andrew Publishing, 2017.

[77] K. Molnár, J. Moczo, M. Murariu, and P. Dubois, "Factors affecting the properties of PLA/CaSO4 composites: homogeneity and interactions," *Express Polymer Letters*, vol. 3, no. 1, pp. 49–61, 2009.

[78] M. Pluta, M.-A. Paul, M. Alexandre, and P. Dubois, "Plasticized polylactide/clay nanocomposites. I. The role of filler content and its surface organo-modification on the physicochemical properties," *Journal of Polymer Science Part B: Polymer Physics*, vol. 44, no. 2, pp. 299–311, 2006.

[79] I. Spiridon, R. N. Darie, and H. Kangas, "Influence of fiber modifications on PLA/fiber composites. Behavior to accelerated weathering," *Composites Part B: Engineering*, vol. 92, pp. 19–27, 2016.

[80] J. Shojaeiarani, D. Bajwa, and K. Hartman, "Esterified cellulose nanocrystals as reinforcement in poly(lactic acid) nanocomposites," *Cellulose*, vol. 26, no. 4, pp. 2349–2362, 2019.

[81] A. Mathew, K. Oksman, and M. Sain, "The effect of morphology and chemical characteristics of cellulose reinforcements on the crystallinity of polylactic acid," *Journal of Applied Polymer Science*, vol. 101, no. 1, pp. 300–310, 2006.

[82] T. Yu, J. Ren, S. Li, H. Yuan, and Y. Li, "Effect of fiber surface-treatments on the properties of poly(lactic acid)/ramie

composites," *Composites Part A: Applied Science and Manufacturing*, vol. 41, no. 4, pp. 499–505, 2010.

[83] F. M. Al-Oqla, "Flexural characteristics and impact rupture stress investigations of sustainable green olive leaves biocomposite materials," *Journal of Polymers and the Environment*, vol. 29, no. 3, pp. 892–899, 2020.

[84] R. Chaaben, R. Taktak, B. Mnif, N. Guermazi, and K. Elleuch, "Innovative biocomposite development based on the incorporation of Salvadora persicain acrylic resin for dental material," *Journal of Thermoplastic Composite Materials*, p. 089270572093916, 2020.

[85] K. Cho, G. Rajan, P. Farrar, L. Prentice, and B. Gangadhara Prusty, "Dental resin composites: A review on materials to product realizations," *Composites Part B: Engineering*, vol. 230, article 109495, 2022.

[86] R. H. Morris, C. L. Trabi, A. Spicer et al., "A natural fibre reinforced composite material for multi-modal medical imaging and radiotherapy treatment," *Materials Letters*, vol. 252, pp. 289–292, 2019.

[87] S.-B. Park, E. Lih, K.-S. Park, Y. K. Joung, and D. K. Han, "Biopolymer-based functional composites for medical applications," *Progress in Polymer Science*, vol. 68, pp. 77–105, 2017.

[88] J. E. Puskas and Y. Chen, "Biomedical application of commercial polymers and novel polyisobutylene-based thermoplastic elastomers for soft tissue replacement," *Biomacromolecules*, vol. 5, no. 4, pp. 1141–1154, 2004.

[89] R. P. Pawar, S. U. Tekale, S. U. Shisodia, J. T. Totre, and A. J. Domb, "Biomedical applications of poly(lactic acid)," *Recent Patents on Regenerative Medicine*, vol. 4, no. 1, pp. 40–51, 2014.

[90] S. Basak, "Thermoplastic elastomers in biomedical industry – evolution and current trends," *Journal of Macromolecular Science, Part A*, vol. 58, no. 9, pp. 579–593, 2021.

[91] T. Casalini, F. Rossi, A. Castrovinci, and G. Perale, "A perspective on polylactic acid-based polymers use for nanoparticles synthesis and applications," *Frontiers in Bioengineering and Biotechnology*, vol. 7, p. 259, 2019.

[92] V. DeStefano, S. Khan, and A. Tabada, "Applications of PLA in modern medicine," *Engineered Regeneration*, vol. 1, pp. 76–87, 2020.

[93] K. S. Sharath Kumar, Y. R. Girish, M. Ashrafizadeh et al., "AIE-featured tetraphenylethylene nanoarchitectures in biomedical application: bioimaging, drug delivery and disease treatment," *Coordination Chemistry Reviews*, vol. 447, p. 214135, 2021.

[94] B. D. Ulery, L. S. Nair, and C. T. Laurencin, "Biomedical applications of biodegradable polymers," *Journal of Polymer Science Part B: Polymer Physics*, vol. 49, no. 12, pp. 832–864, 2011.

[95] S. Wendels and L. Avérous, "Biobased polyurethanes for biomedical applications," *Bioactive Materials*, vol. 6, no. 4, pp. 1083–1106, 2021.

[96] L. Xiao, B. Wang, G. Yang, and M. Gauthier, "Poly(lactic acid)-based biomaterials: synthesis, modification and applications," *Biomedical Science, Engineering and Technology*, vol. 11, 2012.

[97] J. Xu and J. Song, "Polylactic acid (PLA)-based shape-memory materials for biomedical applications," *Shape Memory Polymers for Biomedical Applications*, vol. 197-217, 2015.

[98] L. M. Morawski, "Process for manufacturing a toothbrush," 2006, https://patents.google.com/patent/US7118364B2/en.

[99] S. Budin, N. C. Maideen, M. H. Koay, D. Ibrahim, and H. Yusoff, "A comparison study on mechanical properties of virgin and recycled polylactic acid (PLA)," *Journal of Physics: Conference Series*, vol. 1349, article 012002, 2019.

[100] B. Asaithambi, G. S. Ganesan, and A. K. Srinivasan, "Biocomposites: Development and Mechanical Characterization of Banana/Sisal Fibre Reinforced Poly Lactic Acid (PLA) Hybrid Composites," *Fibers and Polymers*, vol. 15, 2013.

[101] K. S. Sangeetha, S. Umamaheswari, C. U. M. Reddy, and S. N. Kalkura, "Flavonoids: Therapeutic potential of natural pharmacological agents," *International Journal of pharmaceutical sciences and research*, vol. 7, no. 10, p. 3924, 2016.

[102] M. Syaifuddin, H. Suryanto, and S. Suprayitno, "The Effect of Multi-Extrusion Process of Polylactic Acid on Tensile Strength and Fracture Morphology of Filament Product," *Journal of Mechanical Engineering Science and Technology*, vol. 5, no. 1, pp. 62–72, 2021.

[103] R. S. K. M. Babagowda, R. Goutham, and K. R. S. Prasad, "Study of Effects on Mechanical Properties of PLA Filament which is blended with Recycled PLA Materials," *IOP Conference Series: Materials Science and Engineering*, vol. 310, article 012103, 2018.

[104] I. Onuoha, N. Kamarudin, G. Aliagha, S. A. Okeahialam, M. I. Atilola, and F. Atamamen, "Developing Policies and Programmes for Green Buildings: What can Nigeria Learn from Malaysia's Experience?," *International Journal of Real Estate Studies*, vol. 11, no. 2, pp. 49–58, 2017.

[105] Y. Shi, Y. H. Chen, X. J. Yin et al., "Electroacupuncture versus moxibustion for irritable bowel syndrome: a randomized, parallel-controlled trial," *Evidence-Based Complementary and Alternative Medicine*, vol. 2015, Article ID 361786, 12 pages, 2015.

[106] T. I. T. N. Hasanah, D. C. Wijeyesekera, A. J. M. S. Lim, and B. Ismail, "Recycled PP/HDPE Blends: A Thermal Degradation and Mechanical Properties Study," *Applied Mechanics and Materials*, vol. 465-466, pp. 932–936, 2013.

[107] I. Turku, A. Keskisaari, T. Kärki, A. Puurtinen, and P. Marttila, "Characterization of wood plastic composites manufactured from recycled plastic blends," *Composite Structures*, vol. 161, pp. 469–476, 2017.

[108] S. Chattopadhyay, R. Khandal, R. Uppaluri, and A. Ghoshal, "Bamboo Fiber Reinforced Polypropylene Composites and Their Mechanical, Thermal, and Morphological Properties," *Journal of Applied Polymer Science*, vol. 119, no. 3, pp. 1619–1626, 2011.

[109] Protolabs, "Injection molding material selection guide," 2022, https://www.protolabs.com/resources/guides-and-trend-reports/thermoplastic-material-selection-for-injection-molding/.

[110] K. J. Jem and B. Tan, "The development and challenges of poly (lactic acid) and poly (glycolic acid)," *Advanced Industrial and Engineering Polymer Research*, vol. 3, no. 2, pp. 60–70, 2020.

[111] J.-W. Rhim, S.-I. Hong, and C.-S. Ha, "Tensile, water vapor barrier and antimicrobial properties of PLA/nanoclay composite films," *LWT - Food Science and Technology*, vol. 42, no. 2, pp. 612–617, 2009.

[112] H. Al Abdallah, B. Abu-Jdayil, and M. Z. Iqbal, "The effect of alkaline treatment on poly(lactic acid)/date palm wood green

composites for thermal insulation," *Polymers*, vol. 14, no. 6, p. 1143, 2022.

[113] P. Bajpai and V. Chaudhary, "Analysis of wear behavior of thermoplastic bio-composite," *IOP Conference Series: Materials Science and Engineering*, vol. 225, article 012206, 2017.

[114] P. Bajpai, I. Singh, and J. Madaan, "Development and characterization of PLA-based green composites," *Journal of Thermoplastic Composite Materials*, vol. 27, no. 1, pp. 52–81, 2012.

[115] T. Ageyeva, J. G. Kovács, and T. Tábi, "Comparison of the efficiency of the most effective heterogeneous nucleating agents for poly(lactic acid)," *Journal of Thermal Analysis and Calorimetry*, vol. 147, no. 15, pp. 8199–8211, 2021.

[116] L. Aliotta, P. Cinelli, M. Coltelli, M. C. Righetti, M. Gazzano, and A. Lazzeri, "Effect of nucleating agents on crystallinity and properties of poly (lactic acid) (PLA)," *European Polymer Journal*, vol. 93, pp. 822–832, 2017.

[117] C. Correia, T. E. P. Gomes, I. Gonçalves, and V. Neto, "Reprocessability of PLA through chain extension for fused filament fabrication," *Journal of Manufacturing and Materials Processing*, vol. 6, no. 1, p. 26, 2022.

[118] D. Garlotta, "A literature review of poly(lactic acid)," *Journal of Polymers and the Environment*, vol. 9, no. 2, pp. 63–84, 2001.

[119] G. Kfoury, J.-M. Raquez, F. Hassouna et al., "Recent advances in high performance poly(lactide): from "green" plasticization to super-tough materials via (reactive) compounding," *Frontiers in Chemistry*, vol. 1, p. 32, 2013.

[120] L. Suryanegara, H. Okumura, A. N. Nakagaito, and H. Yano, "The synergetic effect of phenylphosphonic acid zinc and microfibrillated cellulose on the injection molding cycle time of PLA composites," *Cellulose*, vol. 18, no. 3, pp. 689–698, 2011.

[121] A. M. Harris and E. C. Lee, "Improving mechanical performance of injection molded PLA by controlling crystallinity," *Journal of Applied Polymer Science*, vol. 107, no. 4, pp. 2246–2255, 2008.

[122] N. Kawamoto, A. Sakai, T. Horikoshi, T. Urushihara, and E. Tobita, "Nucleating agent for poly (l-lactic acid)—an optimization of chemical structure of hydrazide compound for advanced nucleation ability," *Journal of Applied Polymer Science*, vol. 103, no. 1, pp. 198–203, 2007.

[123] H. Li and M. A. Huneault, "Effect of nucleation and plasticization on the crystallization of poly(lactic acid)," *Polymer*, vol. 48, no. 23, pp. 6855–6866, 2007.

[124] H. Liu and J. Zhang, "Research progress in toughening modification of poly(lactic acid)," *Journal of Polymer Science Part B: Polymer Physics*, vol. 49, no. 15, pp. 1051–1083, 2011.

[125] L. T. Lim, R. Auras, and M. Rubino, "Processing technologies for poly(lactic acid)," *Progress in Polymer Science*, vol. 33, no. 8, pp. 820–852, 2008.

[126] S. Chaitanya and I. Singh, "Sisal fiber-reinforced green composites: Effect of ecofriendly fiber treatment," *Polymer Composites*, vol. 39, pp. 4310–4321, 2018.

[127] L. Aliotta, A. Vannozzi, P. Cinelli, S. Fiori, M. Coltelli, and A. Lazzeri, "Wheat bran addition as potential alternative to control the plasticizer migration into PLA/PBSA blends," *Journal of Materials Science*, vol. 57, pp. 1–17, 2022.

[128] B. S. Heidari, E. Oliaei, H. Shayesteh et al., "Simulation of Mechanical Behavior and Optimization of Simulated Injection Molding Process for PLA based Antibacterial Composite and Nanocomposite Bone Screws Using Central Composite Design," *Journal of the Mechanical Behavior of Biomedical Materials*, vol. 65, 2016.

[129] X. Jing, H.-Y. Mi, L.-S. Turng, and X.-F. Peng, "Injection molding of novel polylactic acid/thermoplastic polyurethane (PLA/TPU) blends with shape-memory behavior," *Annual Technical Conference - ANTEC, Conference Proceedings*, vol. 2, pp. 944–948, 2013.

[130] J. Akindoyo, M. Beg, S. Ghazali, H.-P. Heim, and M. Feldmann, "Effects of surface modification on dispersion, mechanical, thermal and dynamic mechanical properties of injection molded PLA-hydroxyapatite composites," *Composites Part A Applied Science and Manufacturing*, vol. 103, pp. 96–105, 2017.

[131] Y. Yang, M. Murakami, and H. Hamada, "Molding Method, Thermal and Mechanical Properties of Jute/PLA Injection Molding," *Journal of Polymers and the Environment*, vol. 20, 2012.

Hindawi
International Journal of Polymer Science
Volume 2022, Article ID 4130440, 7 pages
https://doi.org/10.1155/2022/4130440

Research Article

Mechanical Properties and Electrical Resistivity of the Friction Stir Spot-Welded Dissimilar Al–Cu Joints

N. Mohanraj,[1] N. Mathan Kumar,[2] P. Prathap,[1] P. Ganeshan,[3] K. Raja,[4] V. Mohanavel,[5,6] Alagar Karthick,[7] and M. Muhibbullah[8]

[1]*Department of Mechanical Engineering, Sri Krishna College of Technology, Coimbatore, 641008 Tamil Nadu, India*
[2]*Department of Mechanical Engineering, Akshaya College of Engineering & Technology, Coimbatore, 642109 Tamil Nadu, India*
[3]*Department of Mechanical Engineering, Sri Eshwar College of Engineering, Coimbatore - 641202, Tamil Nadu, India*
[4]*Department of Mechanical Engineering, University College of Engineering Dindigul, Dindigul, 624622 Tamil Nadu, India*
[5]*Centre for Materials Engineering and Regenerative Medicine, Bharath Institute of Higher Education and Research, Chennai 600073, Tamil Nadu, India*
[6]*Department of Mechanical Engineering, Chandigarh University, Mohali-140413, Punjab, India*
[7]*Renewable Energy Lab, Department of Electrical and Electronics Engineering, KPR Institute of Engineering and Technology, Coimbatore, 641407 Tamil Nadu, India*
[8]*Department of Electrical and Electronic Engineering, Bangladesh University, Dhaka 1207, Bangladesh*

Correspondence should be addressed to N. Mohanraj; mohanrajnagarajan@gmail.com and M. Muhibbullah; m.muhibbullah@bu.edu.bd

Received 22 October 2021; Accepted 21 April 2022; Published 3 June 2022

Academic Editor: Ching Hao Lee

Alternative methods for dissimilar metal joining particularly aluminium and copper have gain interest in manufacturing sectors. Friction stir spot welding was carried out on the AA6061 and C11000 wires of 2 mm diameter. This research paper reported the results on microstructures and mechanical properties of the spot-welded joints, and also special attention is provided for electrical resistivity of the welds. The microstructures reveal the information of grain structure and bonding. The width of diffusion layer significantly reduced with low dwell times. For a plunge depth of 1 mm, the maximum tensile strength (294 MPa) is achieved during the higher rotational speed (1400 rpm). For the same plunge depth, lower tensile strength values are exhibited by the joint produced using the lower rotational speed (800 rpm). Hardness of the weld region recorded 70 HV which is less than Cu (115 HV) and greater than Al (40 HV). FSSW joints (0.30 to 0.34 $\mu\Omega$) offered higher range of electrical resistivity than that of base metal (0.02 $\mu\Omega$). The results highlighted in this paper might be helpful for both academic researchers and industrialists.

1. Introduction

The application range of aluminium in automotive industries is expanding due to its many inherent characteristics like low weight, high ductility, and excellent thermal and electrical conductivity. Joining of aluminium with the other metals is still a challenge for many researchers. With advances in welding processes, interest has become more on solid-state welding processes as an alternative for dissimilar metal joining. Friction stir spot welding (FSSW) is a newer technique under solid-state welding processes, which shows the greater efficiency than the existing methods of dissimilar joining of aluminium. Extensive feasibility studies are performed on FSSW of dissimilar metals (aluminium and copper) from manufacturers of aeroplanes, trucks, trains, motor vehicles, and appliances.

FSSW is a modified version of friction stir welding (FSW) originally developed for joining Al-alloys [1–6], with similar working mechanism used for special applications (spot welding process) [7, 8]. A rotating tool (nonconsumable) is positioned perpendicular to the workpiece and pushed towards the workpiece with the application of axial

force for a specific duration also called as dwell time. After the formation of weld, the tool retracts from the workpiece. In FSSW, the heat input and material plasticization are determined through the two significant parameters such as dwell time and tool penetration speed. Based on the material plasticization and heat input, the mechanical properties of the joint are determined [8]. The schematic of FSSW process [9] is shown in Figure 1.

Spot welding techniques are mainly concentrated in the joining of dissimilar wires, sheets, terminals, and contacts to retain its intrinsic metallic properties which are not possible in conventional fusion welding techniques, brazing, and soldering. Solid-state welding processes help avoid the intermetallic compounds formation, whereas conventional welding leads to produce them [10]. Several researchers attempted the dissimilar welding [1] of aluminium and copper through FSW [11–19]. Akinlabi et al. investigated the electrical resistivities of the Al to Cu joints. The authors found the relationship between the resistivity and the heat input, and higher heat inputs lead to the increased electrical resistance. The higher resistivity of joints is about 9.8% more than that of the parent metal resistivity [20]. Similar studies have been performed by the other researchers. Savolainen found that the joint resistivity is 2.5% times more than the average value of both parent materials [21]. Most of the work carried out on FSSW of aluminium to copper deals with mechanical and microstructural properties of the welds. Dissimilar metal joint (aluminium-copper) could be beneficial in electrical connections, wiring circuits in automobiles, and electronic board assemblies. All these applications require the knowledge about weld joint electrical performance. Hence, the present study has been conducted to address the friction stir spot-welded joint electrical performance parameters. The present paper investigates the effect of the FSSW process parameters on electrical resistivity of the weld joints and its relationships. Mechanical and metallurgical properties of the weld joints are reported. This research deals with the dissimilar aluminium-copper spot joint produced by friction stir spot welding. The mechanical properties reveal the joint strength of the weld, and the microstructure highlights the various defects in the joint. The electrical resistivity is also measured to find the resistivity.

2. Experimental Setup

Aluminium, AA6061, and copper, C11000, wires of 2 mm diameter are employed for joining process (friction stir spot welding). Tables 1 and 2 show the elemental composition and mechanical properties of both the metallic wires adopted for experimentation. Before producing weldments, surfaces of the workpiece are cleaned with acetone for the removal of surface contaminants. Welds are produced by placing Cu on the top side of Al. Experimental trials are carried out by different combinations of the process parameters of FSSW process. The FSSW tool is produced with H13 steel tool hardened to 46-48 HRC (with a pin length of 4 mm, shoulder diameter of 10 mm, and diameter of 5 mm). The tool plunge depths of 0.5 and 1 mm with a constant dwell time of 5 s are employed. FSSW rotational speeds are varied from 800 rpm to 1400 rpm. The FSSW torque and axial load values are analyzed through a load cell of six axis attached to the data acquisition system for continuous monitoring. The dimensional indication of workpiece is provided in Figure 2.

For metallographic examination of the weld cross sections, Keller's reagent is used as an etchant for Al side and a solution comprising of HCI (6 ml) + FeCI3 (10 g) + ethanol (C2H50H) (20 ml) + deaerated water (80 ml) was utilized to etch the Cu side. (Morphology and qualitative analysis of the weldments are performed using SEM and EDAS analysis. The electrical resistivity values of the samples are determined using four-point probe meter. Simple device employed for gauging the resistivity of semiconductor specimens is known as four-point probe meter. The substrate resistivity is measured by applying the current through two outer probes and assessed the voltage through the inner probes. Further, weld specimens for tensile tests are machined as per the standard (ASTM A-931). The tensile tests are carried out at the standard room temperature. Vickers hardness apparatus (with a load of 0.98 N) is employed to measure the hardness in the weld region and base metal. An average of five values is taken in each region. Scanning electron microscopy (SEM) is equipped to observe the microstructures of weld joints. Energy-dispersive X-ray spectroscopy is employed to assess the elemental compositions of the weld joints.

3. Results and Discussion

Dissimilar joints (Al and Cu) were successfully obtained through friction stir spot welding according to the experimental design. The cross sections of the joints exhibit the five distinct regions such as base metal (BM), stir zone (SZ), thermo-mechanically affected zone (TMAZ), the heat affected zone (HAZ), and hook region [8].

3.1. Microstructures. Figures 3(a) and 3(b) depict the micrographs of the spot weldments. It is observed that the six intermetallic phases exist below 500°C which are likely some of many metastable intermetallic phases existing in the Al-Cu phase diagram [22–24]. Sound welds are obtained for the selected process parametric range. The width of diffusion layer at the interface is significantly decreased with the decrease in dwell time. The diffusion layer is noticed in Figure 3 for rotational speed of 1400 rpm with dwell time of 5 s. In Figure 4 (rotational speed: 1400 rpm and dwell time: 1 s), the diffusion layer is lower than the Figure 3. The micrographs reveal the negligible pores and defect free weldments. Microstructural studies are performed in all the five distinct zones of weld. The TMAZ constitutes smaller and equiaxed grains because of the mechanical deformation and thermal cycles during stirring action. Stir zone has fully crystallized small and fine grains along the boundaries. Longer grains are observed in the HAZ than that of TMAZ and SZ. Typically, with the increase in distance from weld center, evolution of grain structures takes place. Further, grains in HAZ are randomly distributed in the region.

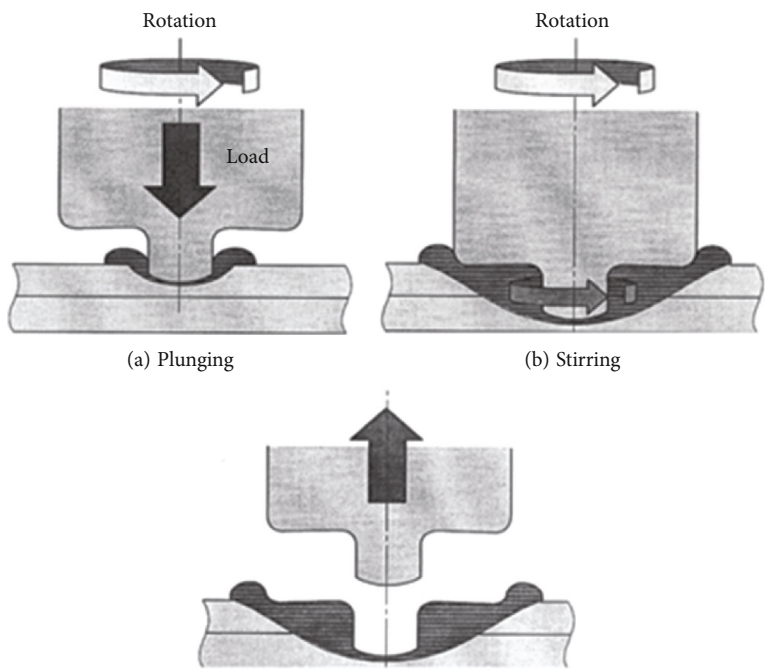

(a) Plunging (b) Stirring

(c) Retracting

Figure 1: Graphic representation of friction stir spot welding process.

Table 1: Chemical composition of AA6061 and C11000 wires.

Materials (wt%)	Cu	Fe	Si	Zn	Pb	Ni	Al
AA6061	0.005	0.3	0.07	0.005	0.003	<0.001	Balance
C11000	Balance	0.05	0.009	4.69	0.03	0.03	0.02

Table 2: Mechanical properties of AA6061 and C11000 used for the experimentation.

Properties	AA6061	C11000
Tensile strength (MPa)	290	455
Elongation (%)	15	33
Hardness (HV)	41	115

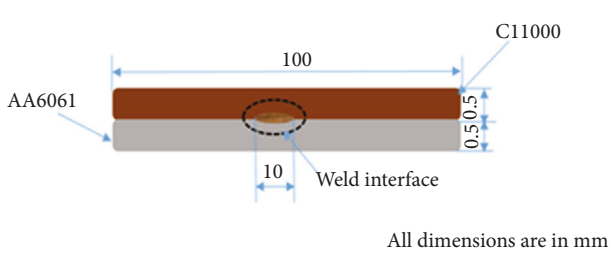

Figure 2: Workpiece dimensions for experimentation.

SEM images are shown in Figures 4(a) and 4(b). The images depict the Cu rings and keyhole of the spot-welded joints by varying process parameter range. Scanning electron microscopy (SEM) analysis performed to find the disparity between two base metals such as Al and Cu. The micrographs clearly reveal the presence of Cu on the Al side and disparity between the base metals. The large variation between the melting points of Al and Cu combined with FSSW tool stirring action and dwell time produce the brittle and hard intermetallic compounds.

The intermetallic compounds in the specimens are analyzed using an electron dispersed X-ray spectroscopy (EDS). Previous literature reports suggested the increased resistivity of the joints due to the presence of long-range–ordered alloys [25, 26]. The long-range–ordered alloys in the weld region of weldment produced with tool rotational speed of 1000 rpm and dwell time of 1 s are noticed in Figure 4(a). Three major intermetallic compounds, namely, Al_2Cu, AlCu, and Al_4Cu_9, are noticed in the SZ of the joints for dwell time of 1 s and rotational speed of 1000 rpm, whereas the joint produced with dwell time of 1 s and 1400 rpm showed only two intermetallic compounds, namely, Al_3Cu_4 and Al_2Cu.

In most of the welded samples, it is observed the accumulation of aluminium particles or aluminium-rich content on the Cu side, particularly in the upper side of keyhole with small percentages of copper. This may be attributed to FSSW tool stirring action which takes bottom side of aluminium particles to the top region. This action promotes the formation of intermetallic compounds or aluminium-rich contents on Cu side.

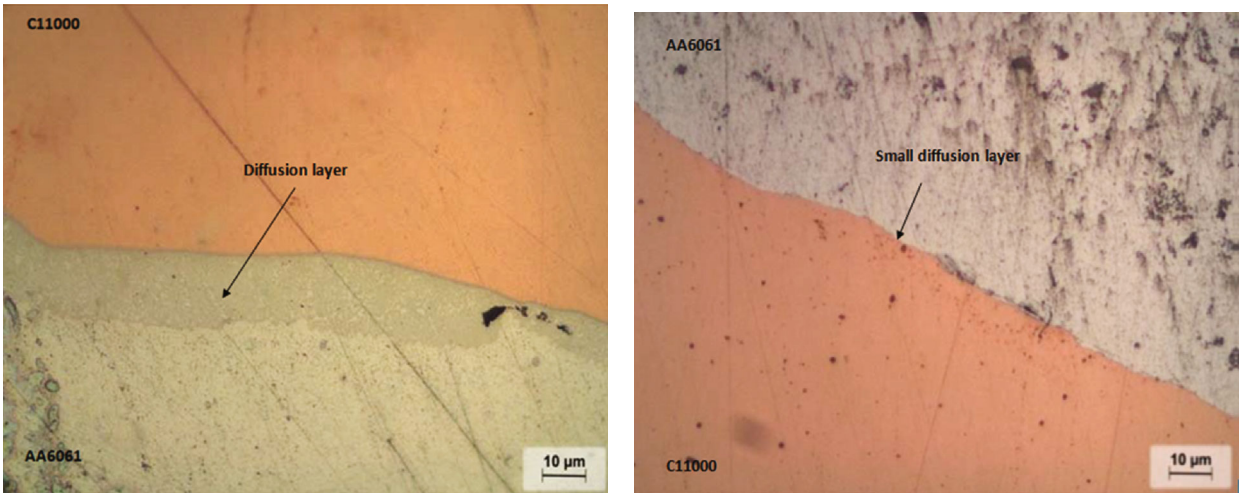

(a) (b)

Figure 3: Microstructures of friction stir spot-welded Al-Cu wires (a) rotational speed: 1400 rpm, dwell time, and 5 s (b) rotational speed: 1400 rpm, dwell time: 1 s.

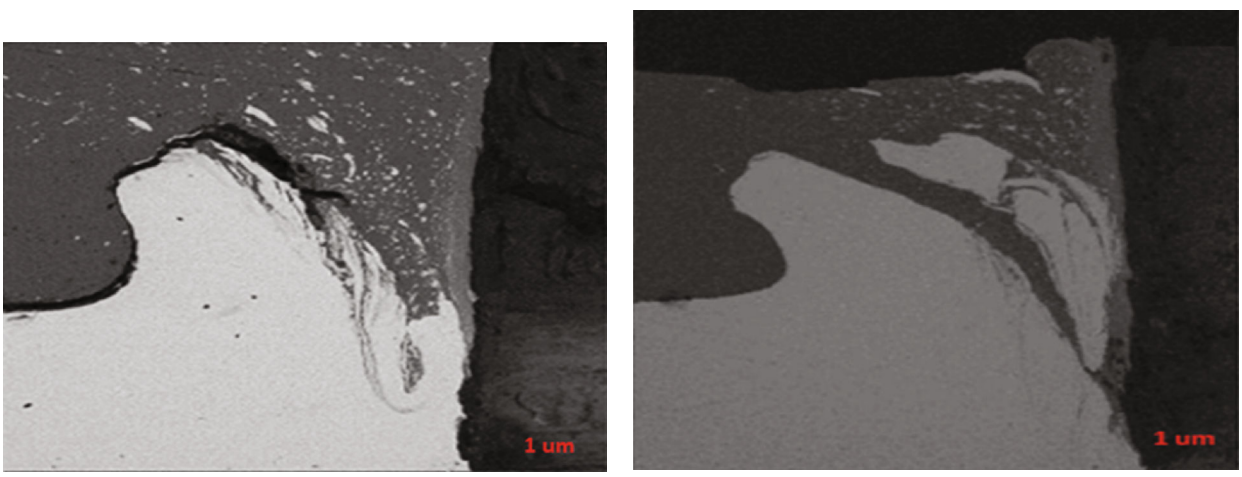

(a) (b)

Figure 4: (a) Microstructure of the spot weld using SEM (1000 rpm, 1 s and 0.5 mm plunge depth). (b) Microstructure of the spot weld using SEM (1400 rpm, 1 s, and 0.5 mm plunge depth).

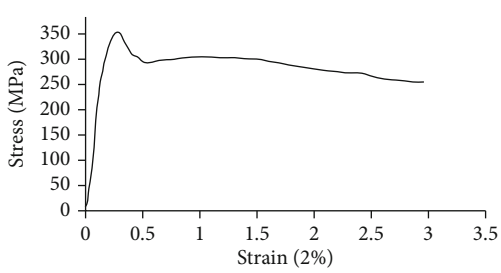

Figure 5: Stress vs. strain curve of spot-welded wire joints (rotational speed: 1400 rpm and plunge depth: 1 mm).

3.2. Mechanical Properties. Figure 5 reveals the weld strength profile of the spot-welded Al-Cu wires for different process parametric range. The results revealed that the weld strength is influenced by many factors such as tool pin length, tool rotational speed, and plunge depth [27]. The least affected parameter in joint strength is weld time and remains to be insignificant. Weld strength is majorly influenced by the tool rotational speed. As the rotational speed increases, weld strength increases. The maximum tensile strength (294 MPa) is achieved during the higher rotational speed (1400 rpm). The minimum tensile strength is yielded during the lower rotational speed (800 rpm). Weld strength remains to be unaffected even for rotational speed more than 1400 rpm. The linear relationship between weld strength and rotational speed exists only for the limited range. All the specimens observed

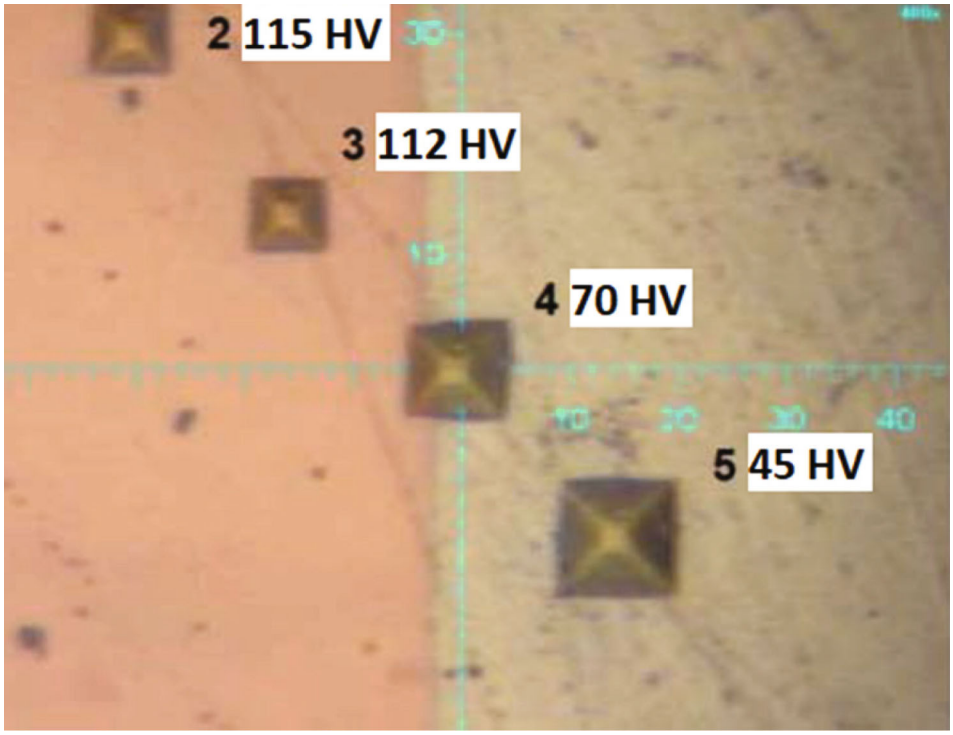

Figure 6: Hardness profile of Al-Cu spot welds (rotational speed: 1200 rpm and plunge depth: 0.5 mm).

Table 3: Electrical resistivities of the base metals and the spot welds of various process parameters (TRS: tool rotational speed; PD: plunge depth).

Material	*Resistivity ($\mu\Omega$)*
Base metal, Al	0.018
Base metal, Cu	0.026
Average value	0.022
Spot welds	*Resistivity ($\mu\Omega$)*
TRS: 800 rpm; PD: 0.5 mm	0.061
TRS: 800 rpm; PD: 1 mm	0.038
TRS: 1000 rpm; PD: 0.5 mm	0.047
TRS: 1000 rpm; PD: 1 mm	0.032
TRS: 1200 rpm; PD: 0.5 mm	0.036
TRS: 1200 rpm; PD: 1 mm	0.030
TRS: 1400 rpm; PD: 0.5 mm	0.029
TRS: 1400 rpm; PD: 1 mm	0.024

failure in the weld region during tensile testing. Weldments are achieved with the average tensile strength of 293.48 MPa and the maximum load of 40.45 kN by using 1400 rpm rotational speed and plunge depth of 1 mm.

Vickers hardness measurements are performed across the weld region and base metal region of the welded specimens (Figure 6). Figure 6 shows the hardness profile of spot-welded specimen with plunge depth of 0.5 mm and rotational speed of 1200 rpm. At the center of the weldment, hardness value observed is 70 HV which is less than Cu and greater than Al. Slight decrease in hardness values on Cu is observed to the contrast in plasticization and thermal cycles during welding process. The increase in hardness value of joint when compared to Al is because of the grain recrystallization in the stir zone.

3.3. Electrical Resistivity. The electrical resistivity at the joint interface of spot-welded dissimilar Al-Cu wires is measured using four-wire probe meter. Similar studies are performed by the authors for ultrasonic spot welding of Al-Cu wires [28, 29]. The electrical resistivity values of joints for process parameters of welding are presented (Table 3).

From Table 3, the electrical resistivity values increased with the rise in magnitudes of plunge depth and tool rotational speed. The tool rotational speed has four values from 800 to 1400 rpm. The plunge depth with two values of 0.5 and 1 mm is used. The electrical resistivities of the spot-welded specimens are higher than the both metals. The difference in electrical resistivity values is huge between spot-welded joints and base metals. This pattern is attributed to the presence of pores and micro cracks at the stir zone of weldments [30–32]. The highest measured of resistivity is 0.061 $\mu\Omega$ for the plunge depth of 0.5 mm and tool rotational speed of 800 rpm. It is observed that the most values of the joint resistivities lies in the range of 0.30 to 0.34 $\mu\Omega$. The average of base metals is 0.022, and when comparing this value to the joint resistivities, a depreciation varies between 0.08 $\mu\Omega$ (42%) and 0.012 $\mu\Omega$ (60%). Along with these values, a maximum value of 0.061 $\mu\Omega$ is 200% rise of base metals average for plunge depth of 0.5 mm and tool rotational speed of 800 rpm. Figure 7 shows the comparison chart of electrical resistivities of the spot welds with various process parameters.

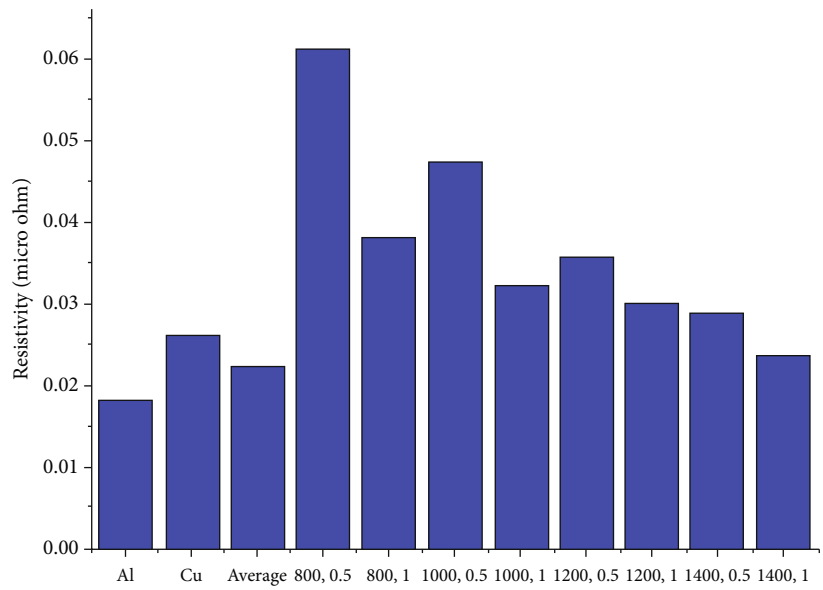

Figure 7: Influence of process parameters on the electrical resistivity of the spot welds when compared to the base metals and their average value.

It can be observed from the measurements that all the joint resistivity values are much more than the parent metal. In FSSW process, the presence of intermetallic compounds affects the electrical resistivity and therefore increases in magnitude. The higher electrical resistivities of the spot welds in the present work are because of the presence of long-range–ordered alloys (intermetallic phases) in the keyhole. This is validated from the energy-dispersive X-ray spectroscopy analysis.

4. Conclusions

Friction stir spot welding between 2 mm AA6061 wires and 2 mm C11000 wires was successfully performed using a hardened H13 steel tool. Within the taken process parametric range, the following important conclusions can be drawn.

(i) Width of diffusion layer is significantly decreased with the decrease in dwell time

(ii) The micrographs clearly reveal the presence of Cu on the Al side and disparity between the base metals which results in formation of harmful brittle and hard intermetallic compounds

(iii) The maximum tensile strength (294 MPa) is achieved during the higher rotational speed (1400 rpm) for a plunge depth of 1 mm. For the same plunge depth, lower tensile strength values are exhibited by the joint produced using the lower rotational speed (800 rpm)

(iv) Hardness of the weld region recorded 70 HV which is less than Cu (115 HV) and greater than Al (40 HV)

(v) The electrical resistivity of the spot welds lies in the range of 0.30 to 0.34 $\mu\Omega$ which is significantly more than the average value of base metals (0.022 $\mu\Omega$)

Data Availability

The data used to support the findings of this study are included within the article.

Conflicts of Interest

The authors declare that they have no conflicts of interest.

References

[1] A. Heidarzadeh, S. Mironov, R. Kaibyshev et al., "Friction stir welding/processing of metals and alloys: a comprehensive review on microstructural evolution," *Progress in Materials Science*, vol. 117, p. 100752, 2021.

[2] G. Çam and G. R. İpekoğlu, "Recent developments in joining of aluminum alloys," *The International Journal of Advanced Manufacturing Technology*, vol. 91, no. 5-8, pp. 1851–1866, 2017.

[3] A. Von Strombeck, G. Çam, J. F. Dos Santos, V. Ventzke, and M. Koçak, "A comparison between microstructure, properties, and toughness behavior of power beam and friction stir welds in al-alloys, Proc. of the TMS," in *Proceeding of the TMS 2001 annual meeting aluminum, automotive and joining*, S. K. Das, J. G. Kaufman, and T. J. Lienert, Eds., pp. 249–264, TMS, Warrendale, PA, USA, 2001.

[4] N. Kashaev, V. Ventzke, and G. Çam, "Prospects of laser beam welding and friction stir welding processes for aluminum airframe structural applications," *Journal of Manufacturing Processes*, vol. 36, pp. 571–600, 2018.

[5] G. Çam, "Friction stir welded structural materials: beyond Al-alloys," *International Materials Review*, vol. 56, no. 1, pp. 1–48, 2011.

[6] G. Çam, G. İpekoğlu, and H. T. Serindağ, "Effects of use of higher strength interlayer and external cooling on properties of friction stir welded AA6061-T6 joints," *Science and Technology of Welding and Joining*, vol. 19, no. 8, pp. 715–720, 2014.

[7] Y. Bozkurt, S. Salman, and G. Çam, "Effect of welding parameters on lap-shear tensile properties of dissimilar friction stir spot welded AA5754-H22/2024-T3 joints," *Science and Technology of Welding and Joining*, vol. 18, no. 4, pp. 337–345, 2013.

[8] H. Badarinarayan, *Fundamentals of Friction Stir Spot Welding*, Missouri University of Science and Technology, 2009.

[9] T. Saeid, A. Abdollah-Zadeh, and B. Sazgari, "Weldability and mechanical properties of dissimilar aluminum-copper lap joints made by friction stir welding," *Journal of Alloys and Compounds*, vol. 490, no. 1-2, pp. 652–655, 2010.

[10] J. Ouyang, E. Yarrapareddy, and R. Kovacevic, "Microstructural evolution in the friction stir welded 6061 aluminum alloy (T6-temper condition) to copper," *Journal of Materials Processing Technology*, vol. 172, no. 1, p. 110, 2006.

[11] A. Abdollah-Zadeh, T. Saeid, B. Sazgari, T. Saeid, and B. Sazgari, "Microstructural and mechanical properties of friction stir welded aluminum/copper lap joints," *Journal of Alloys and Compounds*, vol. 460, no. 1-2, pp. 535–538, 2008.

[12] E. T. Akinlabi, R. D. Reddy, and S. A. Akinlabi, "Microstructural characterizations of dissimilar friction stir welds," *Proceedings of the World Congress on Engineering*, vol. 3, pp. 4–6, 2012.

[13] R. M. Galvao, A. L. Leal, and D. M. Rodrigues, "Material flow in heterogeneous friction stir welding of aluminium and copper thin sheets," *Science and Technology of Welding and Joining*, vol. 15, no. 8, pp. 654–660, 2010.

[14] L. T. Xia-Wei, "Microstructure and mechanical properties of dissimilar pure copper/1350 aluminum alloy butt joints by friction stir welding," *Transactions of Nonferrous Metals Society of China*, vol. 22, no. 6, pp. 1298–1306, 2012.

[15] M. Guerra, C. Schmidt, J. C. McClure, L. E. Murr, and A. C. Nunes, "Flow patterns during friction stir welding," *Materials Characterization*, vol. 49, no. 2, pp. 95–101, 2002.

[16] E. T. Akinlabi and S. A. Akinlabi, "Effect of heat input on the properties of dissimilar friction stir welds of aluminium and copper," *American Journal of Materials Science*, vol. 2, no. 5, pp. 147–152, 2012.

[17] A. O. AI-Roubaiy, S. M. Nabat, and A. D. L. Batako, "Experimental and theoretical analysis of friction stir welding of Al–Cu joints," *International Journal of Advanced Manufacturing Technology*, vol. 71, no. 9-12, pp. 1631–1642, 2014.

[18] M. F. X. Muthu and V. Jayabalan, "Tool travel speed effects on the microstructure of friction stir welded aluminum-copper joints," *Journal of Materials Processing Technology*, vol. 217, pp. 105–113, 2015.

[19] E. T. Akinlabi, D. M. Madyira, and S. A. Akinlabi, "Effect of heat input on the electrical resistivity of dissimilar friction stir welded joints of aluminium and copper," in *IEEE Africon 2011*, pp. 13–15, Victoria Falls, Zambia, Sept. 2011.

[20] K. Savolainen, *Friction stir welding of copper and microstructure and properties of the welds*, Department of Engineering Design and Production, Aalto University Finland, 2012.

[21] D. Hawkins and R. Hultgren, "Metallography, structures, and phase diagrams," in *ASM Metals Handbook, Vol. 8*, p. 258, American Society for Metals, 1973.

[22] T. Massalski, "The Al–Cu (aluminum–copper) system," *Journal of Phase Equilibria*, vol. 1, no. 1, pp. 27–33, 1980.

[23] R. Hultgren, "Al–Cu (aluminum–copper)," in *Ac–Au – Au–Zr*, vol. 5a of Landolt–Bo¨ rnstein – group IV physical chemistry, Springer-Verlag, Berlin, 2006.

[24] R. Heideman, C. Johnson, and S. Kou, "Metallurgical analysis of Al/Cu friction stir spot welding," *Science and Technology of Welding and Joining*, vol. 15, no. 7, pp. 597–604, 2010.

[25] H. J. Kim, J. Y. Lee, K. W. Paik et al., "Effects of CulAl intermetallic compound (IMC) on Copper Wire and aluminum pad bondability," *IEEE transactions on components and packaging technologies*, vol. 26, no. 2, pp. 367–374, 2003.

[26] J. Van der Geer, J. A. J. Hanraads, and R. A. Lupton, "The art of writing a scientific article," *Journal of Science Communication*, vol. 163, pp. 51–59, 2000.

[27] N. Mohan Raj, L. A. Kumaraswamidhas, P. K. Nalajam, and S. Arungalai Vendan, "Studies on electro mechanical aspects in ultrasonically welded Al/cu joints," *Transactions of the Indian Institute of Metals*, vol. 71, no. 1, pp. 107–116, 2018.

[28] N. M. Raj, L. A. Kumaraswamidhas, S. A. Vendan, and P. K. Nalajam, "Investigations on resistance behavior at the Interface of ultrasonically welded dissimilar Al/Cu joints," *Silicon*, vol. 11, no. 4, pp. 1717–1723, 2019.

[29] C. Schmal, G. Meschut, and N. Buhl, "Joining of high strength aluminum alloys by refill friction stir spot welding III-1854-18," *Welding in the World*, vol. 63, no. 2, pp. 541–550, 2019.

[30] K. Chen, X. Liu, and J. Ni, "A review of friction stir based processes for joining dissimilar materials," *International Journal of Advanced Manufacturing Technology*, vol. 104, no. 5-8, pp. 1709–1731, 2019.

[31] X. C. Meng, Y. X. Huang, J. Cao, J. J. Shen, and F. Jorge, "Recent progress on control strategies for inherent issues in friction stir welding," *Progress in Materials Science*, vol. 115, p. 100706, 2021.

[32] M. Awang, *Simulation of friction stir spot welding (FSSW) process: study of friction phenomena*, West Virginia University, 2007.

Hindawi
International Journal of Polymer Science
Volume 2021, Article ID 8587383, 13 pages
https://doi.org/10.1155/2021/8587383

Research Article

Degradation Analysis of Jute Fiber Reinforced Waste Tile Powder-Filled Polymer Composite on Wear Characteristics

G. Sakthi Balan,[1] M. Sridharan,[2] R. Balasundaram,[3] A. Sasikaran,[2] M. Sagar,[2] S. Dinesh,[4] V. Vijayan,[4] and S. Rajkumar[5]

[1]*Research Scholar, School of Mechanical Engineering, Vellore Institute of Technology, Vellore-632014, India*
[2]*Department of Mechanical Engineering, K.Ramakrishnan College of Engineering, Trichy, India*
[3]*Department of Mechanical Engineering, SRM Institute of Science and Technology, Trichy Campus, 621105 Tamil Nadu, India*
[4]*Department of Mechanical Engineering, K.Ramakrishnan College of Technology, Samayapuram, Trichy, 621112 Tamil Nadu, India*
[5]*Department of Mechanical Engineering, Faculty of Manufacturing, Institute of Technology, Hawassa University, Ethiopia*

Correspondence should be addressed to S. Rajkumar; rajkumar@hu.edu.et

Received 7 October 2021; Accepted 30 November 2021; Published 29 December 2021

Academic Editor: Ching Hao Lee

In this study, a polymer composite is made using chemically treated jute fiber and waste floor tile powder as an alternative source for roof tile application. The wear qualities were examined at various ages, and the outcomes were optimized. In order to improve the wetting properties of the jute fiber, it was chemically treated. MINITAB software was used to develop Taguchi method parameters such as jute fiber percentage, waste tile powder percentage, and NaOH chemical treatment using the MINITAB software. It was determined that hardness was the most important characteristic in terms of wear properties after the specimens were subjected to ageing and abrasion wear testing and hardness tests were carried out as per normal protocols. As a result of the waste tile powder addition, the surface and core pore formation rates were reduced and the wear index rates were low. Jute fiber with 15%, 9% tile powder, and 5% NaOH treatment were found to have the lowest wear index of the other specimen compositions tested, according to the wear index. Specimen made with 5% jute fiber addition, 9% tile powder inclusion, and 10% NaOH treatment, on the other hand, had more hardness. Degradation of the fibers and delamination are side effects of the ageing process. The wear resistance of the surface was increased by the use of waste tile powder.

1. Introduction

There are a variety of modern ideas and materials being developed in an effort to create better roofing options. Researchers focus on extending the life of roofing materials by decreasing the degradation of the materials in diverse climatic situations. When exposed to normal environmental conditions, the material will begin to degrade after three to five years. Jute fiber-reinforced polymer composite was explored by [1], who found that rosewood dust boosted thermal stability while padauk wood dust improved adhesion with the matrix. When NaOH treatment of jute fiber and nanoclay inclusion in polymer composites were investigated by [2], they found that the mechanical and vibration characteristics were affected by the concentration of NaOH treatment and inclusion of nanoclay. Improved matrix adhesion was achieved after NaOH treatment. While investigating the material's mechanical and thermal properties, researchers [3] discovered that adding fillers reduced both the material's tensile and flexural qualities while increasing its hardness. Jute fiber and epoxy matrix packed with silicon carbide powder were treated by [4] and characterised for mechanical properties. Reinforcement was added and the SiC particle size had a greater impact on the mechanical properties, which resulted in the installation of reinforcement. It was shown that the mechanical and thermal properties of jute fibers in epoxy composites decreased after exposure to moisture; however, the chemically modified samples showed greater interfacial adhesion than untreated jute fiber samples. A study done by [5] discovered that jute

fiber in epoxy composite was found to be superior to fiber reinforced polyester resin in terms of mechanical qualities, as well as wear resistance. Jute fiber was combined with 304 steel wire mesh, and dynamic characteristics were evaluated, with superior tensile and flexible strengths with 45 orientation wire mesh, according to [6]. It was shown that the SEM pictures of fibers treated with jute fiber modification show better adherence than untreated fibers. The mechanical characteristics and void formation of the treated fibers are affected. Researchers in 2020 used an alkali-treated jute fiber to strengthen a bioepoxy composite and investigated its mechanical properties. Alkali-treated fiber was shown to have improved mechanical capabilities, particularly tensile and flexural qualities. Compressive and tensile strength of jute fiber added epoxy composites were tested and found to increase with the addition of fibers, which can be utilised for construction purposes, partition boards, windows and door frames, and other structural applications. By altering jute fiber surface characteristics with alkaline and benzoyl chloride, [7] were able to conduct abrasive wear tests on jute fiber-reinforced composites. Using chemically treated fibers, wear resistance was found to be significantly improved. Tiles created from recycled bricks and roof tiles exhibit a 13.7-gloss-unit improvement when 15% of the waste is added, according to a study published in 2020 by Filho et al. It has been observed that the thermal time constant of PV roof tiles can be improved by insulating the roof, which results in a longer period of time for the cells to heat and cool. Composites made from laterite tiles and palm broom fibers displayed 12 percent average water absorption and 1221 N/mm^2 average tensile strength after 28 days of curing in [8] experiments. According to [9], the inclusion of 5 percent coal fly ash in the roof tile composite resulted in better mechanical and physical qualities necessary for roof tiles. This study by [10] employed ceramic waste to produce roof tiles by the geopolymerization reaction process and found that the waste is rich in silica and alumina, which boosts its potential for manufacturing roof tiles by the geopolymerization method. Compared to traditional roof tile production, this approach minimises CO_2 emissions. An investigation of the performance of solar roof tiles reinforced with phase change materials by [11] discovered that in winter days, the energy output is 4.1% greater than solar roof tiles without phase change materials. Sludge incorporated fired clay roof tiles were found to be 22.9 percent stronger than traditional tiles when it came to transverse breaking strength, with up to 20 percent clay replacement acceptable for reduced water absorption standards, and 20 percent sludge-incorporated tiles reduced the indoor temperature by 2.8 percent than traditional tiles. Polymer composites reinforced with seashell powder and waste plastic particles were shown to have a higher wear resistance when these materials were used, according to [12], some improvement in the wear resistance was achieved by using seashell powder. With ageing analysis, [12] investigated how the mechanical properties of a PS fiber-reinforced polymer composite filled with palm seed powder changed. They found that the hardness of PS fibers with 15% palm seed powder increased by 30% when compared to the PS fibers with 10% palm seed powder. It has been shown that silica sand has a greater impact on the wear rate and limits pore forms, which also reduces water absorption and boosts the wear resistance of hybrid polymer composites, according to Parkunam et al. According to [13], the minimum water intake levels were discovered to be 10 wt% jute fiber, 30% waste plastic particle addition, and 10% NaOH treatment for a polymer composite with jute fiber reinforcing. [14] gave a common fiber with few advantages, despite the fact that it also has some significant disadvantages as a solution for reduced mechanical properties. An alternative to traditional roofing materials is created by reinforcing jute plants' natural fibers. Waste tile powder filler is employed because pore formation is the most common fault in composites with natural fiber reinforcing. Following typical ageing procedures, the material's wear rate and hardness are assessed, and the findings are evaluated using ANOVA to determine the degree of discrepancy between the actual results and those anticipated using fuzzy logic.

2. Materials and Methods

Many natural and synthetic fibers are reinforced into the polymer matrix and their properties were tested for various applications. The mechanical qualities of materials degrade as they are exposed to the outside world. An alternative roofing tile material must have features such as less water absorption, abrasion, and corrosion as well as good strength and wear resistance in order to compete with traditional roofing tiles. Abrasion wear properties must be increased if the material is used on roofs, where it will be subjected to higher wear. Naturally occurring jute fiber is utilised as reinforcement in this project. Jute fiber is obtained via retting, stripping, and drying jute plants, all of which are included in the extraction process. The final jute fiber can either be utilised as raw long strands or woven into a cloth and then used as reinforcement for other materials [15, 16]. Various amounts of sodium hydroxide (NaOH) are employed in this experiment to cure woven jute fibers. Untreated fibers are hydrophilic and have poor wetting qualities when supplemented with polymers. The NaOH treatment is applied to all of the weaved fibers, and then, they are thoroughly cleaned and dried.

Hard powder fillers are commonly used to enhance the material's wear properties. The more porous a material is, the more faults it has and the lower its characteristics will be. Fillers will reduce the porosity and improve both the surface and core characteristics of the material by increasing its density [17, 18]. In this project, discarded tile powder is employed as a filler in predetermined amounts. Micron-sized ceramic tiles are ground and powdered to produce the tile powder, which is sieved at various stages of grounding. The powder is sieved to ensure a consistent particle size. Clay, silica, and a small amount of feldspar or flint make up the porcelain tile. Porcelain tiles are made up of silica and clay, which contribute to its hardness, corrosion resistance, and abrasion resistance. The hand layup technique is followed by compression moulding, which results in the

Table 1: L9 experimental design with results.

Jute fiber percentage	Percentage of tile powder	Chemical treatment	Wear index in g/min	Shore D hardness
5	3	No treatment	0.27	79
5	6	5% NaOH	0.19	82
5	9	10% NaOH	0.15	83
10	3	5% NaOH	0.26	73
10	6	10% NaOH	0.21	77
10	9	No treatment	0.12	81
15	3	10% NaOH	0.26	69
15	6	No treatment	0.19	72
15	9	5% NaOH	0.11	77

creation of the composite. Porosity due to blow holes can result from hand layups without compression moulding. They are expelled and completed in accordance with prescribed dimensions after curing. The wear and hardness qualities of the fabricated specimens were examined using ANOVA and fuzzy logics, and the results were optimized.

2.1. Ageing Process. After a period of exposure to weather, the materials must be examined for their physical and mechanical qualities in applications like roof tiles. A material's tensile strength can be affected by its exposure to the elements. As a result, hygrothermal ageing is used in which the materials are subjected to thermal heating and cooling conditions as prescribed by the standards, which takes a longer period of time. Testing for mechanical strength was done after the ageing process. The ageing process was carried out in accordance with CSN EN ISO9142 requirements, which called for temperatures ranging from 70°C to -40°C with humidity levels ranging from 50% to 90%. After 16 hours in a deterioration chamber with 90 percent humidity, the specimens were kept at a reduced temperature for three hours before being kept at their highest temperature for five hours with 50 percent humidity. One cycle is completed by repeating this procedure for the whole 24 hours. The specimens are subjected to a wear test after ageing for 35 cycles, which equals 840 hours.

2.2. Abrasive Wear Test. The ASTM G99-17 technique is followed in order to determine a material's wear resistance [19–21]. The pin on the disc wear tester was used to determine the wear index of the material under consideration. Abrasive wear tests and sliding wear tests are the most commonly used for polymer composites, and they are both performed at the same time. Abrasive wear is measured by bringing the specimen into direct contact with the rotating disc, while sliding wear is measured by coating the disc with a layer of abrasive particles of the same grit size and subjecting the material to abrasive wear. During this task, the specimen is subjected to an abrasive wear test with a load of 10 N and a disc speed of 100 rpm for a total of 9 minutes under various conditions. The specimens are trimmed so that they will fit into the pin of the wear testing device. The original weights of the specimens are recorded before they are subjected to testing. The remaining testing parameters, such as the sliding velocity distance and the temperature, were kept at 10 rad/sec, 75 metres, and 30 degrees Celsius, respectively, throughout the experiment. Equation (1) was used to calculate the wear index (or wear rate).

$$\text{Wear Index (WI) in} \left(\frac{\text{grams}}{\text{Minute}}\right) = \frac{W_1 - W_2}{T} \times 1000, \quad (1)$$

where W_1 is the weight of the sample before test in grams, W_2 is the weight of the sample after test in grams, and T is the time of test cycle in minutes

2.3. Shore D Hardness. As part of a comprehensive evaluation of a polymer composite's wear qualities, hardness must also be taken into consideration. Adding ceramic powders, metallic additives, etc., to polymer composites improves their hardness [22–24]. Polymer composite hardness cannot be adjusted by heat treatment procedures, unlike metals, which can be made harder by adding fillers or heat treating. The Shore D hardness tester, which is compact and provides immediate hardness readings, is used to measure the hardness of the samples in this study. The hardness of the samples is determined using the ASTM D2240 method. The indenter on the hardness tester is a hardened steel rod with a conical tip angle of 30 [1]. Using a continuous 5 kg load, a specimen is tested in five separate sites and the average readings are recorded. Table 1 shows the average hardness values of the composites with various compositions.

3. Results and Discussion

Taguchi's method was utilised to determine an experimental design in which a new composite was to be made using the proposed method; there are nine distinct designs that can be generated by modifying the combination of input elements, which are entered into MINITAB. The experimental outcomes of the nine designs are then fed and examined through regression analysis after they have been defined as input factors. When compared to other methods, Taguchi requires fewer experimental variables and yields more accurate results in fewer runs.

Table 2: Process attributes and steps.

Sl. No.	Attributes	Units	Steps		
			1	2	3
1	Constitution of jute fiber	Wt.%	10	20	30
2	Constitution of waste tile powder	Wt.%	5	10	15
3	Chemical concentration	%	No treatment	5	10

Table 3: Analysis of variance for wear and hardness.

ANOVA for abrasive wear					
Source	DF	Adj SS	Adj MS	*F* value	*P* value
Regression	3	0.017833	0.005944	15.11	0.006
Jute fiber percentage	1	0.002017	0.002017	5.13	0.073
Waste tile powder percentage	1	0.015	0.015	38.14	0.002
Chemical treatment	1	0.000817	0.000817	2.08	0.209
Error	5	0.001967	0.000393		
Total	8	0.0198			
ANOVA for hardness					
Source	DF	Adj SS	Adj MS	*F* value	*P* value
Regression	3	158.833	52.9444	128.78	<0.0001
Jute fiber percentage	1	60.167	60.1667	146.35	<0.0001
Waste tile powder percentage	1	96	96	233.51	<0.0001
Chemical treatment	1	2.667	2.6667	6.49	0.051
Error	5	2.056	0.4111		
Total	8	160.889			

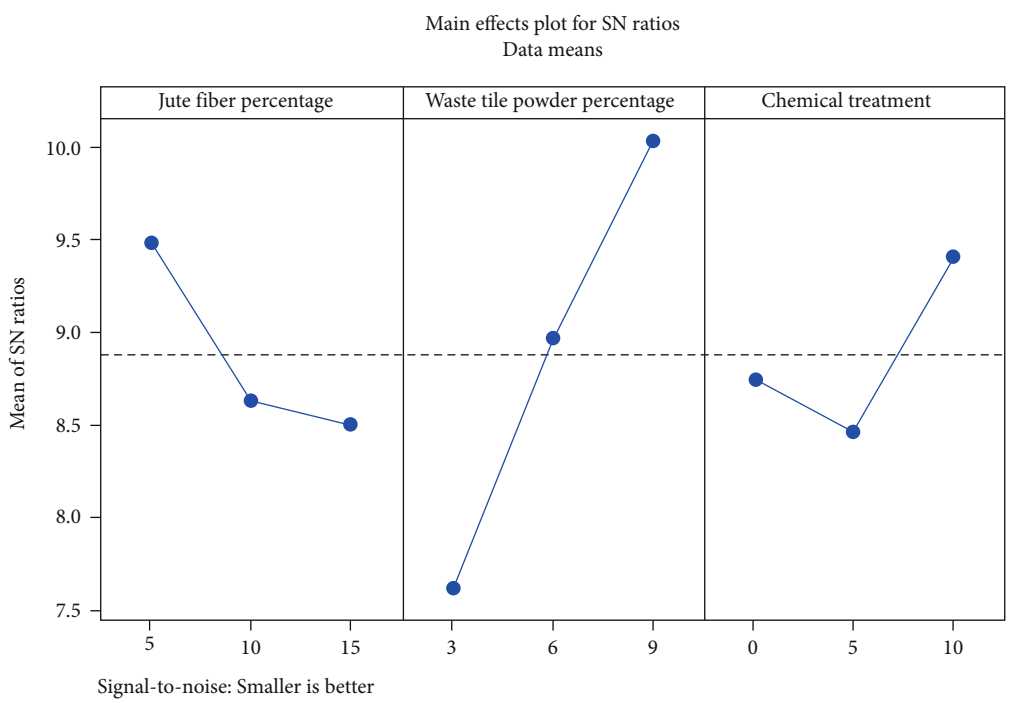

Figure 1: Main plot for effectiveness.

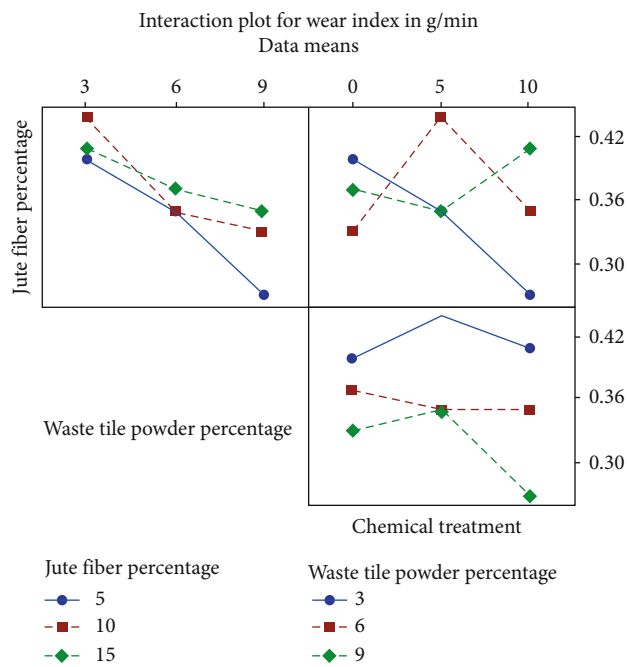

Figure 2: Plot to determine the interactions.

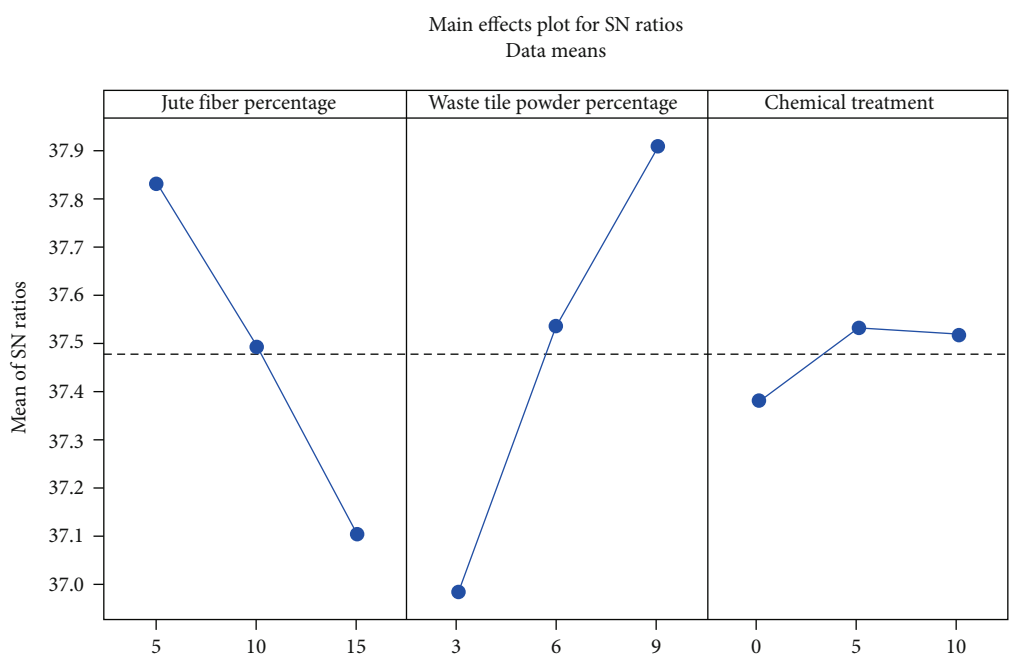

Figure 3: Main effect plot.

$$\begin{aligned}\text{Wear Index in g/min} &= 0.4383 + 0.00367\,(\text{Jute Fiber Percentage})\\ &\quad - 0.01667\,(\text{Waste Tile Powder Percentage})\\ &\quad - 0.00233\,(\text{Chemical Treatment}),\end{aligned} \tag{2}$$

$$\begin{aligned}\text{Shore D Hardness} &= 72.556 - 0.6333\,(\text{Jute Fiber Percentage})\\ &\quad + 1.333\,(\text{Waste Tile Percnetage})\\ &\quad + 0.1333\,(\text{Chemical Treatment}).\end{aligned} \tag{3}$$

Regression equations (2) and (3) were derived from the MINITAB software while ANOVA was used to improve the results. Taguchi's orthogonal array was used to create the experimental design. The regression equation is constructed based on the uploaded data. Using these two equations, we can get the relationship between the wear index in g/min and the Shore D hardness.

There are three tiers of input factors indicated in Table 2. Using MINITAB software, Taguchi's experimental design—L9 orthogonal array—was built, and the input

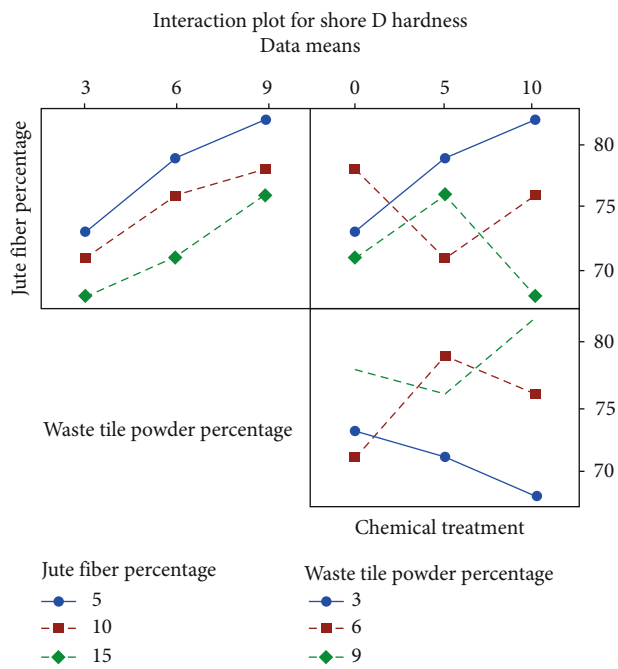

Figure 4: Interaction plot.

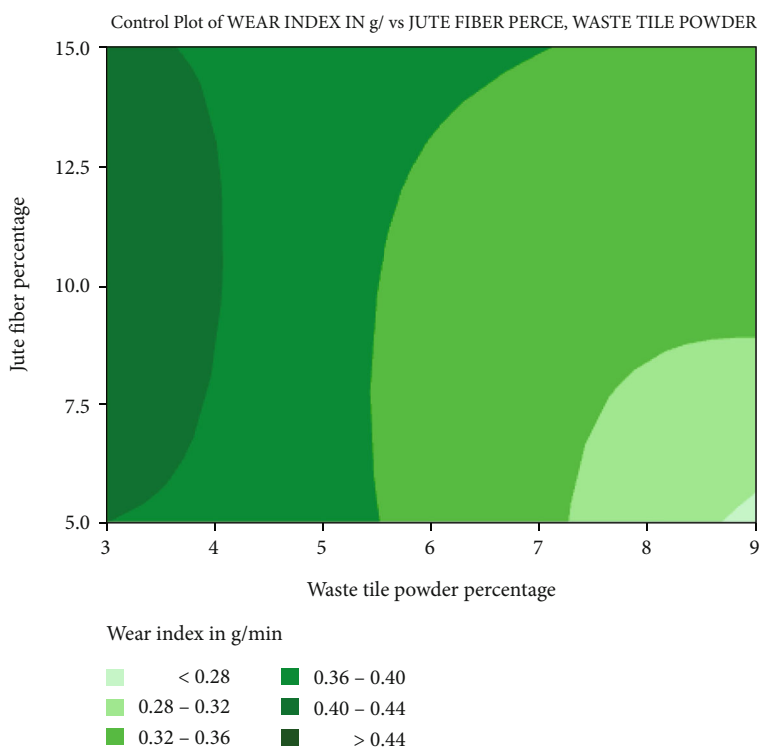

Figure 5: Contour plot for minimum wear index.

factors were shuffled in nine different combinations. The input variables were recognised as jute fiber, waste tile powder, and chemical treatment for the fiber, and the composite samples were manufactured by hand layup in accordance with the design. Table 1 lists the wear index and hardness findings from the experiments. The results were entered into the regression analysis software. As a result of conducting regression analysis, the most significant input element can be identified, as well as the model's relevance. Table 3 shows the ANOVA data for wear index and hardness, and the Fisher value establishes which component has the most impact on the output. Both equations (2) and (3) are

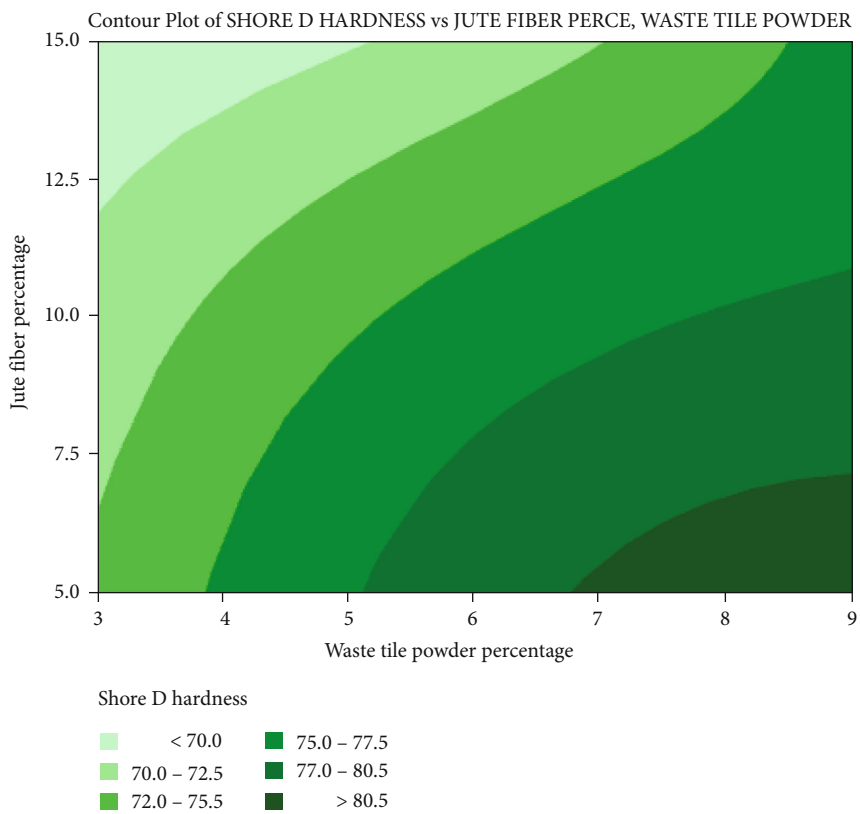

Figure 6: Contour plot for higher hardness.

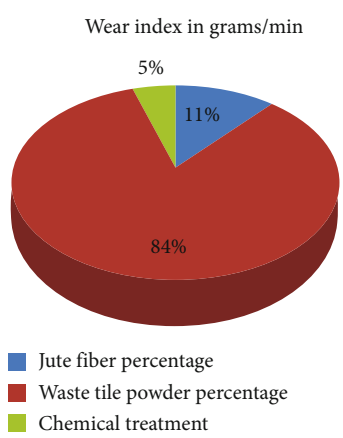

Figure 7: Plot to determine the contribution of factors for optimum results.

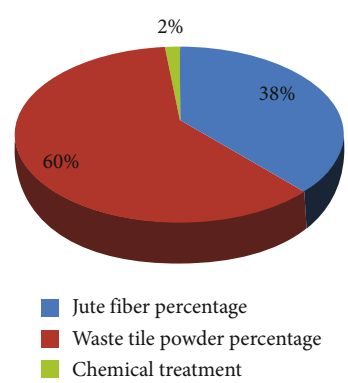

Figure 8: Contribution plot.

regression equations for wear and hardness. Waste tile powder has the greatest impact on both outputs, according to the ANOVA table data. The hardness of a material's surface determines its wear resistance. If the material's surface is less firm, the rubbing material will be able to readily remove the material's surface. So, if the material is more robust, it can withstand greater wear and tear. The hardness and wear resistance of this composite are influenced by the inclusion of waste tile powder. Hardness is increased when ceramics are applied to any other material, which is why ceramic tiles have a higher hardness than other materials. Although the fibers have been treated with chemicals, their attachment to the matrix will not be as strong as with synthetic fibers. Only to a limited extent will the fibers' binding characteristics be improved by chemical treatments. Using the regression square value, we were able to calculate that the model's significance is 90.07 percent and 98.72 percent, respectively, for the wear index and hardness.

The results of a regression analysis can be verified using a variety of charts. If you look at the main effect and interaction plots for wear index in Figures 1 and 2 and for Shore D hardness in Figures 3 and 4, you can get a sense of the relative importance of the various variables. Figures 5 and 6 exhibit contour plots for wear index and hardness, respectively, which demonstrate the optimal input factor for

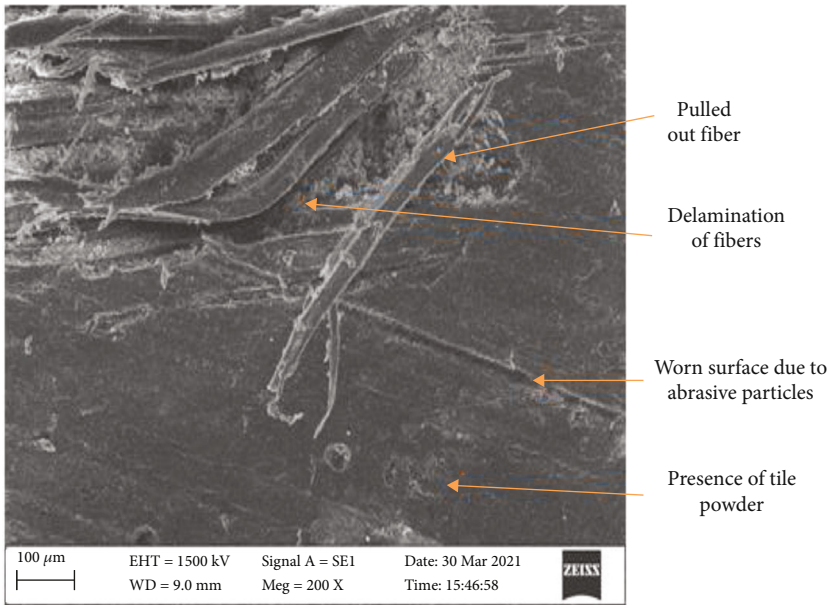

Figure 9: Microstructural image of the composite.

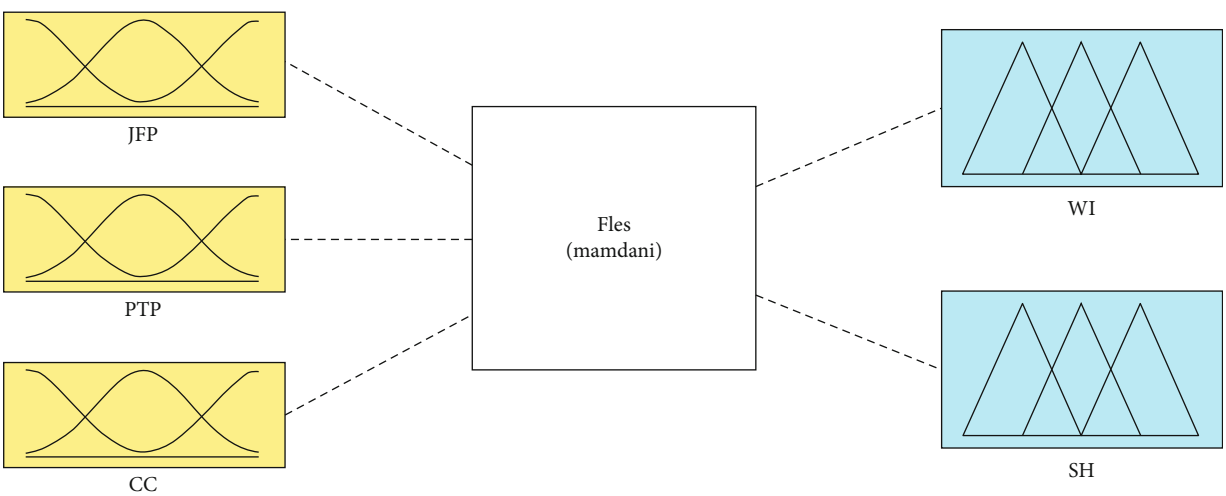

Figure 10: Input, process, and output model of a fuzzy logic system.

achieving the desired result. Figures 7 and 8 provide a pie chart depicting the contribution of each input component to each output. Fillers, such as ceramic powders, may help to improve surface qualities like wear and hardness by providing additional tensile strength. During the curing process, these fillers help to prevent or limit the creation of tiny pores. Curing causes the trapped air in composites to rise to the surface, where it tries in vain to escape. Composite surfaces might have pores that are filled with resin or left as they are because of the air that is escaping from them. Addition of fillers enhances surface characteristics and reduces the number of pores by filling the blowholes and decreasing the number of pores on the surface. Maximum use of tile powder and minimum use of jute fiber are necessary to get the lowest wear index and highest hardness outcomes. Contour plots can confirm this.

3.1. Microscopic Analysis. SEM pictures are taken and analysed to study the specimen's microstructure. It was taken on the surface that is exposed to abrasive wear testing. Figure 9 shows that the friction caused by the abrasive particles causes the jute fibers to be yanked out of their initial position. Because of this, it was clear that the fiber-matrix bond was not strong enough to survive the wear and tear of the rubbing. In some cases, the delamination may be caused by old age. The sample is free of defects like blowholes and cracks, indicating that it was manufactured correctly. In addition to being located on the surface, the waste tile powder was also found in the sample's core.

3.2. Fuzzy Logic Optimization. In addition to the ANOVA analysis, Matlab was used to perform the optimization with fuzzy logic. Numerous inputs and multiple outputs are possible in a

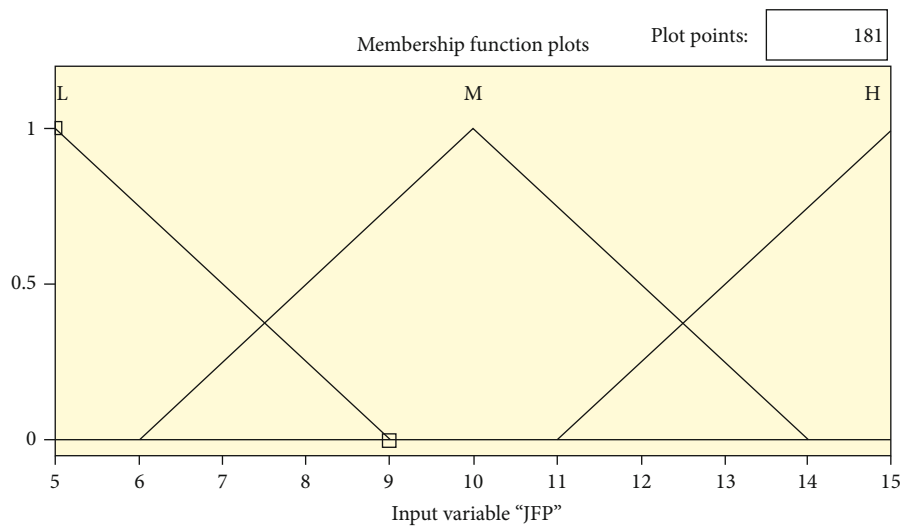

(a)

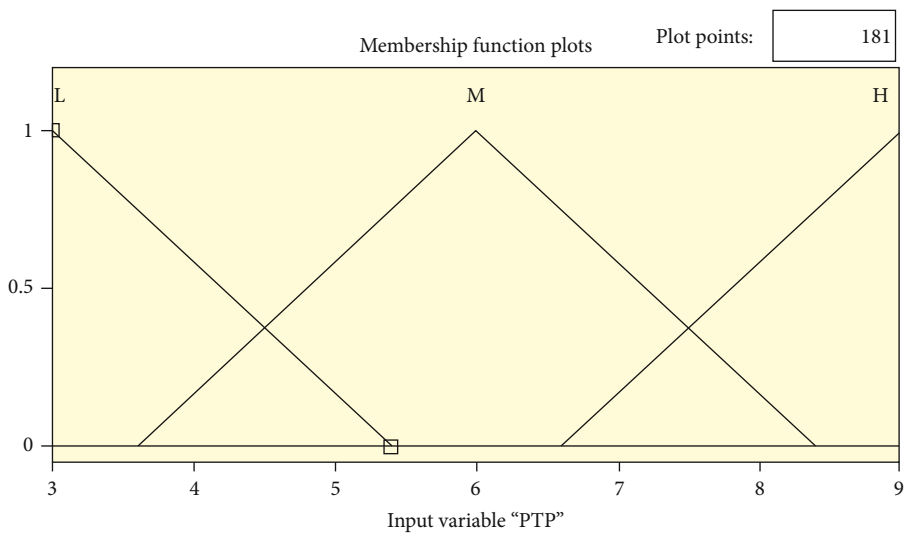

(b)

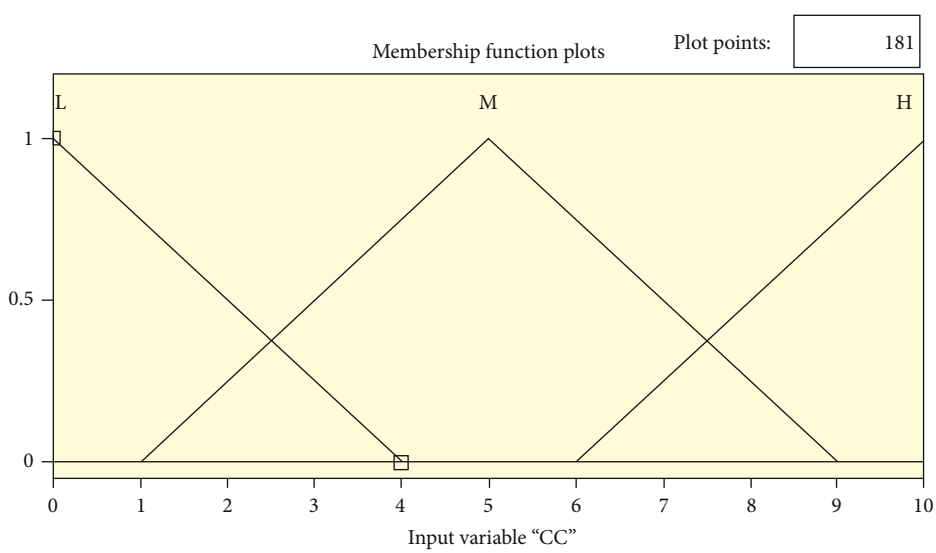

(c)

Figure 11: Continued.

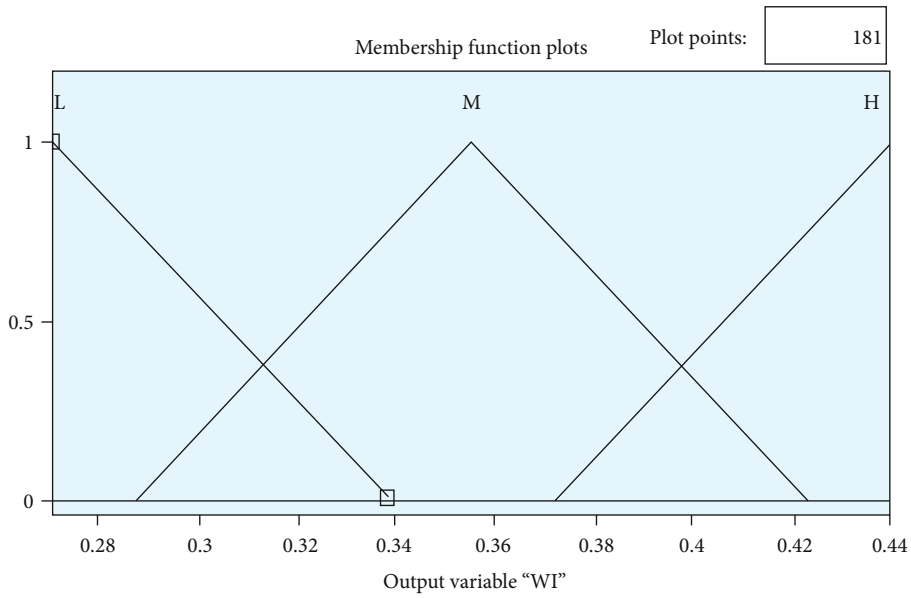

(d)

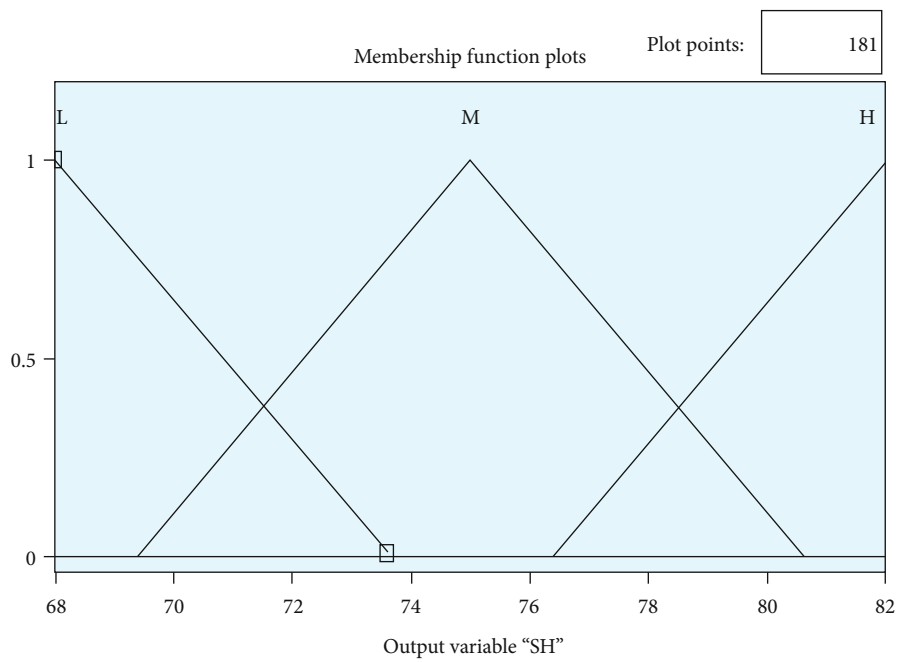

(e)

Figure 11: Input and output levels with membership function plots.

fuzzy logic system. Figure 10 depicts an example of fuzzy logic. Three inputs and two outputs were processed in this case. When a set of rules are supplied to the Mamdani, it uses those rules to make predictions about what the output values will be. Fuzzification and defuzzification take happen in the input and output sections, respectively [25]. The current variables are used to specify the range of the input and output values, and the membership functions are defined. Accuracy may be affected as membership functions are added. Figures 11(a)–11(e) show the membership functions for the input and output taken. Low, medium, and high levels of input were available for the user to choose from [26]. The rule editor supplied a rule for each input. The criteria are formulated based on the outcomes of experiments and information gleaned from the literature. Figure 12 shows the fuzzy logic rule set, while Table 4 shows the fuzzy logic predicted values and the actual experimental values. There is a breakdown of the difference between the experimental and anticipated values in that table. Shore D hardness had an accuracy of 97.91 percent, and wear index had an accuracy of 96.76 percent in this example, which is satisfactory. Figures 13 and 14 show the actual test readings and anticipated values shown on a graph, with error bars appended to show the percentage of variance. All samples, with the exception of one or two, exhibit very little variation from the projected values. In

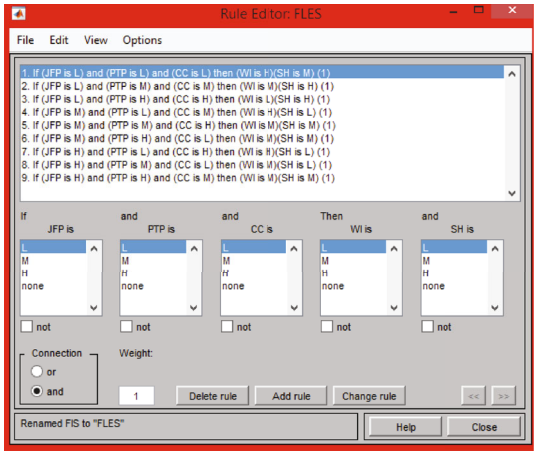

Figure 12: Rules framed in rule editor.

Table 4: Error percentage between actual experimental values and predicted values.

Specimen number	Wear index (grams/min)			Shore D hardness		
	Actual value	Fuzzy predicted	Error%	Actual value	Fuzzy predicted	Error%
1	0.4	0.418	4.306	73	75	2.667
2	0.35	0.35	0.000	79	80.2	1.496
3	0.27	0.29	6.897	82	80.2	2.195
4	0.44	0.41	6.818	71	69.8	1.690
5	0.35	0.35	0.000	76	75	1.316
6	0.33	0.35	5.714	78	75	3.846
7	0.41	0.41	0.000	68	69.8	2.579
8	0.37	0.35	5.405	71	69.8	1.690
9	0.35	0.35	0.000	76	75	1.316
Error percentage			3.2378			2.0883
Accuracy percentage			96.7622			97.9117

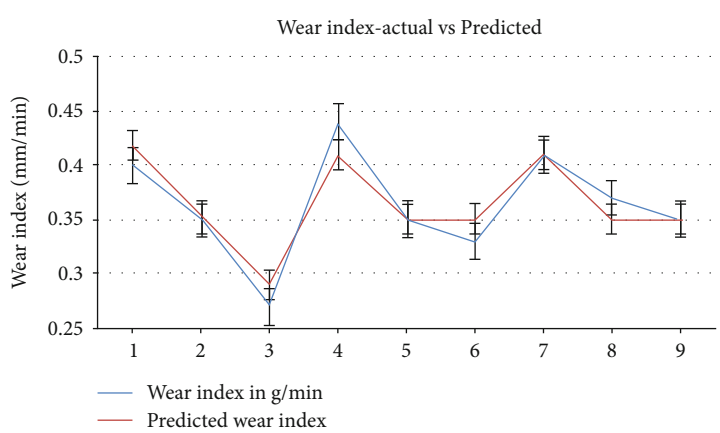

Figure 13: Graph between actual wear index and predicted values.

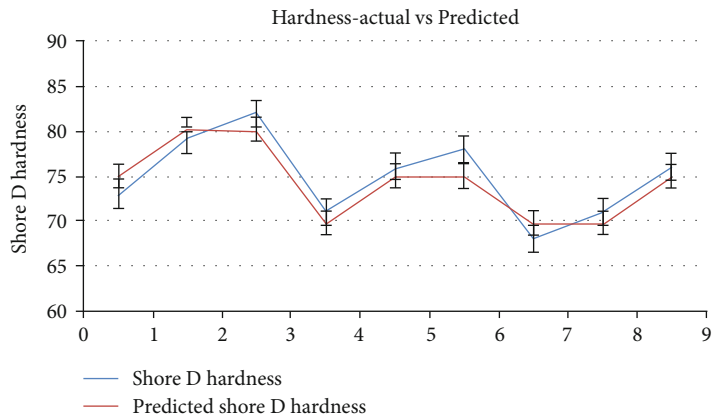

Figure 14: The graph between actual Shore D hardness and predicted hardness values.

other words, it shows that the sample was made and evaluated correctly and that the model is important.

4. Conclusion

To achieve a lower wear index, a high proportion of ceramic powder formed by powdering waste tiles should be used, and the influence of this powder should be the greatest when compared to the addition of jute fiber or the chemical treatment applied to the tiles. In this study, the jute fiber and waste tile powder were used as reinforcement in an epoxy matrix, and the composite samples were made using the hand layup method, which was described previously. The wear index of the generated samples was determined by executing an abrasive wear test on a pin on a disc wear testing machine. The results were then analysed. When employing a Shore D hardness tester, the Shore D hardness of the samples can be determined immediately from the results. Prior to conducting the wear and hardness tests, the samples were subjected to an ageing procedure in which they were maintained at higher temperatures for a specific duration of time and then cooled for a specific period of time while maintaining a regulated level of humidity during the process. After the experiments were completed, the findings were entered into the programme for ANOVA analysis in order to determine the affecting input factor and the optimum value. The findings of the regression predicted that the inclusion of waste tile powder will increase the wear resistance and hardness of the final product. The specimen composition including 15 weight percent jute fiber, 9 weight percent waste tile powder, and jute fiber that had been treated with 5 percent NaOH had the lowest wear index when compared to the other specimen compositions tested. At the same time, specimens created with a 5 weight percent jute fiber addition, a 9 weight percent tile powder inclusion, and a 10 percent NaOH treatment have a higher hardness than those manufactured without these additions.

For extra support, a fuzzy logic optimization procedure was followed, in which the difference between the software's predicted and actual value was calculated, and the accuracy was finally determined to be within an acceptable range of error. Microstructural analysis performed after the wear test confirmed the presence of tile powder all over the surface, and delamination occurred as a result of the wear test. The ageing process weakens the fiber, resulting in a reduction in its stiffness and strength. It is also possible to broaden the scope of the job by conducting tests to assess the tensile and flexural modulus of the steel, as well as corrosion analyses. Engineers can select the appropriate material for the correct application in real life based on the results of these tests.

Data Availability

The data used to support the findings of this study are included in the article. Should further data or information be required, these are available from the corresponding author upon request.

Disclosure

It was performed as a part of the employment at Hawassa University, Ethiopia.

Conflicts of Interest

The authors of this article declare that we have no conflict of interest.

Acknowledgments

The authors appreciate the technical assistance to complete this experimental work from the Department of Mechanical Engineering, K. Ramakrishnan College of Engineering, Tiruchirappalli. The authors thank the technical assistance to complete this experimental work.

References

[1] S. Dinesh, P. Kumaran, S. Mohanamurugan et al., "Influence of wood dust fillers on the mechanical, thermal, water absorption and biodegradation characteristics of jute fiber epoxy composites," *Journal of Polymer Research*, vol. 27, no. 1, p. 9, 2020.

[2] S. Ramakrishnan, K. Krishnamurthy, G. Rajeshkumar, and M. Asim, "Dynamic mechanical properties and free vibration

characteristics of surface modified jute fiber/nano-clay reinforced epoxy composites," *Journal of Polymers and the Environment*, vol. 29, no. 4, pp. 1076–1088, 2021.

[3] M. Pawar, "Investigation on mechanical and thermo-mechanical properties of granite powder filled treated jute fiber reinforced epoxy composite," *Polymer Composites*, vol. 38, no. 4, pp. 736–748, 2017.

[4] K. Manohar Reddy and B. Chandra Mohana Reddy, "Mechanical characterization of chemically treated used jute fiber reinforced epoxy composite with SiC fillers," *Materials Today: Proceedings*, vol. 37, no. 2, pp. 917–921, 2021.

[5] P. Kaushik, J. Jaivir, and K. Mittal, "Analysis of mechanical properties of jute fiber strengthened epoxy/polyester composites," *Engineering Solid Mechanics*, vol. 5, no. 2, pp. 103–112, 2017.

[6] P. Krishnasamy, G. Rajamurugan, and M. Thirumurugan, "Dynamic mechanical characteristics of jute fiber and 304 wire mesh reinforced epoxy composite," *Journal of Industrial Textiles*, vol. 51, no. 4, pp. 540–558, 2019.

[7] P. T. R. Swain and S. Biswas, "Abrasive wear behaviour of surface modified jute fiber reinforced epoxy composites," *Materials Research*, vol. 20, no. 3, pp. 661–674, 2017.

[8] E. Momoh, "Suitability of oil-palm-broom-fibres as reinforcement for laterite-based roof tiles," *IJournals: International Journal of Software & Hardware Research in Engineering*, vol. 5, no. 4, pp. 27–35, 2017.

[9] A. Kantürk Figen, Ü. Özçay, and S. Pişkin, "Manufacturing and characterization of roof tiles a mixture of tile waste and coal fly ash," *Journal of Natural and Applied Sciences*, vol. 21, no. 1, pp. 224–229, 2017.

[10] A. R. G. Azevedo, C. M. F. Vieira, W. M. Ferreira, K. C. P. Faria, L. G. Pedroti, and B. C. Mendes, "Potential use of ceramic waste as precursor in the geopolymerization reaction for the production of ceramic roof tiles," *Journal of Building Engineering*, vol. 29, article 101156, 2020.

[11] M. A. Alim, Z. Tao, M. J. Abden, A. Rahman, and B. Samali, "Improving performance of solar roof tiles by incorporating phase change material," *Solar Energy*, vol. 207, pp. 1308–1320, 2020.

[12] G. Sakthi Balan, V. Santhosh Kumar, S. Rajaram, and M. Ravichandran, "Investigation on water absorption and wear characteristics of waste plastics and seashell powder reinforced polymer composite," *Jurnal Tribologi*, vol. 27, pp. 57–70, 2020.

[13] N. Parkunam, G. Navaneethakrishan, S. Saravanan, B. Sureshkumar, and Sathishkumar, "Mechanical characterization of hybrid laminates composites," *Materials Today: Proceedings*, vol. 21, no. 1, pp. 15–18, 2020.

[14] R. Karthick, S. Gopalakrishnan, and C. Ramesh, "Characterization of palmyra fiber and polyester resins composite," *International Journal of Emerging Trends in Science and Technology*, vol. 6, no. 2, 2020.

[15] A. Dilfi, A. Balan, H. Bin, G. Xian, and S. Thomas, "Effect of surface modification of jute fiber on the mechanical properties and durability of jute fiber-reinforced epoxy composites," *Polymer Composites*, vol. 39, no. S4, pp. E2519–E2528, 2018.

[16] H. Wang, H. Memon, E. Hassan, M. S. Miah, and M. A. Ali, "Effect of jute fiber modification on mechanical properties of jute fiber composite," *Materials*, vol. 12, no. 8, p. 1226, 2019.

[17] B. Shivamurthy, N. Naik, B. H. S. Thimappa, and R. Bhat, "Mechanical property evaluation of alkali-treated jute fiber reinforced bio- epoxy composite materials," *Materials Today: Proceedings*, vol. 28, no. 4, pp. 2116–2120, 2020.

[18] A. Kumar and A. Srivastava, "Preparation and mechanical properties of jute fiber reinforced epoxy composites," *Industrial Engineering & Management*, vol. 6, no. 4, p. 1000234, 2017.

[19] D. Kurz and R. Nawrowski, "Thermal time constant of PV roof tiles working under different conditions," *Science*, vol. 9, no. 8, p. 1626, 2019.

[20] G. H. M. J. Subashi de Silva and M. P. D. P. Mallwattha, "Strength, durability, thermal and run-off properties of fired clay roof tiles incorporated with ceramic sludge," *Construction and Building Materials*, vol. 179, pp. 390–399, 2018.

[21] G. Sakthi Balan, M. Ravichandran, and V. Santhosh Kumar, "Study of ageing effect on mechanical properties of Prosopis juliflora fibre reinforced palm seed powder filled polymer composite," *Australian Journal of Mechanical Engineering*, vol. 18, pp. 1–13, 2020.

[22] G. Navaneethakrishnan, T. Karthikeyan, S. Saravanan et al., "Structural analysis of natural fiber reinforced polymer matrix composite," *Materials Today: Proceedings*, vol. 21, no. 1, pp. 7–9, 2020.

[23] G. Navaneethakrishnan, T. Karthikeyan, S. Saravanan, and V. Selvam, "Influence of boron nitride on morphological, mechanical, thermal and wear characteristics of epoxy nanocomposites," *Materials Research Innovations*, vol. 24, no. 5, pp. 257–262, 2020.

[24] A. K. Sinha, H. K. Narang, and S. Bhattacharya, "Experimental determination, modelling and prediction of sliding wear of hybrid polymer composites using RSM and fuzzy logic," *Arabian Journal for Science and Engineering*, vol. 46, no. 3, pp. 2071–2082, 2021.

[25] R. Vinayagamoorthy, I. V. Manoj, G. Narendra Kumar, I. Sai Chand, G. V. Sai Charan Kumar, and K. Suneel Kumar, "A central composite design based fuzzy logic for optimization of drilling parameters on natural fiber reinforced composite," *Journal of Mechanical Science and Technology*, vol. 32, no. 5, pp. 2011–2020, 2018.

[26] J. E. Soares Filho, Aurich, Sousa, Nascimento, Paskocimas, and Silva, "Polishing performance of eco-friendly porcelain stoneware tiles reusing bricks and roof tiles wastes," *Journal of Cleaner Production*, vol. 256, article 120362, 2020.

Hindawi
International Journal of Polymer Science
Volume 2021, Article ID 1014531, 13 pages
https://doi.org/10.1155/2021/1014531

Review Article

Research Progress on Durability of Cellulose Fiber-Reinforced Cement-Based Composites

Jie Liu[1] and Chun Lv[2]

[1]*College of Light-Industry and Textile Engineering, Qiqihar University, Qiqihar 161006, China*
[2]*College of Architecture and Civil Engineering, Qiqihar University, Qiqihar 161006, China*

Correspondence should be addressed to Chun Lv; lvchun8603@163.com

Received 15 April 2021; Revised 26 June 2021; Accepted 31 July 2021; Published 17 August 2021

Academic Editor: Ching Hao Lee

The performance of cellulose fiber-reinforced cement-based composites (CFCCs) depends not only on the characteristics of the cement matrix and fibers but also on the bonding property of the matrix and fibers. The durability of cement-based composites including various properties such as impermeability, frost resistance, and carbonization resistance has an important impact on the long-term service life of the matrix structure. The presence of a large number of hydroxyl groups on the molecular chain of cellulose can promote the formation of intra- and intermolecular hydrogen bonds of cellulose. This special structure imparts the cellulose high hydrophilicity, which leads the cement hydration C-S-H gel to adhere to the surface of cellulosic fibers (CFs) and induce its growth. The cavity of CFs has good water absorption and can be used as an internal curing fiber for the continuous hydration of cement-based composites. But CFs in the Portland cement matrix tend to deteriorate under strong alkali conditions. This paper presents a review of the research on the durability of CFCCs. The methods and paths to improve the durability of CFCCs are summarized and analyzed from the perspectives of the internal curing of CFs, the deterioration of the performance of CFs in the matrix, and the use of many types of supplementary cementitious materials. Finally, the development and engineering application of CFCCs have been prospected.

1. Introduction

In the last few years, more and more different types of fibers have been used to reinforce cement-based composites. As is known, these fibers include steel, organic synthetic, carbon, and glass fibers. The commonly used fibers for reinforcements exhibit a set of advantages, such as long application time, relatively mature technology, and interesting physical and mechanical properties. However, compared to CFs, the commonly used fibers have their own limitations [1]. As far as we know, the density of steel fibers is relatively large, which cannot meet the requirements of reducing the weight of composites. At the same time, the size of the steel fiber is too large, there is an interface transition zone in the cement matrix, and it also lacks inducing the growth of the hydrate gel in the cement matrix interface transition zone. The organic synthetic fiber has poor compatibility with the cement matrix and is not easy to disperse in the cement matrix. It pollutes the environment greatly, which is contrary to the concept of green cement-based composites [2–4]. The carbon fiber is easy to agglomerate in the cement matrix, and the cost is relatively high [5–8]. The glass fiber is brittle and has poor wear resistance [9, 10].

Plant fibers such as crop straws are composed of cellulose, hemicellulose, lignin, and other substances, and cellulose is the main component. CFs are widely found in nature. They are inexpensive, have low density, are renewable, are biodegradable, are rich in sources, and have good reinforcement effects on cement-based composites [11–13]. The geometric characteristics, mechanical properties, volume mixing ratio of CFs, and bonding property of the fiber and matrix interface are important factors that affect the strength and toughness of the matrix. Compared with traditional fibers, CFs have a larger specific surface area, aspect ratio, excellent toughness, and bonding ability. It disperses evenly in the cement matrix, has good compatibility, and has a filling and bridging effect on the cement matrix [14]. At the same time, the addition of CFs also greatly reduces the density of cement-based

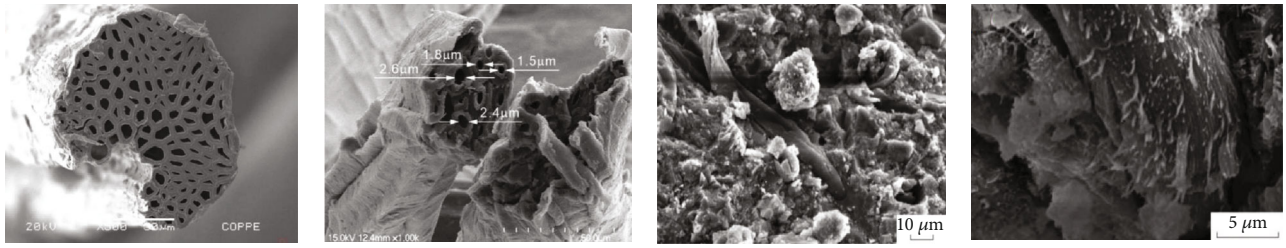

(a) (b) (c) (d)

Figure 1: SEM images of CFs. (a) Sisal fibers [39]. (b) Jute fibers [13]. (c, d) Combination of the macroscale fiber and cement matrix [37].

composites, improves their flexural strength [15–17], inhibits the occurrence and development of microcracks within the matrix [18, 19], and enhances the impact resistance of cement-based composites [20].

Over the last few years, studies on the toughening modification of cement-based composites using CFs have focused on the macromechanical properties of composites, the microstructure of the interface between the cement matrix and the fibers, the effect of fiber cracking and toughening, and the durability [21–24]. The durability of cement-based composites includes impermeability, frost resistance, carbonization resistance, and resistance to sulfate attack, which have an important impact on the long-term service life of the structure [25]. The durability of CFCCs is the main reason which limits their engineering application [26].

This paper presents a review of the research done in the area of the durability of CFCCs during the last years (2005.01-2021.05), which used Chinese journal literature retrieval databases, including China Journal Network and CNKI Scholar, English journal literature retrieval databases, and so on. Search keywords include cellulose fiber, concrete durability, internal curing, impermeability, frost resistance, and carbonization. In the searched literature, no relevant similar reviews have been found, and works of literature that are not related to the content of the paper have also been excluded. Only a few book chapters or reviews provide a general overview of the durability of CFCCs [27, 28], summarizing the main improvements and findings from a few research papers. There are also overviews of nanocellulose fibers, which are different from the contents discussed in this paper [29, 30]. The durability of CFCCs such as impermeability, frost resistance, and carbonization resistance is reviewed, and the impact of CFs on the durability of composites and the internal curing of CFs is discussed in this paper. From the perspectives of the performance, the degradation of CFs in the matrix, and the application of multiple types of auxiliary gel materials, a summary analysis is made to improve the durability of CFCCs, and the solutions are proposed.

2. Performance of CFs

As one of the most abundant renewable resources, CFs have the advantage of being low cost and environmentally friendly [31]. In 1932, scientists studied the chemical structure of cellulose [32]. Cellulose is a straight-chain polymer formed by linking countless D-glucopyranose anhydrides(1-5) with β(1-4) glycosides. The structure of cellulose is highly regular and unbranched, and the chemical formula is $(C_6H_{10}O_5)_n$. There are a large number of hydroxyl groups on the molecular chain of cellulose. The presence of this polar group promotes the formation of intra- and intermolecular hydrogen bonds of cellulose [33, 34]. CFs can be made from renewable resources such as straw, they have a porous cell structure, and their specific surface area is better than other fibers [35]. As described above, there are many pores in the cross-section of the fibers, as shown in Figures 1(a) and 1(b). The properties of CFs mainly depend on the type of cellulose. The cellulose content of different types of plants varied greatly, among which the cellulose content of cotton is the highest. Table 1 shows the performance index data of commonly used CFs and other commonly used fibers [36]. The physical and mechanical properties of CFs can be seen in Table 1. The mechanical properties of CFs such as tensile strength and Young's modulus are weaker than those of the commonly used fibers such as carbon fiber and aramid fiber. Flax, jute, ramie, sisal, and hemp fibers have better mechanical properties as similar to glass fiber in tensile strength and Young's modulus, so they can be directly used as CFCCs.

The performance of CFCCs includes working performance, mechanical properties, and durability. The effect of CFs on the working performance and mechanical properties of composites is similar to that of traditional fibers, but the impact on durability is very different. As mentioned above, the existence of a large number of hydroxyl groups on the molecular chain of cellulose promotes the formation of intra- and intermolecular hydrogen bonds of cellulose. This special structure renders the cellulose extremely hydrophilic, makes the CFs compatible with the cement matrix, and has a good cohesive force. C-S-H gel, the main hydration product of the cement, grows on the surface of CFs, as shown in Figures 1(c) and 1(d). Wu et al. [37] analyzed the SEM (Figures 1(c) and 1(d)) and found that the cement hydration around CFs was more complete. The reason is that the CFs can induce the orderly and directional growth of hydration products in the initial stage of cement hydration. After the cement hardens, when the load exceeds its cracking load, the fibers can share the load, which greatly increases the load of the cement matrix, avoiding or delaying the growth of microcracks. In Figure 1(d), the CF surface has peeled off and separated countless microfibers with a diameter less than 1 μm. Some of the microfiber ends are embedded in the cement hydration product. The formation of the

Table 1: Performance of CFs and commonly used fibers.

Fibers	Density (g/cm^3)	Elongation (%)	Tensile strength (MPa)	Young's modulus (GPa)
Cotton fiber	1.5-1.6	7.0-8.0	287-597	5.5-12.6
Jute fiber	1.3	1.5-1.8	393-773	26.5
Flax fiber	1.5	2.7-3.2	345-1035	27.6
Ramie fiber	1.5	3.6-3.8	400-938	61.4-128.0
Sisal fiber	1.5	2.0-2.5	511-635	9.4-22.0
Coir fiber	1.2	30.0	175	4.0-6.0
Cork fiber	1.5	—	1000	40.0
E-glass fiber	2.5	2.5	2000–3500	70.0
S-glass fiber	2.5	2.8	4570	86.0
Aramid fiber	1.4	3.3-3.7	3000-3150	63.0-67.0
Carbon fiber	1.4	1.4-1.8	4000	230.0-240.0

Table 2: Performance of CFs and commonly used fibers.

CFs	Length (nm)	Diameter (nm)	Tensile strength (MPa)	Young's modulus (GPa)	Ref.
Macroscale CFs (cotton)	2,000,000-3,000,000	11,540	287-597	5.5-12.6	[36]
Microcrystalline CFs	100-3,000	1,440	7,500	100.0-140.0	[37, 40, 41]
Nanocrystalline CFs	50-500	1-100			

microstructure of the cement paste will be accompanied by complex chemical reactions and physical changes. When the shrinkage of the matrix is restricted, the cement-based material will crack. The degree of cracking depends on the tensile strength and shrinkage stress of the cement paste. These microfibers play a bridging and filling role in the composites. The moisture absorbed in the CFs supplements the lack of moisture in the cement hydration process and can induce the hydration of the cement surface, and the hydration product can fill the microcracks so as to achieve the composites' effect of enhancing impermeability.

However, the lignin and hemicellulose in CFs are easily dissolved in the alkaline solution of the cement matrix, and the strong alkali material enters the fiber cavity to cause the mineralization and degradation of the fiber structure, thereby affecting the durability. The CFs applied to cement-based composites can be classified by the function of their size. CFs can be found as macroscale, microcrystalline, and nanocrystalline CFs. Macroscale CFs include strands (long fibers of lengths around 20 to 100 cm), staple fibers (short fibers with lengths between 1 and 20 cm), and pulp (very short fibers with lengths between 1 and 10 mm), which can be processed by chemical methods to form micron-scale microcrystalline CFs and nanosized nanocrystalline CFs [37, 38].

In general terms, micron-sized microcrystalline CFs and nanosized nanocrystalline CFs can be produced in chemical or enzymatic ways. The loosely arranged amorphous regions in the cellulose are destroyed, and the crystalline regions are retained to obtain micron-sized microcrystalline CFs and nanosized nanocrystalline CFs with higher crystallinity. The preparation methods of nanocrystalline CFs mainly include the physical mechanical method, acid hydrolysis method, and biological method. Nanocrystalline CFs have a rigid rod-like structure, and their properties are shown in Table 2.

3. Research Status of Durability of CFCCs

Anselme Payen, a French scientist, extracted a compound from wood in 1838 and named it cellulose. The majority of the fabrication methods for cement composites reinforced with CFs in the pulp form are based on the Hatschek process, patented by L. Hatschek in 1900 [27]. After a century, the research and application of CFCCs have become increasingly widespread. The research on CFs is from mechanical property to durability, from the bonding phenomenon between the CFs and the matrix to the bonding mechanism, and from macroscale application to microscale application. Only a few studies have been focused on the bond adhesion of CFs with cement matrices. For instance, some studies analyzed the effect of CF shape and curing age on the bond strength of CFCCs using pull-out tests [28, 42], and the other studies analyzed the fiber matrix bond adhesion indirectly [14–16].

At this stage, research studies on the durability of CFCCs include frost resistance, carbonization resistance, water penetration resistance, chloride ion penetration resistance, gas penetration resistance, sulfate erosion resistance, early anticracking performance, compressive creep performance, and compressive fatigue deformation performance. In general terms, the durability of the composites depends on the resistance to chloride ion permeability, frost resistance, and carbonization resistance. As can be seen in Table 3, it is a summary of related studies on the durability of CFCCs.

Table 3 shows that CFCCs are rich in varieties, and their durability involved a wide range, which are closely related to the service life of the composites. The test methods for resistance of CFCCs to freezing and thawing usually include slow freezing and thawing, rapid freezing and thawing, and single-side freezing and thawing. The test methods for resistance of CFCCs to chloride penetration adopt the rapid chloride

Table 3: Summary of studies on durability of CFCCs.

Durability	CFs	CFs (wt.%)	Fiber form	Cementitious	Test methods	Ref.
Antichloride ion penetration	UF500 CF	0.45~1.5	Randomly dispersed	P·O42.5	RCM method; water seepage height	[43–45]
	Bokai super fiber	0.6~1.2		P·O52.5	Water seepage pressure	[46]
Antifreezing	Flake fiber	0.9	Randomly dispersed	P·O42.5	Rapid freezing	[43, 47]
	UF500 CF	0.1~0.2				[48]
Carbonization	Cork kraft pulp	8.0	Aligned	P·II42.5R	Accelerate carbonization	[49]
	Rape straw fiber	0.5~2.00	Randomly dispersed	SAC		[50, 51]
	Coir fiber	2.0		Slag cement	12 years	[52]
Antidry and wet cycle	Sisal fiber	1.5~8.0	Randomly dispersed	P·O42.5R	CBI method	[53, 54]
	Cork CF	4.0		P·O42.5	25 dry/wet cycles	[55]
	Sisal fiber	0.6	Aligned	Calcined clay	100 dry/wet cycles	[56]
Antisulfate attack	UF500 CF	0.9	Randomly dispersed	P·II42.5R	Sulfate-wet and dry cycle coupling	[51]
Anticrack	Sisal fiber	2.0	Aligned	MK/PC	Instron 5948 test system	[57]

migration (RCM) coefficient test and coulomb electric flux test. The procedures for preparing CFCCs reported in the literature can be divided into two main groups depending on the fiber form: fibers randomly dispersed in the cement matrix [58–60] and aligned fibers or fibrous structures [43, 46, 50, 53]. In view of the fibers randomly dispersed in the matrix, it has certain limitations in the mechanical properties of reinforced composites, and aligned fibers or fibrous structures are also used to strengthen the cement matrix [49, 56, 57, 61].

Cement-based composite is a kind of porous material, which provides a channel for harmful external impurities to penetrate into the matrix. Adding CFs to the cement matrix can reduce the generation of early microcracks, inhibit the development of microcracks during the service period of the matrix, and improve the durability of CFCCs. After absorbing water, the CFs are evenly dispersed into the cement matrix, forming a plurality of microwater flow channels inside the matrix. These pores can continue to provide water for the later cement hydration, make it fully hydrated, ensure the mechanical properties of the cement matrix, prevent the cement matrix from cracking, and also improve the cement matrix's antipermeability, antifreezing, and anticarbonization capabilities. The uniform distribution of the fiber network enhances the adhesion between the matrix components, the matrix structure has good integrity, and the impact resistance is also significantly improved [62].

3.1. Impermeability of CFCCs. Impermeability is an important factor that affects the durability of CFCCs. CFs are evenly distributed in the cement matrix, which can reduce the segregation effect in the initial stage of the cement hydration, inhibit the formation of shrinkage cracks in the cement matrix, reduce the porosity of the matrix, improve the compactness of the matrix, and effectively prevent harmful substances from penetrating into the matrix. It is usually determined by the rapid chloride ion migration coefficient test or the water penetration height test [44]. The chloride ion diffusion coefficient and the water penetration height are reduced after the CFs have been mixed, and the impermeability of the CFs is better than that of the polypropylene fibers under the same dosage. The test results showed that when the CF volume fraction was 0.9%, the effect of improving the impermeability of the matrix was the best [45]. CFs have little effect on the compressive strength of the matrix but significantly improve the splitting tensile strength, axial tensile strength, and ultimate tensile value and effectively block the penetration of chloride ions. At the same time, the cracking time and the width of the matrix crack have been improved [63, 64]. It has been found through experiments that the bubble content in the CF cement matrix decreases by 40%, and the bubble spacing becomes smaller [65].

CFs are effectively bonded to the cement matrix and distributed in random directions, forming a uniform support system, optimizing the pore structure of the cement matrix, and blocking the internal communication channels of the matrix. Due to the toughening and cracking resistance of CFs, the number of initial cracks can be significantly reduced, the long-term cracks of the matrix can be effectively inhibited, and the possibility of forming through cracks in the matrix can be reduced. In this way, the microcrack pattern of the cement-based composite is further refined, and its impermeability is significantly improved.

3.2. Effect of Freeze-Thaw Cycles on the Durability of CFCCs. Due to the effect of negative temperature, the water in the pores of CFCCs in a water-saturated state freezes and produces a volume change to form tensile stress. Under the action of the freeze-thaw cycle, the cement matrix damage gradually accumulates and expands, which will eventually lead to the destruction of the cement matrix. CFs can significantly improve the frost resistance of CFCCs. On the one hand, the addition of CFs reduces the water penetration in the cement matrix. On the other hand, the CFs can absorb parts of the unfrozen free water and reduce the hydrostatic pressure in the cement matrix. A large number of comparative tests have shown that polypropylene fibers and CFs have improved frost resistance to cement-based composites [47, 66, 67], and CFs are better than polypropylene fibers.

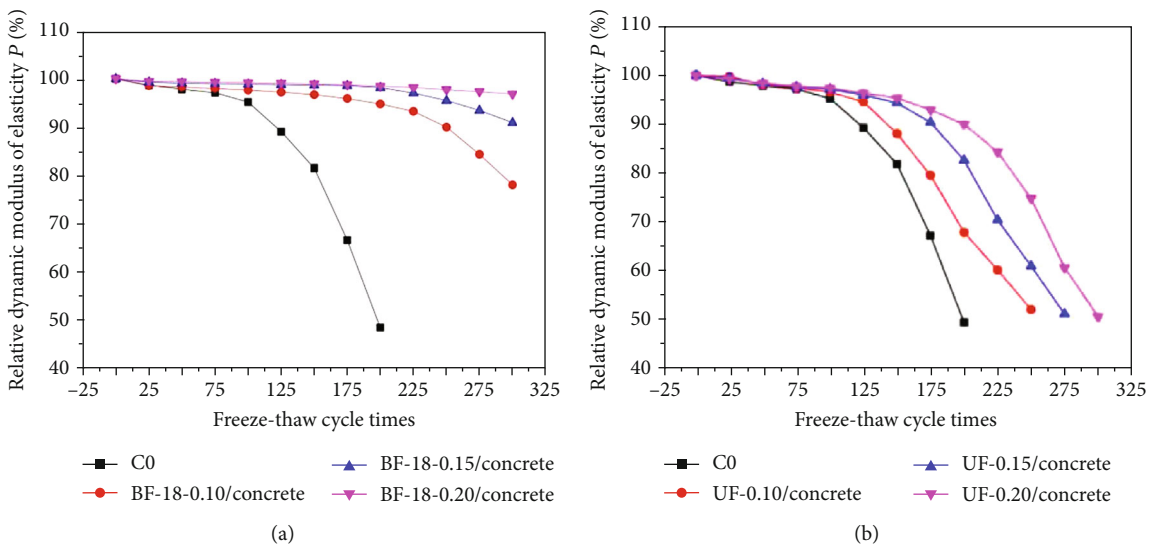

Figure 2: (a) The relative dynamic elastic modulus of basalt fibers and (b) CF with different fiber volume fraction changes with the number of freeze-thaw cycles [48].

When the volume fraction of CFs is 0.9%, the antifreezing effect of CFCCs is the best. Under the action of the freeze-thaw cycle, the CFs have the effect of binding the surface slurry of the matrix, and its appearance damage is improved to a certain extent.

The addition of CFs slows down the rate of decrease of relative dynamic elastic modulus, increases the number of freeze-thaw cycles that the test piece can withstand, and improves the frost resistance of the CFCCs; it can be seen from Figure 2 [48]. As the number of freeze-thaw cycles increases, the relative dynamic elastic modulus of the specimens decreases. At the beginning of the freeze-thaw cycle (within 100 freeze-thaw cycles), for basalt fibers and CFs, when the fiber volume fraction is 1.0, 1.5, or 2.0%, the relative dynamic elastic modulus decreases slowly, and the effect of fiber content is not much different. In the late freeze-thaw period (the number of freeze-thaw cycles is greater than 100), the decline rate increases, indicating that the internal damage of the concrete gradually increases after the freeze-thaw cycle. The relative dynamic elastic modulus of plain concrete decreases faster than that of fiber concrete. When the freeze-thaw cycle reaches 200 times, the freeze-thaw damage rate is far less than 60%. However, the relative dynamic elastic modulus of fiber-reinforced concrete with a fiber volume fraction of 2% decreases more gently than that of concrete with fiber volume fractions of 1.0% and 1.5%.

Since the elastic modulus and tensile properties of basalt fibers are higher than those of CFs, the basalt fibers can more effectively improve the tensile strength of concrete, inhibit the expansion of internal cracks in concrete, reduce the entry of water into the matrix, and delay the frost heave damage of the internal structure. Therefore, when the number of freeze-thaw cycles is high, basalt fibers improve the freeze resistance of concrete more significantly than CFs. In general, the effect of improving the frost resistance is not significant when the fiber volume fraction is increased from 1.5% to 2.0%. Therefore, it is more economical and reasonable to choose the fiber volume fraction of 1.5%.

3.3. Effect of Carbonization on the Durability of CFCCs. When CFCCs are applied as the protective layer of steel bars, the impact of carbonization on the steel bars must be paid attention to. The high alkalinity inside the matrix passivates the surface of the steel bar, and the passivated film can prevent the steel bar from corroding by the external environment. The hydration product of cement-based composites has stable performance in an alkaline environment and can maintain good cementing ability. Carbonization is the process of neutralizing the cement matrix, which can reduce the alkalinity of CFCCs and can induce the corrosion of the stressed steel bars and the destruction of the structure [68, 69]. The essence of carbonization is the diffusion process of carbon dioxide gas from the surface to the inside of the matrix. Both compactness of the matrix structure and internal defects affect the diffusion rate. The hydrophilicity and unique hollow structure of CFs optimize the pore structure of cement-based composites, which reduce internal defects and enhance carbonization resistance. In the case of loading, the generated microcracks become channels for the diffusion of carbon dioxide gas, which reduce its anticarbonization performance. After adding CFs to the matrix, the carbonization of cement-based composites is still a diffusion-dominated process [70–72].

Analysis of the pore size distribution data obtained based on the mercury intrusion experiment method shows that the fiber has a significant influence on the microstructure of cement-based composites [73]. After the fiber volume fraction reaches 0.6%, it can be observed that the unimodal width on the pore distribution curve of cement-based materials increases, and the number of large-scale pores (radius greater than or equal to 200 nanometers) increases, which confirms that the micromatrix structure is coarsened due to the introduction of fibers. The addition of fibers can change the working performance of the fresh cement paste, thereby producing an air-entraining effect [74]. At the 0.6% fiber volume fraction, the effect of this phenomenon exceeds the internal curing effect, which causes the degradation of the

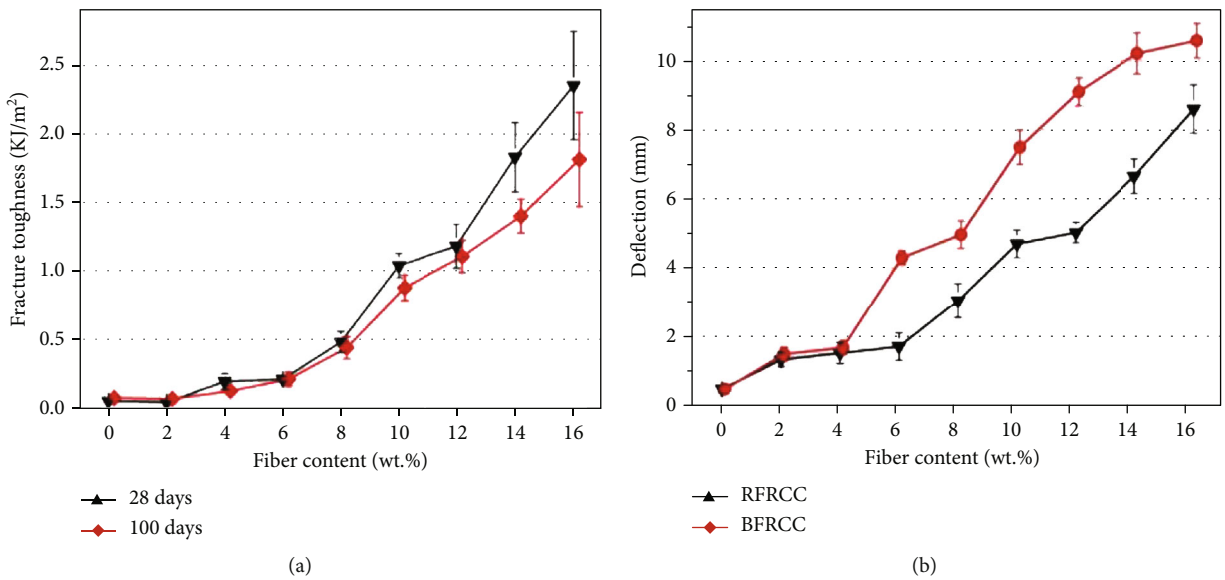

Figure 3: (a) Influence of fiber content on fracture toughness and (b) influence of fiber content on composite deformation [78].

Table 4: Bulk density of CFCCs at 28 days (g/cm^3).

CFs	Fiber content (wt.%)				
	0	4	8	12	16
RFRCC	2.01 ± 0.04	1.70 ± 0.01	1.49 ± 0.03	1.38 ± 0.04	1.26 ± 0.01
BFRCC	2.01 ± 0.04	1.71 ± 0.01	1.50 ± 0.04	1.36 ± 0.04	1.30 ± 0.05

overall microstructure of cement-based composites. Compared with the 0.6% fiber volume fraction, at the 0.3% fiber volume fraction, the pore size distribution before and after carbonization is less different, indicating that the 0.3% fiber volume fraction has a limited effect on the microstructure of cement-based composites.

4. Constitutive Relationship between CFs and Composite Durability

According to the fiber spacing theory proposed by the concept of fiber crack resistance, the use of densely spaced fibers as a crack barrier can reduce the stress intensity factor of the microcrack tip inside the matrix and inhibit the propagation of microcracks in the matrix, thereby improving the initial cracking strength of the composites. It is known from the previous studies that there is a certain limit on the amount of CF, which has a significant impact on the durability of composites due to the internal curing of the cement matrix and the long-term alkaline environment.

In fact, CFs increase the air content of the concrete and relieve the hydrostatic pressure and osmotic pressure during low-temperature cycles. Secondly, dense microfibers improve the internal quality of the concrete, reduce internal defects, and improve concrete's tensile properties such as ultimate tensile strain and fracture energy. In addition, due to the small diameter of CFs and the large number of fibers per unit weight, the fiber spacing is small, which increases the energy loss during the concrete damage process and effectively inhibits the cracking of the concrete.

4.1. Internal Curing Fiber of Cement-Based Composites. Different from other types of fibers, CFs have a unique hollow lumen structure and good water absorption. It can be used as the internal curing fiber of cement-based composites, as shown in Figures 1(a) and 1(b). In the absence of an external water supply for maintenance, it can play its role in the internal maintenance of the cement matrix, improve the water loss of the cement matrix under natural conditions, and promote continuous hydration for a long time. Therefore, its later strength increases greatly [75, 76]. CFs can also harmonize the workability of composites and improve construction performance. In addition, the use of the curing properties of CFs can improve the interlayer deposition and stacking process of 3D printed cement-based composites, reduce interlayer voids and longitudinal defects, and enhance durability [77].

CFs can effectively reduce the shrinkage of the cement matrix and significantly improve the flexural strength and fracture toughness of composites. The 28-day fracture toughness and 100-day fracture toughness of the composite vary with the fiber content, as shown in Figure 3(a). The physical parameter of CFCCs varies with fiber content. As the amount of CFs increases, the density of the composites decreases. Table 4 shows the density of CFCCs [78]. When the fiber content is 16% by mass, the 28-day fracture toughness is increased by 37 times. Figure 3(b) shows the relationship

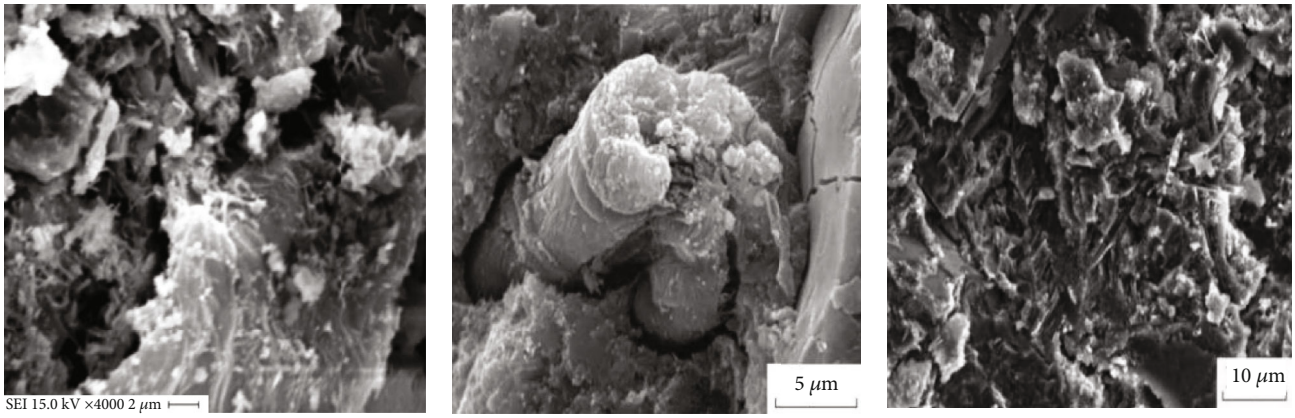

(a) (b) (c)

Figure 4: (a) Microstructure [72]. (b) Voids around the CFs. (c) Micro-nano-level microcrystalline cellulose [35].

between the deflection and the fiber content of two CFCCs of rice straw (RFRCC) and bamboo (BFRCC) [78]. It can be seen that as the CF content increased, the deflection of the test piece also increased, which further shows that the fiber improved the deformability and toughness of the composite, thereby enhancing the durability of the composites. As shown in Figure 3, composites reinforced with CFs experience a significant reduction in fracture toughness along with the prolongation of time. This means that the CF-reinforced composites will become stiffer and more brittle with time. Melo Filho and his coworkers [39] suggested that the weakening of energy absorbability of the CF was probably due to the deposition of calcium hydroxide crystals on the CF surface.

4.2. Deterioration of CFs in the Cement Matrix. The structural characteristics of CFs are the root cause of their deterioration in the environment of a high alkaline cement matrix. Studies have shown that the fiber is in an alkaline environment for a long time, and the lignin and hemicellulose in fibers are easy to dissolve in the alkaline solution of the cement-based composite, resulting in partial fiber breakage and tensile strength weakening. On the other hand, the strong alkali substance of the cement matrix enters into the fiber cavity to cause the mineralization of the fiber structure, which can reduce the mechanical properties of the fiber. At the same time, the extremely strong hydrophilicity of CFs causes its volume to change, which affects the overall structure durability [49, 57]. The sisal fiber and coconut husk fiber were immersed in a calcium hydroxide-saturated solution, the strength test was conducted for 28 days, and it was found that the tensile strength decreased by about 50% [52]. When CFs are immersed in water, saturated lime water, and sodium hydroxide solution, the lignin, cellulose, and hemicellulose contents of the fibers are all reduced [37, 58]. The application of these deteriorated fibers in cement-based composites will inevitably cause the mechanical properties of cement-based composites to decrease.

4.3. Ways to Improve the Durability of CFCCs. At present, there are generally two methods to improve the durability of CFCCs based on the internal curing and prone to deterioration characteristics of CFs. One method is to modify the cement matrix to consume the calcium hydroxide content of the alkaline component produced during cement hydration. Another method is to modify the fibers to improve the stability of the fibers in the cement matrix by physical or chemical methods.

4.3.1. Modification of the Cement Matrix. The reinforced concrete structure should be prevented from carbonization, and as for cement-based composites reinforced with single CFs, carbonization needs to be accelerated in order to enhance their durability. The purpose of carbonization is to make the cement hydration product calcium hydroxide react with carbon dioxide to form calcium carbonate. Pizzol et al. [79] have done the strengthened and accelerated carbonization test of the composite with sisal and kraft pulp, which increased the load-bearing capacity of the composite by 25% and the toughness by 80%, and reduced the fiber degradation in the cement medium. Carbonization reduced the porosity, water absorption, and nitrogen permeability of the composite, increased the matrix interface density, and made the fiber and cement matrix bond tighter, as shown in Figure 4(a). Carbonization improved the compressive strength and the durability and weather resistance of the composites, and their service life was extended [70, 71, 80]. Due to the chemical stability of the carbonized product and its reduced capillary porosity, the CFCCs have better flexural strength and can improve the adhesion between the cement-based matrix and the CFs.

Studies have shown that the optimal water content of the carbonized matrix is 40% to 60% [72], and carbonization significantly improves the durability of the matrix against dry and wet freezing and thawing. Both carbonization and the addition of mineral admixtures can reduce the calcium hydroxide content in the cement matrix. The cement-based composite is mixed with mineral admixtures such as silica fume, metakaolin, blast furnace slag, and fly ash, which can undergo secondary hydration reaction with calcium hydroxide in the cement to obtain hydrated calcium silicate or hydrated calcium aluminate [81]. Replacing part of cement

Table 5: Use of supplementary cementitious materials of CFCCs.

Cementitious materials	Weight of cement (%)	CFs	Extent of improvement	Ref.
MK	50 MK	Sisal	Significant reduction of the calcium hydroxide formation; no signs of fiber degradation	[38, 64, 83]
MK and SF	15 SF or 15 MK	Sisal	Improved the mechanical properties and the durability	[81]
SL, SF, and MK	70 SL/10 MK or 70 SL/10 SF	Kraft pulp	Effective in preventing degradation	[82]
RHA, MK, and NC	30 RHA, MK, and NC	Sisal	The durability of composites was improved owing to the mitigation of fiber degradation	[53]
SF and SL	10 SF and 40% SL	Cannabinus	Slowing down the strength loss and embrittlement	[84]
SF, SL, FA, MK	10% SF/70% SL, 10% MK/70% SL, and 10% MK/10% SF/70% FA	Softwood kraft pulp	Prevented composite degradation due to a reduction in the calcium hydroxide content and the stabilization of the alkali content	[85]
SL, GY, LI	88 SL/10 GY/2 LI (0 cement)	Coir and sisal	Do not appear to have a significant effect on the prevention of ductility dropping	[86]
SF, NRL	13.55 SF/14.55 CF/1.40 NRL	Cellulose	Improved material durability	[20]

Table 6: Modification of CFs and the extent of improvement.

Type	Method	CFs	Extent of improvement	Ref.
Physical modification	Polyelectrolyte adsorption	Blue eucalyptus paper	Antibacterial effect	[91]
	Nonelectrolyte adsorption	Cellulose nanocrystals	Changed the surface structure and properties of cellulose	[92]
Chemical modification	Small molecule modification	Pulp	Promoted the preparation of nanocellulose	[93]
	Graft modification	Softwood cellulose fiber	Formed a strong nanocomposite	[94]
	Cross-linking modification	Cellulose nanocrystals	Improved thermal stability and water resistance, decreased swelling degree	[95]
Biological modification	*In situ* modification	6-Carboxyfluorescein-modified glucose	With nonnatural characteristic fluorescent function	[96]
	Ex situ modification	Proanthocyanidins as cross-linking agent	Novel bacterial cellulose/gelatin composite	[97, 98]

with mineral admixtures significantly reduces the content of calcium hydroxide, avoids the deterioration of fiber performance, and ensures the strength and toughness of cement-based composites [82]. More studies revealed that it can produce cementitious materials without calcium hydroxide by using calcined metakaolin and calcined waste crushed clay bricks instead of ordinary Portland cement [53].

There are many types of supplementary cementitious materials used, and the extent of improvement varies. As shown in Table 5, the abbreviations of each component are as follows: silica fume (SF), blast furnace slag (SL), fly ash (FA), metakaolin (MK), rice husk ash (RHA), natural rubber latex (NRL), nanoclay (NC), gypsum (GY), and lime (LI).

4.3.2. Modification of CFs. Improving the water resistance of CFs and the adhesion between the matrix and the fiber interface is a necessary method to develop composites with good mechanical and environmental properties. However, the various types of CFs, geographical and climatic conditions, and growth cycles make the performance of CFs different. Some CFs have poor chemical resistance and low strength. These fibers can be modified to improve their internal and external structures and mechanical performance. The modification of CFs mainly includes physical modification, chemical modification, and biological modification, among which chemical modification is the most common [87–90], as shown in Table 6.

In the modification method of cellulose, the physical method is simple, convenient, and easy to operate, but the performance of the modified product is unstable, and the modifier is easy to fall off from the cellulose, resulting in product performance reduction. The chemical method is a better modification method [91, 92]. Compared with small molecule modification, graft polymerization has obvious advantages. It imparts other properties to cellulose without changing the properties of cellulose, and the modification effect is very stable. However, there are also disadvantages such as difficulty in operation and difficulty in controlling the reaction [93–95]. The biological modification to cellulose should be modified *in situ* or *ex situ* according to the actual situation [96–98].

The fibers are chemically modified to remove hemicellulose, lignin, pectin, and other substances on its surface so that

the structure of CFs becomes fibrillation and, which have a relatively rough appearance. The cement matrix interface forms a mechanical interlocking morphology [99–101].

When eucalyptus fibers are modified with 3-mercaptopropyltrimethoxysilane [102], it is found that the fiber reduces the water retention and meanwhile improves the dimensional stability of the composite. Through the dry-wet cycle treatment of abaca, agave, and sisal fibers [103], the cross-section of the fiber is reduced, Young's modulus is increased, and the tensile strength and tensile strain are reduced. At the same time, the cavity becomes thinner. The modified fibers increase the interfacial shear strength of the cement-based composite and also improve the durability. By adding 5% styrene-acrylic copolymer for treatment, after 200 dry and wet cycles, the water absorption ratio of the test piece is reduced by 50%, the elastic modulus value is reduced by 40%, and the shrinkage rate is reduced by 15%, which improves the stiffness and dimensional stability of the specimen [104]. After the modification treatment, the interface between the fibers and the cement matrix forms a dense and cohesive transition zone, which makes the fiber adhere to the cement surface to prevent the fiber from mineralizing.

4.3.3. Multitype CFs. Macroscale CFs are of large diameter and cavity, so they will absorb water and swell in the initial stage of mixing with the cement matrix. In the later stage of cement hydration, the fiber moisture gradually loses, the fiber shrinks and collapses in the matrix interface, and some voids are left at the fiber and cement matrix interface, which affects the performance of the composite, as shown in Figure 4(b). In order to improve this situation, the acid hydrolysis method can be used to prepare micron-sized microcrystalline CFs and nanosized nanocrystalline CFs [105, 106].

Microcrystalline CF is super absorbent, which can supplement the lack of moisture in the cement matrix at the later stage of hydration so that the cement matrix can be fully hydrated. A large amount of cement hydration gel can be induced around the microcrystalline CFs in the cement matrix to fill the microcracks and voids of the matrix and reduce the dry shrinkage cracks of the cement matrix at the initial stage of hydration. Nanocrystalline CF is of the same size as the cement hydration gel, which can induce the cement matrix hydration C-S-H gel to adhere to the surface of the nanocrystalline CFs, so they are connected and fused to form a uniform continuous C-S-H gel phase in the cement matrix. The cement matrix hydrate can completely embed in the nanocrystalline CFs, avoiding the negative effects of volume instability caused by macroscale CFs and microcrystalline CFs, and can further improve the durability of the composite, as shown in Figure 4(c). The shrinkage rate and mechanical properties of the material have been improved by using micro-nano-microcrystalline cellulose to toughen the concrete [107, 108]. Compared with ordinary samples, the network structure formed by the multitype fibers can transmit and share the stress generated by the plastic shrinkage of the cement matrix. The combination of the fiber and the matrix improved the crack resistance of the material and also enhanced its durability.

5. Conclusions

When microcracks appear during the service period of cement-based composites, the fibers share the load through the bridging action, which slows down the continuous development of the microcracks and increases the durability of the composites. The main conclusions are as follows.

The hydrophilicity and unique hollow structure of CFs optimize the pore structure of cement-based composites, so CFs can significantly improve the permeability, frost resistance, and carbonization resistance of CFCCs.

CFs uniformly dispersed in the cement matrix, and it can induce the orderly growth of cement hydration products at the initial stage of hydration and enhance the compactness of the cement matrix.

The internal curing characteristics of CFs on the cement matrix can enhance the durability of CFCCs. The utilization of microcrystalline CFs and nanocrystalline CFs has further improved the durability of CFCCs.

Cementitious materials with low alkali corrosion have been used to reduce the long-term performance degradation of CFs, such as magnesium silicate cement, magnesium phosphate cement, and geopolymer cement.

Fiber modification is an important measure to improve the durability of CFCCs, and in particular, chemical modification has been usually used.

Data Availability

All underlying data are provided in full within this paper.

Disclosure

The funders had no role in the design of the study; in the collection, analyses, or interpretation of data; in the writing of the manuscript; or in the decision to publish the results.

Conflicts of Interest

The authors declare no conflict of interest.

Acknowledgments

This research was funded by the "General items of basic scientific research business expenses of provincial universities in Heilongjiang Province" (grant number "135409313") and "Heilongjiang Province Higher Education Teaching Reform Project" (grant number "SJGY20200784").

References

[1] A. K. Pandey, T. Pal, R. Sharma, and K. K. Kar, "Study of matrix–filler interaction through correlations between structural and viscoelastic properties of carbonous-filler/polymer-matrix composites," *Journal of Applied Polymer Science*, vol. 137, no. 27, pp. 48660–48660, 2020.

[2] F. Pacheco-Torgal and S. Jalali, "Cementitious building materials reinforced with vegetable fibres: a review," *Construction and Building Materials*, vol. 25, no. 2, pp. 575–581, 2010.

[3] A. M. Mohamed, M. H. Osman, H. Smaoui, and M. A. M. Ariffin, "Durability and microstructure properties of concrete with arabic gum biopolymer admixture," *Advances in Civil Engineering*, vol. 2018, pp. 1–9, 2018.

[4] O. Karahan and C. D. Atis, "The durability properties of polypropylene fiber reinforced fly ash concrete," *Materials and Design*, vol. 32, no. 2, pp. 1044–1049, 2011.

[5] I. Ahmad, P. Y. Wong, and I. Abdullah, "Effects of fiber composition andgraft-copoly(ethylene/maleic anhydride) on thermoplastic natural rubber composites reinforced by aramid fiber," *Polymer Composites*, vol. 27, no. 4, pp. 395–401, 2006.

[6] J. Zhu, J. Wei, Q. Yu, M. Xu, and Y. Luo, "Hybrid effect of wollastonite fiber and carbon fiber on the mechanical properties of oil well cement pastes," *Advances in Materials Science and Engineering*, vol. 2020, pp. 1–9, 2020.

[7] P. Agnihotri, S. Basu, and K. K. Kar, "Effect of carbon nanotube length and density on the properties of carbon nanotube-coated carbon fiber/polyester composites," *Carbon*, vol. 49, no. 9, pp. 3098–3106, 2011.

[8] R. Kumar, K. K. Kar, and K. Dasgupta, "Enhanced electrical, mechanical, and viscoelastic properties of carbon-carbon composites using carbon nanotubes coated carbon textile as reinforcement," *Journal of Composite Materials*, vol. 55, no. 13, pp. 1733–1748, 2021.

[9] A. Rahaman and K. K. Kar, "E-glass fibers coated with nickel phosphorous by electroless deposition technique," *Composite Interfaces*, vol. 23, no. 7, pp. 689–699, 2016.

[10] A. Rahaman and K. K. Kar, "Carbon nanomaterials grown on E-glass fibers and their application in composite," *Composites Science and Technology*, vol. 101, no. 12, pp. 1–10, 2014.

[11] A. K. Mohanty, S. Vivekanandhan, J.-M. Pin, and M. Misra, "Composites from renewable and sustainable resources: challenges and innovations," *Science*, vol. 362, no. 6414, pp. 536–542, 2018.

[12] S. Venkatarajan and A. Athijayamani, "An overview on natural cellulose fiber reinforced polymer composites," *Materials Today: Proceedings*, vol. 37, no. 2, pp. 3620–3624, 2021.

[13] H. Choi and Y. C. Choi, "Setting characteristics of natural cellulose fiber reinforced cement composite," *Construction and Building Materials*, vol. 271, no. 15, p. 121910, 2021.

[14] M. Sargaphuti, S. P. Shah, and K. D. Vinson, "Shrinkage cracking and durability characteristics of cellulose fiber reinforced concrete," *Materials Journal*, vol. 90, no. 4, pp. 309–318, 1993.

[15] Ö. Andiç-Çakir, M. Sarikanat, H. B. Tüfekçi, C. Demirci, and U. H. Erdogan, "Physical and mechanical properties of randomly oriented coir fiber- cementitious composites," *Composites Part B Engineering*, vol. 61, no. 5, pp. 49–54, 2014.

[16] H. Savastano, S. F. Santos, M. Radonjic, and W. O. Soboyejo, "Fracture and fatigue of natural fiber-reinforced cementitious composites," *Cement and Concrete Composites*, vol. 31, no. 4, pp. 232–243, 2009.

[17] A. Sellami, M. Merzoud, and S. Amziane, "Improvement of mechanical properties of green concrete by treatment of the vegetals fibers," *Construction and Building Materials*, vol. 47, no. 10, pp. 1117–1124, 2013.

[18] X. Liu, J. Li, F. Li, J. Wang, and H. Lu, "Study on the properties of an ecotype mortar with rice husks and sisal fibers," *Advances in Civil Engineering*, vol. 2021, Article ID 5513303, pp. 1–11, 2021.

[19] J. M. Ferraz, C. H. S. del Menezzi, M. R. Souza, E. Y. A. Okino, and S. A. Martins, "Compatibility of pretreated coir fibres (Cocos nucifera L.) with Portland cement to produce mineral composites," *International Journal of Polymer Science*, vol. 2012, no. 9, Article ID 290571, 7 pages, 2012.

[20] G. Ramakrishna and T. Sundararajan, "Impact strength of a few natural fibre reinforced cement mortar slabs: a comparative study," *Cement and Concrete Composites*, vol. 27, no. 5, pp. 547–553, 2004.

[21] M. A. S. Mohamed, E. Ghorbel, and G. Wardeh, "Valorization of micro-cellulose fibers in self-compacting concrete," *Construction and Building Materials*, vol. 24, no. 12, pp. 2473–2480, 2010.

[22] H. Ez-zaki, L. Riva, M. Bellotto et al., "Influence of cellulose nanofibrils on the rheology, microstructure and strength of alkali activated ground granulated blast-furnace slag: a comparison with ordinary Portland cement," *Materials and Structures*, vol. 54, no. 1, p. 23, 2021.

[23] S. Beck-Candanedo, M. Roman, and D. G. Gray, "Effect of reaction conditions on the properties and behavior of wood cellulose nanocrystal suspensions," *Biomacromolecules*, vol. 6, no. 2, pp. 1048–1054, 2005.

[24] H. Xu, Z. Shao, Z. Wang et al., "Experimental study on mechanical properties of fiber reinforced concrete: effect of cellulose fiber, polyvinyl alcohol fiber and polyolefin fiber," *Construction and Building Materials*, vol. 261, no. 20, p. 120610, 2020.

[25] M. Şahmaran and V. C. Li, "Durability properties of micro-cracked ECC containing high volumes fly ash," *Cement & Concrete Research*, vol. 39, no. 11, pp. 1033–1043, 2009.

[26] D. Romanzini, H. L. Ornaghi Jr., S. C. Amico, and A. J. Zattera, "Influence of fiber hybridization on the dynamic mechanical properties of glass/ramie fiber-reinforced polyester composites," *Journal of Reinforced Plastics and Composites*, vol. 31, no. 23, pp. 1652–1661, 2012.

[27] M. Ardanuy, J. Claramunt, and R. D. Toledo Filho, "Cellulosic fiber reinforced cement-based composites: a review of recent research," *Construction and Building Materials*, vol. 79, no. 3, pp. 115–128, 2015.

[28] A. Balea, E. Fuente, M. C. Monte, Á. Blanco, and C. Negro, "Fiber reinforced cement based composites," *Fiber Reinforced Composites*579–648.

[29] A. Sharma, M. Thakur, M. Bhattacharya, T. Mandal, and S. Goswami, "Commercial application of cellulose nanocomposites - a review," *Biotechnology Reports*, vol. 21, no. 3, article e00316, 2019.

[30] D. Lasrado, S. Ahankari, and K. Kar, "Nanocellulose-based polymer composites for energy applications—a review," *Journal of Applied Polymer Science*, vol. 137, no. 27, pp. 48959–48959, 2020.

[31] S. Mohan, E. Francis, S. Thomas, and N. Ninan, *Natural Polymers, Biopolymers, Biomaterials, and Their Composites, Blends, and IPNs*, Apple Academic Press, 1st edition, 2012.

[32] G. Tonoli, S. F. Santos, A. P. Joaquim, and H. Savastano Jr., "Effect of accelerated carbonation on cementitious roofing tiles reinforced with lignocellulosic fibre," *Construction and Building Materials*, vol. 24, no. 2, pp. 193–201, 2010.

[33] H. Kargarzadeh, M. Mariano, D. Gopakumar et al., "Advances in cellulose nanomaterials," *Cellulose*, vol. 25, no. 4, pp. 2151–2189, 2018.

[34] I. Hamawand, S. Seneweera, P. Kumarasinghe, and J. Bundschuh, "Nanoparticle technology for separation of cellulose, hemicellulose and lignin nanoparticles from lignocellulose biomass: a short review," *Nano-Structures & Nano-Objects*, vol. 24, no. 10, p. 100601, 2020.

[35] S. K. Singh, M. J. Akhtar, and K. K. Kar, "Hierarchical carbon nanotube-coated carbon fiber: ultra lightweight, thin, and highly efficient microwave absorber," *ACS Applied Materials & Interfaces*, vol. 10, no. 29, pp. 24816–24828, 2018.

[36] A. K. Bledzki and J. Gassan, "Composites reinforced with cellulose based fibres," *Progress in Polymer Science*, vol. 24, no. 2, pp. 221–274, 1999.

[37] W. Jing, Z. Weijun, and W. Luoxin, "Effect of submicron cellulosic fiber on the micro-structure of cement paste," *Journal of Building Materials*, vol. 21, no. 2, pp. 309–313, 2018.

[38] Y. A. Mubarak, "Tensile and impact properties of microcrystalline cellulose nanoclay polypropylene composites," *International Journal of Polymer Science*, vol. 2018, Article ID 1708695, 13 pages, 2018.

[39] J. d. A. Melo Filho, F. d. A. Silva, and R. D. Toledo Filho, "Degradation kinetics and aging mechanisms on sisal fiber cement composite systems," *Cement and Concrete Composites*, vol. 40, no. 7, pp. 30–39, 2013.

[40] W. Yong, S. Huijuan, and X. Shaoxiang, "Study on properties of polyurea/acrylic resin composite film reinforced by nanocrystalline cellulose," *Materials Review*, vol. 29, no. 6, pp. 11–14, 2015.

[41] P. Klemm, F. Kramer, S. Moritz et al., "Nanocelluloses: a new family of nature-based materials," *Angewandte Chemie International Edition*, vol. 50, no. 24, pp. 5438–5466, 2011.

[42] F. D. A. Silva, B. Mobasher, C. Soranakom, and R. D. T. Filho, "Effect of fiber shape and morphology on interfacial bond and cracking behaviors of sisal fiber cement based composites," *Cement and Concrete Composites*, vol. 33, no. 8, pp. 814–823, 2011.

[43] B. He, L. Xie, Q. Liu, and S. Zhang, "Influence of fiber hydrophilic to improve the frost resistance of concrete," *Journal of Sichuan University (Engineering Science Edition)*, vol. 48, no. 2, pp. 225–230, 2016.

[44] Q. Hongping, "Experimental study and engineering application of anti-cracking and impermeability performance of concrete mixed with cellulose fiber and hybrid fiber," *New Building Materials*, vol. 39, no. 3, pp. 40–42, 2012.

[45] Y. J. Li and J. Jian, "Experimental study on anti-permeability of cellulose fiber and hybrid fiber concrete," *Advanced Materials Research*, vol. 482, no. 484, pp. 1334–1337, 2012.

[46] J. Wei, S. Ma, and D.'. S. G. Thomas, "Correlation between hydration of cement and durability of natural fiber- reinforced cement composites," *Corrosion Science*, vol. 106, no. 5, pp. 1–15, 2016.

[47] M. Nili, A. Azarioon, A. Danesh, and A. Deihimi, "Experimental study and modeling of fiber volume effects on frost resistance of fiber reinforced concrete," *International Journal of Civil Engineering*, vol. 16, no. 3, pp. 263–272, 2016.

[48] C. Li, J. Hu, C. Yuan, and G. Yu, "Experimental study on the freezing resistance of fiber reinforced high strength concrete," *Acta Materiae Compositae Sinica*, vol. 36, no. 8, pp. 1977–1983, 2019.

[49] P. Soroushian, J.-P. Won, and M. Hassan, "Durability characteristics of CO_2-cured cellulose fiber reinforced cement composites," *Construction and Building Materials*, vol. 34, no. 9, pp. 44–53, 2012.

[50] G. Ramakrishna, T. Sundararajan, and S. Kothandaraman, "Evaluation of durability of natural fibre reinforced cement mortar composite- a new approach," *Journal of Engineering & Applied Sciences*, vol. 5, no. 6, 2010.

[51] L. Guo, W. Zhang, W. Sun, Z. Shen, and C. Ding, "Durability of cellulose fiber reinforced concrete under bending load in tunnel engineering," *Journal of Southeast University (Natural Science Edition)*, vol. 46, no. 3, pp. 612–618, 2016.

[52] V. M. John, M. A. Cincotto, C. Sjöström, V. Agopyan, and C. T. A. Oliveira, "Durability of slag mortar reinforced with coconut fibre," *Cement and Concrete Composites*, vol. 27, no. 5, pp. 565–574, 2004.

[53] J. Wei and C. Meyer, "Utilization of rice husk ash in green natural fiber-reinforced cement composites: mitigating degradation of sisal fiber," *Cement and Concrete Research*, vol. 81, no. 3, pp. 94–111, 2016.

[54] B. J. Mohr, H. Nanko, and K. E. Kurtis, "Durability of kraft pulp fiber–cement composites to wet/dry cycling," *Cement and Concrete Composites*, vol. 27, no. 4, pp. 435–448, 2005.

[55] B. J. Mohr, H. Nanko, and K. E. Kurtis, "Durability of thermomechanical pulp fiber-cement composites to wet/dry cycling," *Cement and Concrete Composites*, vol. 35, no. 8, pp. 1646–1649, 2005.

[56] J. Wei and C. Meyer, "Degradation mechanisms of natural fiber in the matrix of cement composites," *Cement and Concrete Research*, vol. 73, pp. 1–16, 2015.

[57] J. Wei and C. Meyer, "Sisal fiber-reinforced cement composite with Portland cement substitution by a combination of metakaolin and nanoclay," *Journal of Materials Science*, vol. 49, no. 21, pp. 7604–7619, 2014.

[58] G. A. Holt, P. Chow, J. D. Wanjura, M. G. Pelletier, and T. C. Wedegaertner, "Evaluation of thermal treatments to improve physical and mechanical properties of bio-composites made from cotton byproducts and other agricultural fibers," *Industrial Crops & Products*, vol. 52, no. 1, pp. 627–632, 2014.

[59] A. A. Belkadi, S. Aggoun, C. Amouri, A. Geuttala, and H. Houari, "Effect of vegetable and synthetic fibers on mechanical performance and durability of metakaolin-based mortars," *Journal of Adhesion Science and Technology*, vol. 32, no. 15, pp. 1670–1686, 2018.

[60] L. Zhang, Z. Jiang, H. Wu et al., "Flexural properties of renewable coir fiber reinforced magnesium phosphate cement, considering fiber length," *Materials*, vol. 13, no. 17, pp. 3692–3692, 2020.

[61] F. d. A. Silva, D. Zhu, B. Mobasher, C. Soranakom, and R. D. Toledo Filho, "High speed tensile behavior of sisal fiber cement composites," *Materials Science & Engineering A*, vol. 527, no. 3, pp. 544–552, 2009.

[62] P. J. C. Machado, R. A. dos Reis Ferreira, L. A. de Castro Motta, and D. Pasquini, "Characterization and properties of cementitious composites with cellulose fiber, silica fume and latex," *Construction and Building Materials*, vol. 257, no. 10, p. 119602, 2020.

[63] R. S. Teixeira, G. H. D. Tonoli, S. F. Santos et al., "Different ageing conditions on cementitious roofing tiles reinforced with alternative vegetable and synthetic fibres," *Materials and Structures*, vol. 47, no. 3, pp. 433–446, 2014.

[64] S. V. Bharathi, S. Vinodhkumar, and M. M. Saravanan, "Strength characteristics of banana and sisal fiber reinforced

composites," *IOP Conference Series Materials Science and Engineering*, vol. 1055, no. 1, article 012024, 2021.

[65] M. Ardanuy, J. Clarmunt, and R. Filho, "Evaluation of durability to wet/dry cycling of cement mortar composites reinforced with nanofibrillated cellulose," *Brittle Matrix Composites*, vol. 10, pp. 33–41, 2012.

[66] N. H. El-Ashkar, B. Mohr, H. Nanko, and K. E. Kurtis, "Durability of pulp fiber-cement composites to wet/dry cycling," *Advances in Building Technology*, vol. 35, no. 8, pp. 233–237, 2002.

[67] S. U. N. Jia-ying, "Frost resistance characteristics of fiber concrete," *Journal of Building Materials*, vol. 16, no. 3, pp. 437–440, 2013.

[68] A. E. F. S. Almeida, G. H. D. Tonoli, S. F. Santos, and H. Savastano, "Improved durability of vegetable fiber reinforced cement composite subject to accelerated carbonation at early age," *Cement and Concrete Composites*, vol. 42, no. 9, pp. 49–58, 2013.

[69] A. F. Almeida, G. Tonoli, S. Santos, and H. S. Junior, "Accelerated carbonation in the early ages of cellulose pulps reinforced cement composites," *Ambiente Construído*, vol. 10, no. 4, pp. 233–246, 2010.

[70] J. Claramunt, M. Ardanuy, and L. J. Fernandez-Carrasco, "Wet/dry cycling durability of cement mortar composites reinforced with micro- and nanoscale cellulose pulps," *BioResources*, vol. 10, no. 2, 2015.

[71] V. da Costa Correia, S. F. Santos, and H. Savastano, "Vegetable fiber as reinforcing elements for cement based composite in housing applications – a Brazilian experience," *MATEC Web of Conferences*, vol. 149, p. 01007, 2018.

[72] Z. He, Y. Jia, and S. Wang, "Maximizing CO_2 sequestration in cement-bonded fiberboards through carbonation curing," *Construction and Building Materials*, vol. 213, pp. 51–60, 2019.

[73] C. Dong, W. Sun, and N. Banthia, "Use of tomography to understand the influence of preconditioning on carbonation tests in cement-based materials," *Cement and Concrete Composites*, vol. 88, pp. 52–63, 2018.

[74] D. N. Winslow and S. Diamond, "A mercury porosimetry study of the evolution of porosity in portland cement," *Gels*, 1969.

[75] G. Ma, X. Zheng, and P. Guo, "Early-age cracking resistance and self-shrinkage behavior of recycled cellulose fibers-reinforced cement mortar," *Journal of Civil and Environmental Engineering*, vol. 42, no. 3, pp. 127–132, 2020.

[76] K. Jiang, C. Qi, Y. Cui, T. Li, and Z. Lu, "Effects of several factors such as cellulose on the properties of polyethylene fiber reinforced pervious concrete," *Materials Review*, vol. 34, Supplement 1, pp. 189–192, 2020.

[77] G. Ma, N. M. Salman, L. Wang, and F. Wang, "A novel additive mortar leveraging internal curing for enhancing interlayer bonding of cementitious composite for 3D printing," *Construction and Building Materials*, vol. 244, no. 5, p. 118305, 2020.

[78] X. Xie, H. David, Z. Wang, X. Xu, and Z. Zuowan, "Cellulosic fibers from rice straw and bamboo used as reinforcement of cement- based composites for remarkably improving mechanical properties," *Composites Part B Engineering*, vol. 78, pp. 153–161, 2015.

[79] V. D. Pizzol, L. M. Mendes, L. Frezzatti, H. Savastano Jr., and G. H. D. Tonoli, "Effect of accelerated carbonation on the microstructure and physical properties of hybrid fiber-cement composites," *Minerals Engineering*, vol. 59, no. 5, pp. 101–106, 2014.

[80] R. Mac Vicar, L. M. Matuana, and J. J. Balatinecz, "Aging mechanisms in cellulose fiber reinforced cement composites," *Cement and Concrete Composites*, vol. 21, no. 3, pp. 189–196, 1999.

[81] R. M. de Gutiérrez, L. N. Díaz, and S. Delvasto, "Effect of pozzolans on the performance of fiber-reinforced mortars," *Cement and Concrete Composites*, vol. 27, no. 5, pp. 593–598, 2004.

[82] G. H. D. Tonoli, A. P. Joaquim, M. A. Arsene, K. Bilba, and H. Savastano, "Performance and durability of cement based composites reinforced with refined sisal pulp," *Materials and Manufacturing Processes*, vol. 22, no. 2, pp. 149–156, 2007.

[83] R. D. Toledo Filho, F. D. A. Silva, E. M. R. Fairbairn, and J. D. A. M. Filho, "Durability of compression molded sisal fiber reinforced mortar laminates," *Construction and Building Materials*, vol. 23, no. 6, pp. 2409–2420, 2009.

[84] R. D. Tolêdo Filho, K. Ghavami, G. L. England, and K. Scrivener, "Development of vegetable fibre-mortar composites of improved durability," *Cement and Concrete Composites*, vol. 25, no. 2, pp. 185–196, 2003.

[85] B. J. Mohr, J. J. Biernacki, and K. E. Kurtis, "Supplementary cementitious materials for mitigating degradation of kraft pulp fiber-cement composites," *Cement and Concrete Research*, vol. 37, no. 11, pp. 1531–1543, 2007.

[86] V. Agopyan, H. Savastano, V. M. John, and M. A. Cincotto, "Developments on vegetable fibre-cement based materials in Sao Paulo, Brazil: an overview," *Cement & Concrete Composites*, vol. 27, no. 5, pp. 527–536, 2005.

[87] S. Kalia, A. Dufresne, B. M. Cherian et al., "Cellulose-based bio- and nanocomposites: a review," *International Journal of Polymer Science*, vol. 2011, Article ID 837875, 35 pages, 2011.

[88] M. I. D. Dulmalik and S. N. Kumala, "The effect of NaOH concentration variation in the process of paper making from bamboo fiber," *IOP Conference Series: Materials Science and Engineering*, vol. 535, no. 1, 2019.

[89] J. Liu and C. Lv, "Synthesizing environmentally friendly non-silicone oxygen bleaching stabilizer for linen yarn using oligomeric acrylic acid," *Scientific Reports*, vol. 11, no. 1, p. 10355, 2021.

[90] E. Yuanita, Y. A. Husnil, M. A. Mochtar, R. Lailani, and M. Chalid, "The effect of alkalization treatment on fiber-matrix compatibility in natural fiber reinforced composite," *Key Engineering Materials*, vol. 847, no. 6, pp. 28–33, 2020.

[91] N. C. T. Martins, C. S. R. Freire, and R. J. B. Pinto, "Electrostatic assembly of Ag nanoparticles onto nanofibrillated cellulose for antibacterial paper products," *Cellulose*, vol. 19, no. 4, pp. 1425–1436, 2012.

[92] J. Majoinen, J. S. Haataja, and D. Appelhans, "Supracolloidal multivalent interactions and wrapping of dendronized glycopolymers on native cellulose nanocrystals," *Journal of the American Chemical Society*, vol. 136, no. 3, pp. 866–869, 2014.

[93] O. Nechyporchuk, M. N. Belgacem, and J. Bras, "Production of cellulose nanofibrils: a review of recent advances," *Industrial Crops and Products*, vol. 93, no. 11, pp. 2–25, 2016.

[94] C. Chuensangjun, T. Kitaoka, Y. Chisti, and S. Sirisansaneeyakul, "Optimal ring-opening polymerization

for producing surface-modi-fied cellulose nanofibers-graft-poly(lactic acid) s," *New Biotechnology*, vol. 44s, no. 10, pp. s105–s105, 2018.

[95] H. Zhengzheng, T. Xiuzhi, J. Xue, W. Hongbo, and G. Weidong, "Preparation and properties of dialdehyde nanocellulose cross-linked polyvinyl alcohol membranes," *Journal of Materials Science and Engineering*, vol. 37, no. 4, pp. 578–582, 2019.

[96] M. Gao, J. Li, and Z. Bao, "A natural in situ fabrication method of functional bacterial cellulose using a microorganism," *Nature Communications*, vol. 10, no. 1, pp. 437–437, 2019.

[97] J. Wang, Y. Z. Wan, H. L. Luo, C. Gao, and Y. Huang, "Immobilization of gelatin on bacterial cellulose nanofibers surface via crosslinking technique," *Materials Science & Engineering C*, vol. 32, no. 3, pp. 536–541, 2012.

[98] T. Almalkawi Areej and S. Parviz, "Aerated cement slurry and controlling fungal growth of low-cost biomass-based insulation materials," *Scientific Reports*, vol. 9, no. 1, p. 19237, 2019.

[99] A. Shahzad, "Effects of alkalization on tensile, impact, and fatigue properties of hemp fiber composites," *Polymer Composites*, vol. 33, no. 7, pp. 1129–1140, 2012.

[100] X. Xie, Z. Zhou, and Y. Yan, "Flexural properties and impact behaviour analysis of bamboo cellulosic fibers filled cement based composites," *Construction and Building Materials*, vol. 220, no. 9, pp. 403–414, 2019.

[101] X. Xie, G. Gou, and X. Wei, "Influence of pretreatment of rice straw on hydration of straw fiber filled cement based composites," *Construction and Building Materials*, vol. 113, no. 6, pp. 449–455, 2016.

[102] G. H. D. Tonoli, M. N. Belgacem, and G. Siqueira, "Processing and dimensional changes of cement based composites reinforced with surface-treated cellulose fibres," *Cement and Concrete Composites*, vol. 37, no. 3, pp. 68–75, 2013.

[103] M. Ardanuy and Claramunt, "Effect of water treatment on the fiber-matrix bonding and durability of cellulose fiber cement composites," *Journal of Biobased Materials and Bioenergy*, vol. 9, no. 5, pp. 486–492, 2015.

[104] E. O. Cruz, M. J. Radler, and M. Perello, "Fiber cement boards modified with styrene-acrylic copolymer: an approach to address dimensional stability and cellulose fiber preservation," *Journal of Composite Materials*, vol. 55, no. 3, pp. 437–452, 2021.

[105] A. Balea, E. Fuente, and A. Blanco, "Nanocelluloses: natural-based materials for fiber-reinforced cement composites. A critical review," *Polymers*, vol. 11, no. 3, p. 518, 2019.

[106] S. Ahankari, T. George, A. Subhedar, and K. K. Kar, "Nanocellulose as a sustainable material for water purification," *SPE Polymers*, vol. 1, no. 2, pp. 69–80, 2020.

[107] T. Wenrui, M. Changwen, and D. Bei, "Properties study and mechanism analysis of concrete reinforced by microcrystalline cellulose," *New Building Materials*, vol. 37, no. 7, pp. 4–6, 2010.

[108] H.-J. Lee, S.-K. Kim, and H.-S. Lee, "A study on the drying shrinkage and mechanical properties of fiber reinforced cement composites using cellulose nanocrystals," *International Journal of Concrete Structures and Materials*, vol. 13, no. 1, pp. 1–11, 2019.

Hindawi
International Journal of Polymer Science
Volume 2021, Article ID 7491679, 10 pages
https://doi.org/10.1155/2021/7491679

Research Article

Study on Compaction and Machinability of Silicon Nitride (Si3N4) Reinforced Copper Alloy Composite through P/M Route

T. Sathish,[1] **V. Mohanavel**,[2] **Alagar Karthick**,[3] **M. Arunkumar**,[4] **M. Ravichandran**,[5] **and S. Rajkumar**[6]

[1]*Department of Mechanical Engineering, Saveetha School of Engineering, SIMATS, 602105 Chennai, Tamil Nadu, India*
[2]*Centre for Materials Engineering and Regenerative Medicine, Bharath Institute of Higher Education and Research, Chennai, 600073 Tamil Nadu, India*
[3]*Department of Electrical and Electronics Engineering, KPR Institute of Engineering and Technology, Coimbatore, 641407 Tamil Nadu, India*
[4]*Department of Agriculture Engineering, Sri Shakthi Institute of Engineering and Technology, Coimbatore, 641062 Tamil Nadu, India*
[5]*Department of Mechanical Engineering, K.Ramakrishnan College of Engineering, Trichy 621112, Tamil Nadu, India*
[6]*Department of Mechanical Engineering, Faculty of Manufacturing, Institute of Technology, Hawassa University, Ethiopia*

Correspondence should be addressed to S. Rajkumar; rajkumar@hu.edu.et

Received 11 April 2021; Accepted 23 June 2021; Published 8 July 2021

Academic Editor: Ching Hao Lee

Nowadays, most of the products are used in the electrical and electronics field, and copper alloy is playing a significant role such as Springs for relay contacts and switchgear, Rotor bars, and Busbars. In this work, the copper alloys consider as base alloy, and the reinforced factor of silicon nitride (Si_3N_4) is processed of reinforcement as 3 wt. %, 6 wt. %, 9 wt. %, 12 wt. % Si_3N_4 through powder metallurgy performance. The ball mill process is used for this work to obtain an enhanced homogeneous mixture of both base material as well as reinforced particles. Using a hydraulic press, the blended powders are compacted with applying 3 kN and 10 min period for obtained good strength of green compact specimens. Further, the green compacted specimens are sintered, and the sintered billets are machined in the conventional lathes with different cutting speeds 50 m/min, 100 m/min, and 150 m/min; feed rate of 0.1 mm/rev (fixed); and depth of cut of 0.5 mm, 0.8 mm, 1 mm, 1.2 mm, 1.4 mm, and 1.6 mm. Cutting speed and depth of cut to find the composites' cutting force is ingenious. A wear test also can be conducted to find the wear resistance of the reinforced particles of the copper alloy material.

1. Introduction

With the development of new materials, the composite functions majorly with low mass ratio to potency ratios and enhanced properties. The standard composite is metal matrix composites. These are high strength, magnificent wear, and corrosion behavior and have high mechanical properties. The powder metallurgy route is the best way to fabricate all parts in simple compacting and heating metal powders [1, 2]. The machining of MMCs is complex due to superior hardness value, the tool wear is more, and the surface finish attains poor condition. The Aluminium Matrix Composites (AMCs) are simple ones to replacing MMCs by their nature of strength and lightweight, and these alloys are suitable for structural work, aerospace, and automotive sectors. The polymer composite is also used for the fabrication of automotive components to improve their strength. Polymer composites possess high strength and lightweight [3, 4].

Powder metallurgy is a versatile process of producing composites within a short period. The preparation of powders, blending of powders, and the compaction process are indirect effects of the composites' machinability process [5–7]. The sintering process increases the strength of the composites and affects the cutting force of the tool. Based

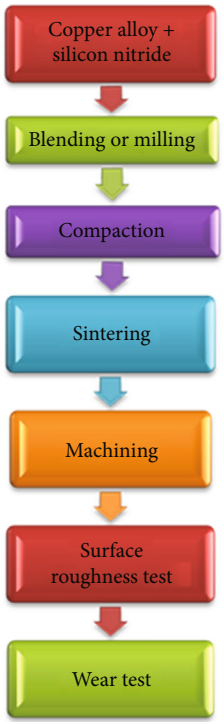

Figure 1: Flowchart of the proposed study.

on the material, the tool selection was an important one [8–11]. The compaction process in the P/M tightens the loose powder effectively by applying different compaction pressure and selects the proper die and punch. There are forced particles mixed into the base material due to the blending or milling process [12]. The effects of reinforcement in the composite reflect in the tool wear. Most of the tool materials are affected by machining speed and feed rate [13]. Numerous methodologies are used to manufacture aluminum composites and other composites. Most composites are prepared by powder metallurgy and stir casting approach; most researchers develop their composites through these techniques. The stir casting method is termed liquid state processing which the base material has to be melted well and stir continually with the addition of solid reinforcement particles. This process considers the time for carrying out stirring action to increase the composites' strength. After stirring, action followed the solidification process to improve the solid strength of the composites. Stir casting examination offered the low-cost, simple in-process control of liquid state molten material. But some of the limitations are caused by the stir casting process, such as difficulty obtaining homogeneous mixture and possibly producing porosity in the composites. High temperature leads to poor wetting and a chance to form a reaction between the base and reinforced particles. The researchers undertake all these considerations. The powder metallurgy process is used to prepare the composites with multiple reinforcement particles in a single process. It can be provided the enhanced mechanical strength as well as tribological properties of the hybrid composites.

Some researchers carried out the PM method, mixing Al_2O_3into the aluminum and copper powders; the excellent mechanical strength was found. When developing composites, ductility is considered a factor in improving the composites' strength [14]. In some literature, the silicon nitride (Si_3N_4) was used to reinforce into the alloys the composites' ductility has to be obtained excellently and improve fracture toughness. Silicon nitride is one of the hard ceramic particles. It possesses high fracture toughness. Few of the literature only considered the silicon nitride ceramic particles into the aluminum alloy composites. The copper alloys have exceptional corrosion resistance. It has widely used in mechanical areas such as the joining of rivets and screws. Usually, copper alloys are called metal alloys. In that alloy, copper has a chief element of the copper alloys.

In general, copper and its alloys possess high electrical and thermal properties, continually better corrosion resistance, and superior ductility in nature for use in various engineering applications [15]. These alloys' limitations are low tensile strength and minimum wear resistance; this limitation needs enforcement in the silicon nitride ceramic particles to solve the limitations. Silicon nitride reinforced particles have

Table 1: Chemical composition of copper alloy.

Elements	Cu	Al	Mg	Mn	Si	Cr
Weight%	98.05	0.42	0.29	0.47	0.24	0.24

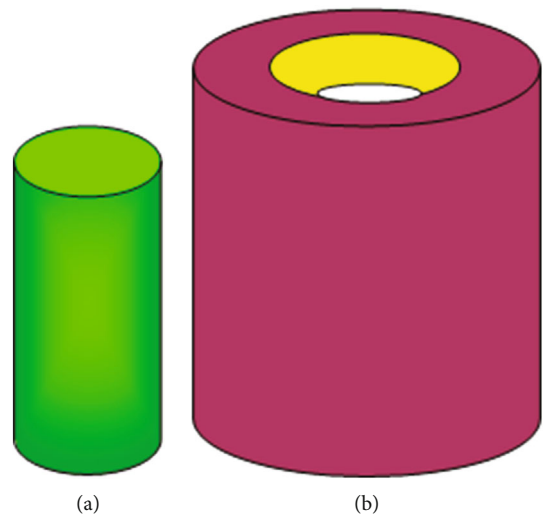

Figure 2: Punch and die for the compaction.

Table 2: Sintering process sequence.

Sintering process	Temperature		Time
	Starting	Ending	
Heating process	35°C	400°C	50 min
Soaking process	400°C	400°C	40 min
Heating process	400°C	500°C	40 min
Soaking process	500°C	500°C	40 min
Heating process	500°C	600°C	40 min
Soaking process	600°C	600°C	50 min
Allowed to cooling in the furnace	600°C	35°C	—

(a) (b)

Figure 3: Compacted billets (a) before sintering and (b) after sintering.

high thermal, mechanical, and wear properties to reinforce the base material to enhance material strength. Si_3N_4 ceramic particles offered better compressive strength than any composites since they possess superior compressive strength and yield strength [16]. Copper alloys and silicon carbide hard particles improve the microhardness of the composite materials. The wear resistance of the composites also increases hugely. Using silicon nitride, the homogeneous mixture was obtained in the P/M process route. The ball milling process was enhanced the mixture strength, such as base alloys and silicon nitride hard particles. The sintering process lifted the strength of the composites through melting. Both the base alloys and silicon nitride was moved to red hot condition and obtained uniform distribution [17]. This study planned to prepare the copper alloys with reinforced silicon nitride by implementing powder metallurgy practice. The main objectives of this work were mentioned, such as to find the machinability characteristics and wear property of the copper alloy composites prepared by the powder metallurgy practice with different input parameters. The sintered composites are machined by using of conventional lathe machine with different machining parameters such as cutting speed, feed rate, and depth of cut. The result of cutting force is measured by the influence of cutting speed and depth of cut. The machinability study is focusing on machining of the copper nozzle and bushes, a wear study aimed to prevent the wear in the commutator in an electric motor.

2. Materials and Method

This experiment considers the copper alloys to reinforce silicon nitrite with a different weight percentage of composition [18]. The experiment plan was illustrated in Figure 1, and the material selection is the initial phase of this work. The material is chosen for this work as copper alloys and silicon nitride. Copper alloys are primarily used in electrical items such as motor winding and electrical wire. The powder metallurgy process highly blends both the materials; continually, the compaction process is carried out. Further, green compaction is sintered and extruded. Finally, the machinability, surface roughness, and wear test were conducted. Table 1 presented the constituent elements of copper alloys generally X-ray fluorescence (XRF) technique was used to measure the material's elemental composition. The atomized powder particles of copper alloys and the different weight percentages of the silicon nitride were mixed into the ball mill with a uniform speed of 400rpm, with a few steel balls being induced the powders'.

Table 3: Machining parameters.

Tool bit material	High-speed steel (HSS)
Cutting speed in m/min	50, 100,150
Feed rate in mm/rev	0.1 (fixed)
Depth of cut in mm	0.5, 0.8, 1, 1.2,1.4,1.6
Percentage of reinforcement % wt. Si_3N_4	3, 6, 9,12

Uniform mixing in the ball mill, the blending operation carried out 1 hour 30 minutes [19]. The mixed powder particles are filled in the cylindrical die cavity. The powders are pressed by the application of pressure, the punch and die of the experiment were illustrated in Figure 2. The hydraulic press complied under the specifications of 10 kN capacity and the ram's stroke length as 300 mm. The 3 kN pressure was applied while compaction with maintaining the pressure for 10 min [20]. The sintering sequence is presented in Table 2, and the Green compact billets are further sintered by using of sintering process in the furnace. The billets are placed inside the furnace in the order of reinforcement percentage to collect the billets after sintering [21]. Initially, the starting temperature of the sintering process at 35°C was applied, continually heating up to 400°C after reaching 400°C to maintain the same temperature for 40 min. Further heating 400°C to 500°C, the furnace reached 500°C to maintain the same temperature at the time of 40 min [22–24]. In the last attempt of heating 500°C to 600°C, the furnace reached the temperature of 600°C and maintains the same temperature for 40 min. After that, they allowed reducing

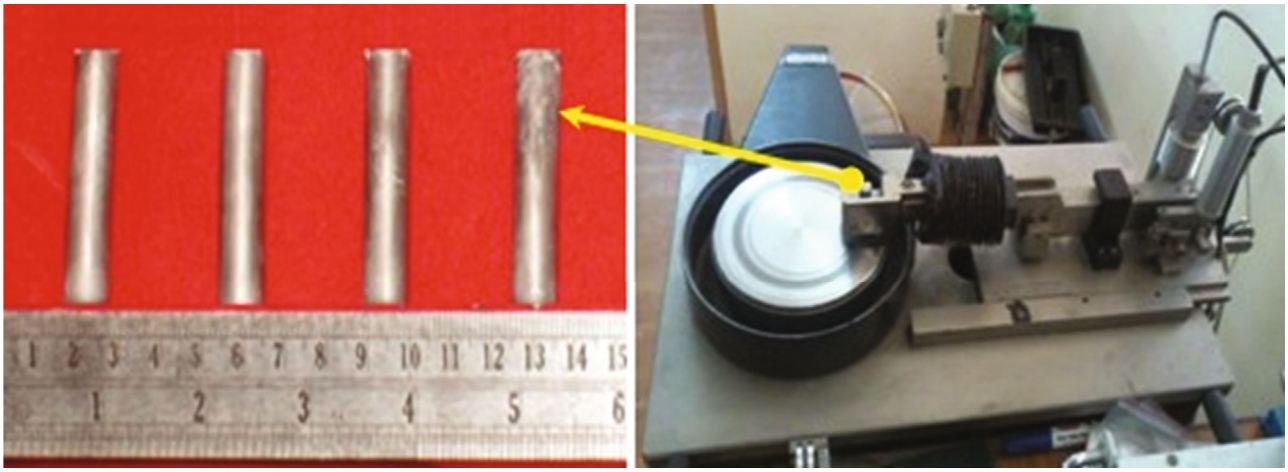

Figure 4: DUCOM dry sliding wear tester with specimens.

Table 4: Summary of machining parameters with the result of surface roughness.

S. no	Feed rate in (mm/rev)	Cutting speed in (m/min)	Depth of cut (mm)	Surface roughness values in microns			
				3 wt. %	6 wt. %	9 wt. %	!2 wt. %
1	0.1	50	0.5	0.58	1.52	2.08	2.65
2			0.8	0.75	1.58	2.09	2.68
3			1.0	0.92	1.68	2.10	2.74
4			1.2	0.67	1.54	1.07	2.69
5			1.4	0.69	1.63	2.15	2.72
6			1.6	0.83	1.57	2.17	2.78
7		100	0.5	0.95	1.68	2.23	2.8
8			0.8	1.02	1.72	2.37	2.81
9			1.0	1.34	1.86	2.29	2.80
10			1.2	1.25	1.67	2.34	2.76
11			1.4	1.34	1.73	2.42	2.84
12			1.6	1.21	1.81	2.45	2.83
13		150	0.5	1.32	1.92	2.53	2.94
14			0.8	1.42	1.96	2.57	2.97
15			1.0	1.28	1.89	2.74	3.01
16			1.2	1.34	1.94	2.64	3.11
17			1.4	1.47	2.01	2.58	3.12
18			1.6	1.39	2.05	2.62	3.16

the temperature of 600°C to 35°C. The compact green billets before sintering and after sintering are shown in Figure 3. The soaking process is essential to modifying the composite billets' microstructure [25–28].

The conventional machining process was carried out in the lathe machine with different speeds, constant feed rates, and depth of cut. The HMT lathe machine was used for machining the composites with the aid of a high-speed steel tool material. The Mitutoyo surface roughness tester is measured by the machined components' surface roughness [29–31]. The cutting force was measured by using of lathe tool dynamometer made by National instruments effectively; the machining parameters of this investigation are presented in Table 3.Wear test experiments under the influence of 3.0 kgf of applied, sliding velocity of 2 m/s, the sliding distance of 1500 m, and the wear track diameter of 120 mm [32–34]. The disc rotational speed is maintained at 160 rpm with a

Table 5: Cutting force summary (cutting speed 50 m/min).

S. no	Depth of cut (mm)	Cutting force (kgf)			
		3 wt. %	6 wt. %	9 wt. %	12 wt. %
1	0.5	2.34	2.89	3.01	3.76
2	0.8	4.56	5.32	4.56	6.37
3	1.0	6.75	7.24	7.34	8.28
4	1.2	8.24	9.15	10.45	10.72
5	1.4	10.23	12.34	12.78	14.89
6	1.6	12.74	13.24	14.23	16.76

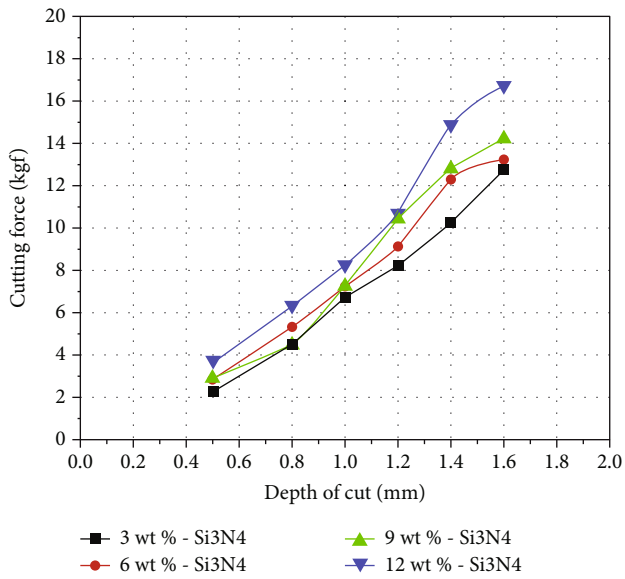

Figure 5: Depth of cut vs. cutting force (cutting speed 50 m/min).

Table 6: Cutting force summary (cutting speed 100 m/min).

S. no	Depth of cut (mm)	Cutting force (kgf)			
		3 wt. %	6 wt. %	9 wt. %	12 wt. %
1	0.5	3.45	3.84	3.67	3.76
2	0.8	6.24	5.23	6.24	7.36
3	1.0	7.23	9.15	10.21	1.24
4	1.2	9.45	12.12	11.54	12.76
5	1.4	12.62	14.67	16.92	15.43
6	1.6	14.67	18.23	19.84	17.98

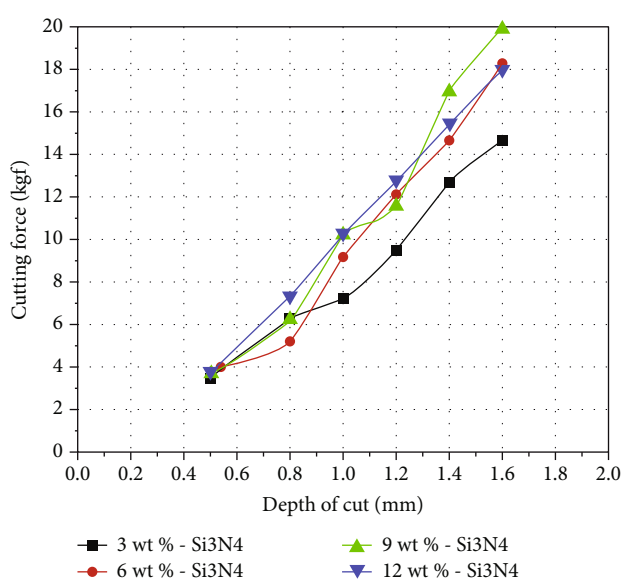

Figure 6: Depth of cut vs. cutting force (cutting speed 100 m/min).

time of 25 minutes. The dry sliding wear test specimens and apparatus of the DUCOM machine are effectively utilized for this research, as shown in Figure 4.

Table 7: Cutting force summary (cutting speed 150 m/min).

S. no	Depth of cut (mm)	Cutting force (kgf)			
		3 wt. %	6 wt. %	9 wt. %	12 wt. %
1	0.5	1.89	2.37	3.01	2.56
2	0.8	3.65	4.62	4.52	5.34
3	1.0	7.23	8.34	8.24	9.37
4	1.2	8.24	11.24	10.34	12.76
5	1.4	10.29	13.47	14.78	13.27
6	1.6	13.64	17.23	16.34	15.49

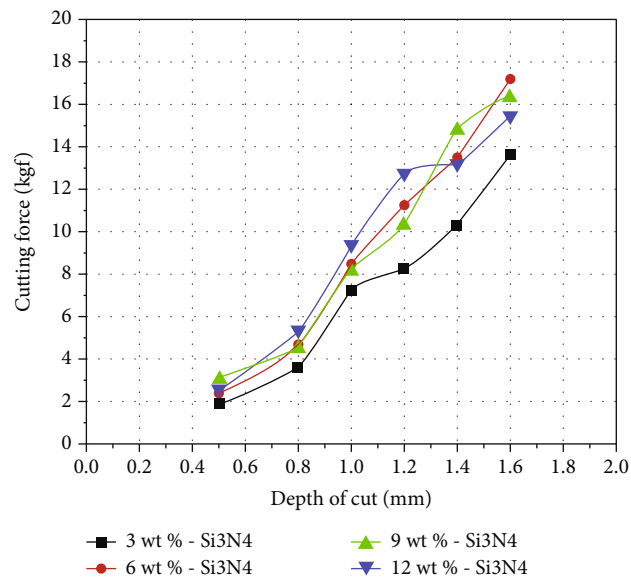

Figure 7: Depth of cut vs. cutting force (cutting speed 150 m/min).

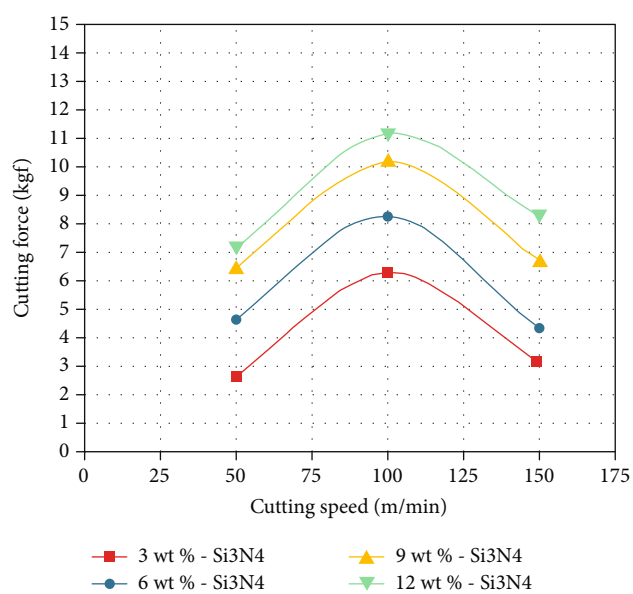

Figure 8: Cutting speed vs. cutting force (depth of cut 0.5 mm).

Different reinforcement percentages of wear test specimens are prepared under 10 mm diameter and 40 mm length with power tool cutting. Specimens are cleaned well before

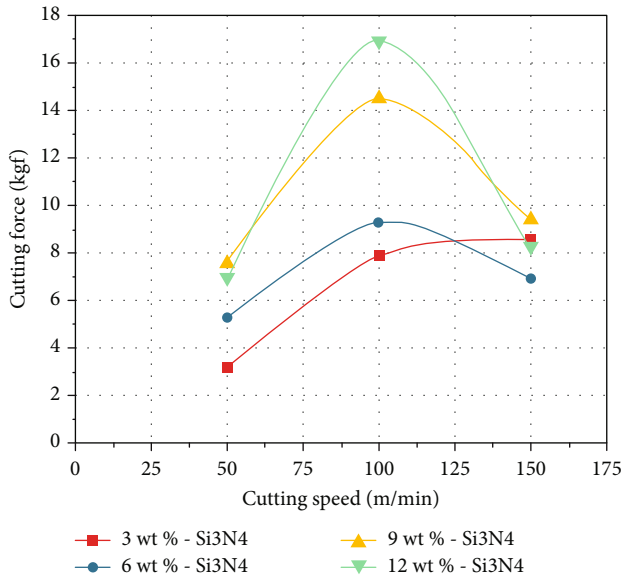

Figure 9: Cutting speed vs. cutting force (depth of cut 0.8 mm).

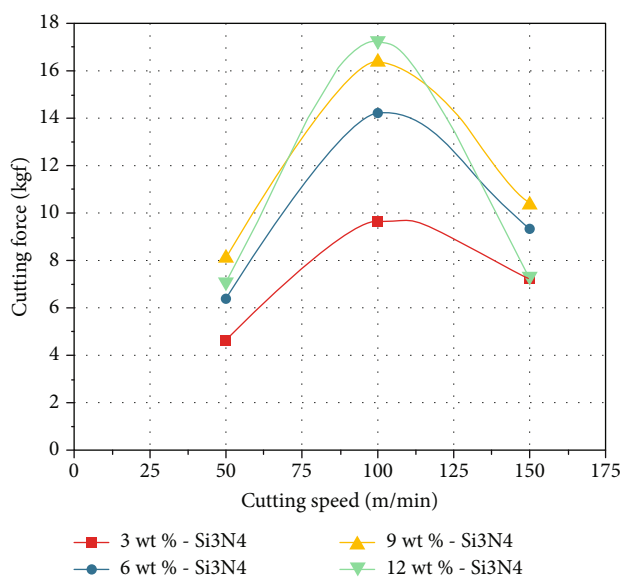

Figure 10: Cutting speed vs. cutting force (depth of cut1.0 mm).

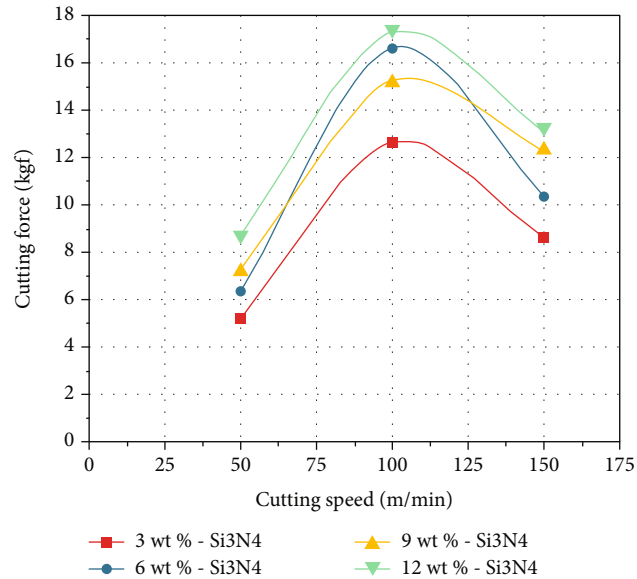

Figure 11: Cutting speed vs. cutting force (depth of cut 1.2 mm).

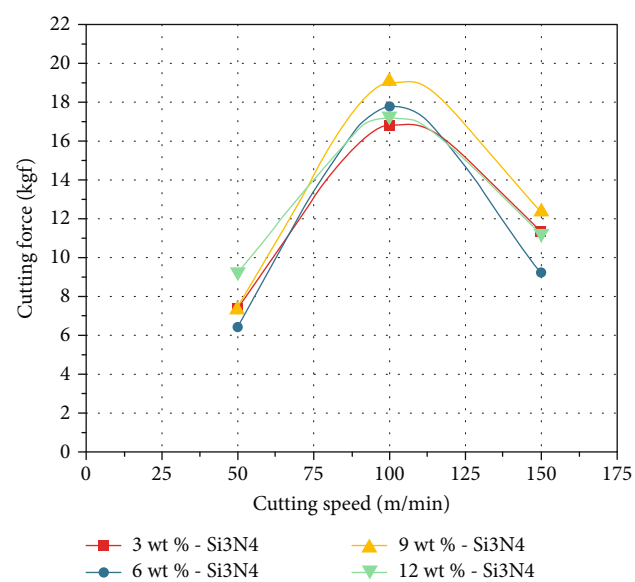

Figure 12: Cutting speed vs. cutting force (depth of cut 1.4 mm).

carried out the wear test. All the samples are prepared and wear-tested as per the American Society of Testing Materials (ASTM G99) standard procedure [35–37].

3. Results and Discussion

Table 4 clearly illustrated the influence of machining parameters and the result of surface roughness value. The surface roughness values are increased by increasing of reinforcement percentage of silicon nitride. The cutting speed and the reinforcement percentage were directly influenced to maximize the surface roughness value. The maximum surface roughness value was obtained as 3.16 microns by reinforcement of 12 wt. %, cutting speed of 150 m/min, depth of cut 1.6 mm, and the constant federate 0.1 mm/rev. The minimum surface roughness value obtained is 0.58 microns. Increasing reinforcement increases the tool wear and increases the surface roughness value. Increasing reinforcement increases the strength of the composites in terms of toughness and hardness, leading to affect the tool edges. Further, it can be reflected by poor surface finish.

3.1. Effects of Cutting Speed. The Cutting force summary of influencing Cutting speed 50 m/min is presented. The cutting force increases by increasing the depth of the cut and increasing reinforcement percentage Table 5. The maximum cutting force attained was 16.76 kgf at reinforcement of 12 wt. % of silicon nitride with the depth of cut as 1.6 mm. The minimum cutting force is 2.34 kgf by influencing 3 wt. % of reinforcement and the 0.5 depth of cut as shown in Figure 5.

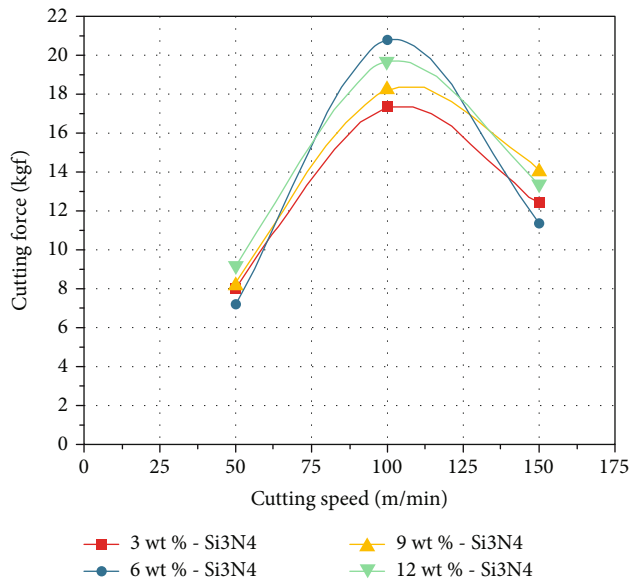

Figure 13: Cutting speed vs. cutting force (depth of cut 1.6 mm).

Table 8: Summary of wear test.

S. no	Load (*N*)	Sliding velocity (m/s)	Sliding distance (m)	Track diameter (mm)	Wear time (min)	Reinforcement %	Wear results Wear (microns)	Frictional force
1						3	211	1.2
2	30	2	1500	120	25	6	182	1.4
3						9	174	1.5
4						12	188	1.4

The cutting force analysis by influencing cutting speed 100 m/min is illustrated. The cutting force constantly increases with increasing depth of cut and increasing reinforcement weight percentage. Maximum cutting force obtained as 17.98 kgf by the reinforcement of 12 wt. % with the depth of cut as 1.6 mm in Table 6. The low cutting force was 3.45 kgf by persuading 3 wt. % of reinforcement and the 0.5 depth of cut, as shown in Figure 6.

In the cutting force study, by influencing cutting speed 150 m/min, the cutting force regularly increases with increasing cut and increasing reinforcement weight percentage in Table 7. The maximum value of cutting force was 15.49 kgf by their enforcement of 12%, with the depth of cut as 1.6 mm. The 1.89 kgf cutting force was attained by inducing 3 wt. % of reinforcement and the 0.5 depth of cut, as shown in Figure 7. Compared to cutting speed 100 m/min, the cutting force value decreased by applying 100 m/min.

3.2. Effects of Depth of Cut. The cutting force's effects were analyzed by variation of cut depth shown in Figures 8–13. The minimum cutting force obtained as 2.58 kgf with 50 m/min influence was shown in Figure 9. The maximum cutting force was obtained as 20.86 kgf with 12 wt. % reinforcement and the 100 m/min cutting speed, as shown in Figure 13, which presented the wear results. The constant values of applied load (30 N), sliding velocity (2 m/s), track diameter (120 mm), and wear time (25 min) were continued to all four specimens with different reinforcement percentages. Increasing reinforcement particles (Si_3N_4) conversely reduced the wear. Further increasing of reinforcement percentage can be turned to increases the wear rate Table 8.

The wear graph was presented in Figure 14 effectively; the maximum wear was 211 microns using 3 wt. % of Si_3N_4. Using a testing time of 25 minutes, the average frictional force was illustrated as 1.0. During the wear process, the temperature would be continually maintained as 287°C. For increasing reinforcement, reduction reduces the wear finally reached the maximum reinforcement it caused to increase wear. Minimum wear was obtained as 174 microns with 9 wt. % of reinforcement. High reinforcement percentage was induced lower mixing level. Further, it can be the origin of high weight loss. These reinforcement composites offered better wear resistance even in increasing temperature and the higher speed of the wear test.

4. Conclusion

The powder metallurgy technique carried out the machinability study of copper alloys with silicon nitride. The different machining parameters as cutting speed, feed rate, depth

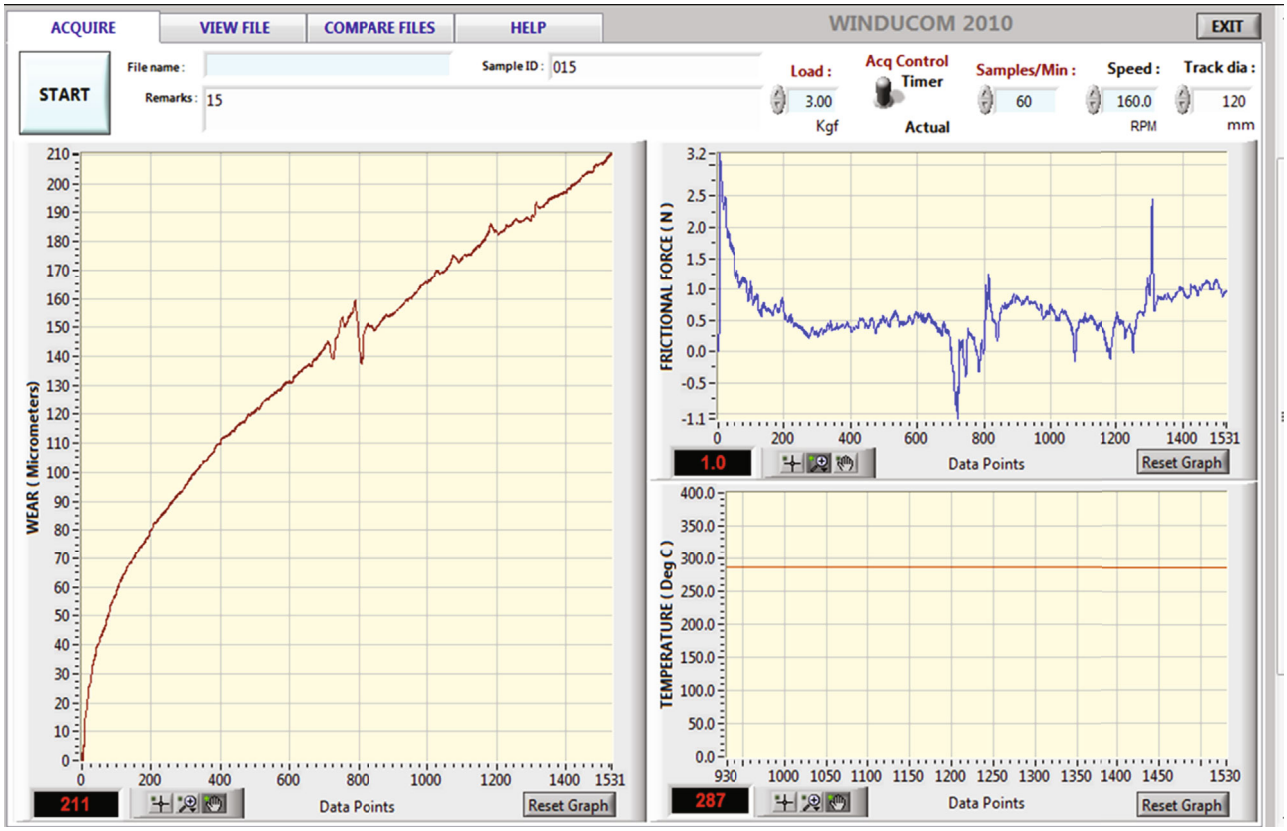

Figure 14: Wear test output in graphical view.

of cut, and reinforcement percentage were executed to measure the composite's surface roughness and cutting force effectively. The result of this investigation was presented as follows:

(i) The cutting speed and the reinforcement percentage were directly influenced to maximize the surface roughness value from the analysis. The maximum surface roughness value obtained was 3.16 microns by reinforcement of 12 wt. %, cutting speed of 150 m/min, depth of cut 1.6 mm, and the constant feed rate 0.1 mm/rev. The minimum surface roughness value obtained is 0.58 microns. Increasing reinforcement increases the tool wear and increases the surface roughness value

The maximum cutting force attained is 16.76 kgf at reinforcement of 12 wt. % of silicon nitride with the depth of cut as 1.6 mm. The minimum cutting force is 2.34 kgf by influencing 3 wt. % of reinforcement and the 0.5 depth. The cutting speed is 100 m/min, and the maximum cutting force is obtained as kgf by the reinforcement of 12 wt. % with the cut's depth as 1.6 mm. The low cutting force was 3.45 kgf by persuading 3 wt. % of reinforcement and 0.5 depth. For the cutting speed of 150 m/min, the maximum value of cutting force was 15.49 kgf by their enforcement of 12 wt. % with the depth of cut as1.6 mm. The 1.89 kgf cutting force was attained by inducing 3 wt. % of reinforcement and the 0.5 depth of cut.

(ii) From the analysis, the maximum cutting force obtained was 20.86 kgf with the influence of 12 wt. % reinforcement and the 100 m/min cutting speed. The minimum cutting force obtained was 2.58 kgf with an influence of 50 m/min

(iii) From the wear test, the minimum wear was obtained as 174 microns with 9 wt. % of reinforcement. Maximum wear was obtained as 211 microns by reinforcement of 3 wt. % of Si_3N_4. The increasing tendency of reinforcement reduces the wear and finally reached the 9 wt. % to 12 wt. % of reinforcement it caused to increase wear

Data Availability

The data used to support the findings of this study are included within the article.

Conflicts of Interest

The authors declare that there is no conflict of interest regarding the publication of this article.

References

[1] M. Kilic, D. Ozyurek, and T. Tuncay, "Dry sliding wear behaviour and microstructure of the W–Ni–Fe and W–Ni–Cu heavy alloys produced by powder metallurgy technique," *Powder*

Metallurgy and Metal Ceramics, vol. 55, no. 1-2, pp. 54–63, 2016.

[2] S. Chand and P. Chandrasekhar, "Influence of B4C/BN on solid particle erosion of Al6061 metal matrix hybrid composites fabricated through powder metallurgy technique," *Ceramics International*, vol. 46, no. 11, pp. 17621–17630, 2020.

[3] D. Rahmadiawan, A. Hairul, N. Nasruddin, and Z. Fuadi, "Stability, viscosity, and tribology properties of polyol ester oil-based biolubricant filled with TEMPO-oxidized bacterial cellulose nanofiber," *International Journal of Polymer Science*, vol. 2021, Article ID 5536047, 9 pages, 2021.

[4] Y. Zeleke and G. K. Rotich, "Design and development of false ceiling board using polyvinyl acetate (PVAc) composite reinforced with false banana fibres and filled with sawdust," *International Journal of Polymer Science*, vol. 2021, Article ID 5542329, 10 pages, 2021.

[5] H. Alihosseini, K. Dehghani, and J. Kamali, "Microstructure characterization, mechanical properties, compressibility and sintering behavior of Al-B4C nanocomposite powders," *Advanced Powder Technology*, vol. 28, no. 9, pp. 2126–2134, 2017.

[6] S. L. G. Petroni, "PM compaction equations applied for the modelling of titanium hydride powders compressibility data," *Powder Metallurgy*, vol. 63, no. 1, pp. 35–42, 2020.

[7] F. Güner, Ö. N. Cora, and H. Sofuoğlu, "Numerical modeling of cold powder compaction using multi particle and continuum media approaches," *Powder Technology*, vol. 271, pp. 238–247, 2015.

[8] N. Sharma and K. Kumar, "Mechanical characteristics and bioactivity of porous Ni50-xTi50Cux (x =0, 5and 10) prepared by P/M," *Materials Science*, vol. 34, no. 8, pp. 934–944, 2018.

[9] A. Saboori, C. Novara, M. Pavese, C. Badini, F. Giorgis, and P. Fino, "An investigation on the sinterability and the compaction behavior of aluminum/graphene nanoplatelets (GNPs) prepared by powder metallurgy," *Journal of Materials Engineering and Performance*, vol. 26, no. 3, pp. 993–999, 2017.

[10] P. Verma, R. Saha, and D. Chaira, "Waste steel scrap to nanostructured powder and superior compact through powdermetallurgy: powdergeneration, processing and characterization," *Powder Technology*, vol. 326, pp. 159–167, 2018.

[11] A. Saker, M. G. Cares-Pacheco, P. Marchal, and V. Falk, "Powders flowability assessment in granular compaction: what about the consistency of Hausner ratio?," *Powder Technology*, vol. 354, pp. 52–63, 2019.

[12] A. Fathy, E.-K. Omyma, and M. M. M. Mohammed, "Effect of iron addition on microstructure, mechanical and magnetic properties of Al-matrix composite produced by powder metallurgy route," *Transactions of Nonferrous Metals Society of China*, vol. 25, no. 1, pp. 46–53, 2015.

[13] M. A. Sohag, P. Gupta, N. Kondal, D. Kumar, N. Singh, and A. Jamwal, "Effect of ceramic reinforcement on the mi- crostructural, mechanical and tribological behavior of Al-Cu alloy metal matrix composite," *Materials Today: Proceedings*, vol. 21, pp. 1407–1411, 2020.

[14] Y. Tian, Z. Dou, L. Niu, and T. Zhang, "Effect of nanoboron carbide particles on properties of copper-matrix/graphite composite materials," *Materials Research*, vol. 6, no. 9, pp. 950–957, 2019.

[15] M. Zhou, S. Huang, L. Yu, W. Liu, and S. Yan, "Investigation on compaction densification behaviors of multicomponent mixed metal powders to manufacture silver-based filler metal sheets," *Arabian Journal for Science and Engineering*, vol. 44, no. 2, pp. 1321–1335, 2019.

[16] W. Chen, J. Wang, S. Wang, P. Chen, and J. Cheng, "On the processing properties and friction behaviours during compaction of powder mixtures," *Materials Science and Technology*, vol. 36, pp. 1057–1064, 2020.

[17] C. Ayyappadas, A. Muthuchamy, A. R. Annamalai, and D. K. Agrawal, "An investigation on the effect of sintering mode on various properties of copper-graphene metal matrix composite," *Advanced Powder Technology*, vol. 28, no. 7, pp. 1760–1768, 2017.

[18] A. H. Jaafar and H. Al-Ethari, "Optimization of machining nickel aluminum bronze matrix composite prepared by powder metallurgy," in *International Conference on Advances in Sustainable Engineering and Applications (ICASEA)*, pp. 255–260, Wasit - Kut, Iraq, 2018.

[19] D. Sujit, R. Behera, G. Majumdar, B. Oraon, and G. Sutradhar, "An experimental investigation on the machinability of powder formed silicon carbide particle reinforced aluminium metal matrix composites," *International Journal of Scientific & Engineering Research*, vol. 2, no. 7, pp. 2229–5518, 2011.

[20] M. B. N. Shaikh, S. Arif, and M. A. Siddiqui, "Fabrication and characterization of aluminium hybrid composites reinforced with fly ash and silicon carbide through powder metallurgy," *Materials Research Express*, vol. 5, no. 4, 2018.

[21] K. Halil, O. İsmail, D. Sibel, and Ç. Ramazan, "Wear and mechanical properties of Al6061/SiC/B4C hybrid composites produced with powder metallurgy," *Journal of Materials Research and Technology*, vol. 8, no. 6, pp. 5348–5361, 2019.

[22] P. V. Badiger, V. Desai, M. R. Ramesh, B. K. Prajwala, and K. Raveendra, "Cutting forces, surface roughness and tool wear quality assessment using ANN and PSO approach during machining of MDN431 with TiN/AlN-coated cutting tool," *Arabian Journal for Science and Engineering*, vol. 44, no. 9, pp. 7465–7477, 2019.

[23] M. O. Shabani, A. Baghani, A. Khorram, and F. Heydari, "Evaluation of fracture mechanisms in Al-Si metal matrix nanocomposites produced by three methods of gravity sand casting, squeeze casting and compo casting in semi-solid state," *Silicon*, vol. 12, no. 12, pp. 2977–2987, 2020.

[24] R. Harichandran and N. Selvakumar, "Microstructure and mechanical characterization of (B4C+ h-BN)/Al hybrid nanocomposites processed by ultrasound assisted casting," *International Journal of Mechanical Sciences*, vol. 144, pp. 814–826, 2018.

[25] M. S. Kumar, M. Vanmathi, and G. Sakthivel, "SiC reinforcement in the synthesis and characterization of A356/AL2O3/-Sic/Gr reinforced composite-paving a way for the next generation of aircraft applications," *Silicon*, pp. 1–18, 2020.

[26] K. A. Ali, V. Mohanavel, M. Ravichandran, S. A. Vendan, T. Sathish, and A. Karthick, "Microstructure and mechanical properties of friction stir welded SiC/TiB 2 reinforced aluminum hybrid composites," *Silicon*, pp. 1–11, 2021.

[27] A. Nirala and A. Upadhyaya, "Experimental characterization and sintering behavior in mixed atmosphere (N 2 and H 2) of Fe 3 P-added ferritic stainless steel (434L)," *Journal of Materials Engineering and Performance*, vol. 29, no. 5, pp. 2926–2935, 2020.

[28] R. K. Behera, S. C. Panigrahi, B. P. Samal, and P. K. Parida, "Mechanical properties and micro-structural study of sintered aluminium metal matrix composites by P/M technique,"

Journal of Modern Manufacturing Systems and Technology, vol. 3, no. 2, pp. 89–97, 2019.

[29] V. Kavimani, B. Stalin, P. M. Gopal, M. Ravichandran, A. Karthick, and M. Bharani, "Application of r-GO-MMT hybrid nanofillers for improving strength and flame retardancy of epoxy/glass fibre composites," *Advances in Polymer Technology*, vol. 2021, 9 pages, 2021.

[30] R. Bhagat, "Advanced aluminium powder metallurgy alloy and composites," in *ASM Hand Book*, vol. 7, pp. 840–858, ASM International, Cleveland OH, 2018.

[31] N. Sharma, T. Raj, and K. K. Jangra, "Microstructural evaluation of NiTi-powder, steatite, and steel balls after different milling conditions," *Materials and Manufacturing Processes*, vol. 31, no. 5, pp. 628–632, 2016.

[32] S. A. Daniel, M. Sakthivel, P. M. Gopal, and S. Sudhagar, "Study on tribological behaviour of Al/SiC/MoS2 hybrid metal matrix composites in high temperature environmental condition," *Silicon*, vol. 10, no. 5, pp. 2129–2139, 2018.

[33] I. Gunes, T. Uygunoglu, and M. Erdogan, "Effect of sintering duration on some properties of pure magnesium," *Powder Metallurgy and Metal Ceramics*, vol. 54, no. 3-4, pp. 156–165, 2015.

[34] N. Radhika, J. Sasikumar, and R. Jojith, "Effect of grain modifier on mechanical and tribological properties of Al-Si alloy and composite," *Silicon*, vol. 13, no. 3, pp. 841–855, 2021.

[35] N. Raj and N. Radhika, "Tribological characteristics of LM13/Si3N4/Gr hybrid composite at elevated temperature," *Silicon*, vol. 11, no. 2, pp. 947–960, 2019.

[36] M. I. Haq and A. Anand, "Dry sliding friction and wear behavior of AA7075-Si3N4 composite," *Silicon*, vol. 10, no. 5, pp. 1819–1829, 2018.

[37] P. V. Badiger, V. Desai, M. R. Ramesh, B. K. Prajwala, and K. Raveendra, "Effect of cutting parameters on tool wear, cutting force and surface roughness in machining of MDN431 alloy using Al and Fe coated tools," *Materials Research Express*, vol. 6, no. 1, pp. 89–97, 2018.